Universidad Autónoma de Madrid
Doctorado en Biociencias Moleculares

Mitochondrial DNA transfer through exosomes during immune synapsis primes antiviral innate immune response in dendritic cells

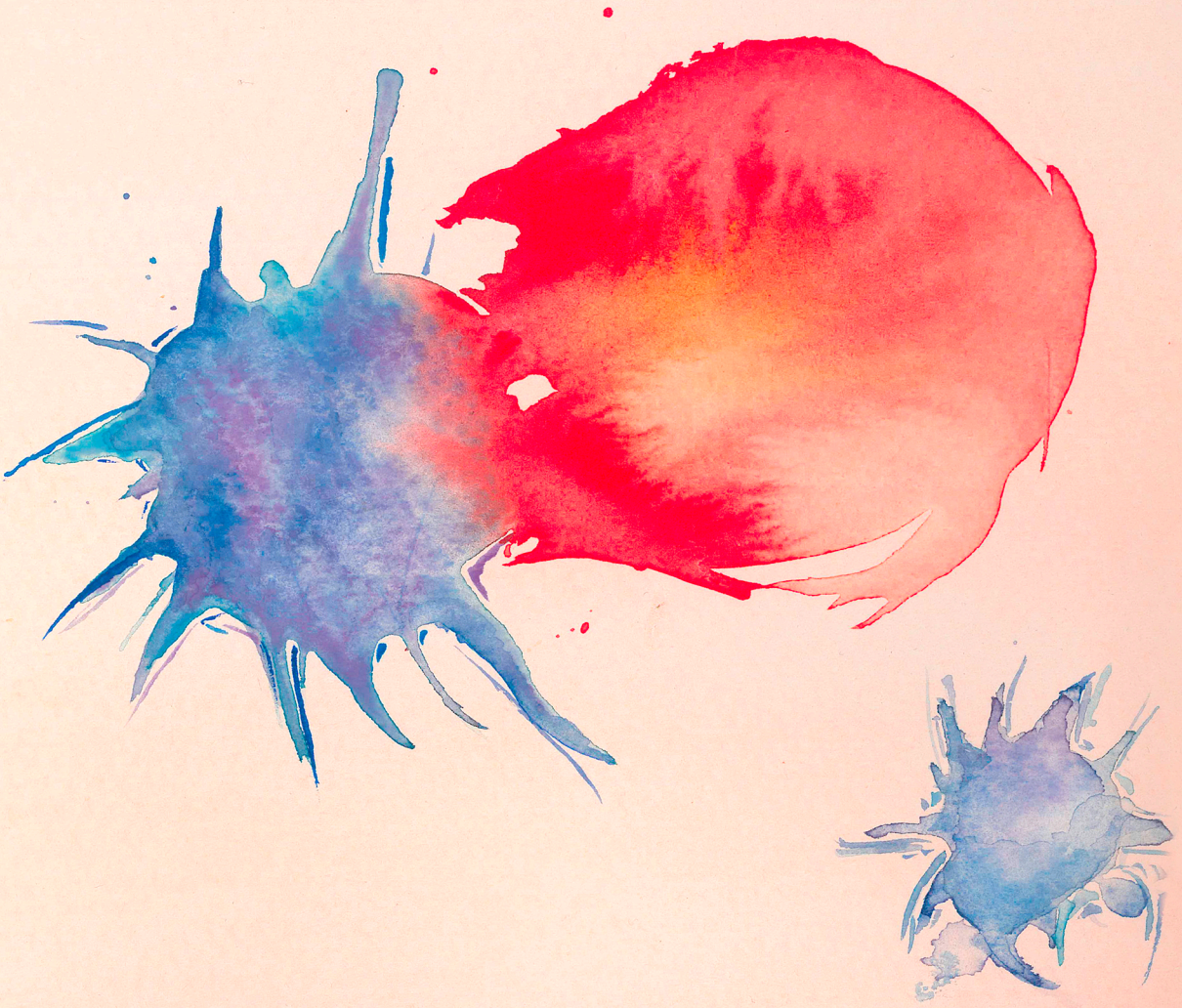

Daniel Torralba Grajales

Madrid, 2019

Universidad Autónoma de Madrid

Departamento de Bioquímica

Facultad de Medicina

Mitochondrial DNA transfer through exosomes during immune synapsis primes antiviral innate immune response in dendritic cells.

Doctoral Thesis

Daniel Torralba Grajales

Madrid, 2019

Universidad Autónoma de Madrid

Programa de Doctorado en Biociencias Moleculares

Facultad de Medicina

Departamento de Bioquímica

Mitochondrial DNA transfer through exosomes during immune synapsis primes antiviral innate immune response in dendritic cells.

Memoria presentada por el Licenciado en Bioquímica:

Daniel Torralba Grajales

Para optar al título de Doctor por la Universidad Autónoma de Madrid

Director de tesis: **Dr. Francisco Sánchez Madrid**, Doctor en Ciencias Biológicas y Catedrático de Inmunología de la Universidad Autónoma de Madrid

Este trabajo ha sido realizado en el Centro Nacional de Investigaciones Cardiovasculares (CNIC) y Servicio de Inmunología del Hospital Universitario de la Princesa

Madrid, 2019

Francisco Sánchez Madrid, Doctor en Ciencias Biológicas y Catedrático de Inmunología de la Universidad Autónoma de Madrid

CERTIFICA:

Que Daniel Torralba Grajales, Licenciado en Bioquímica por la Universidad Autónoma de Madrid, ha realizado bajo mi dirección el trabajo de investigación correspondiente a su Tesis Doctoral con el título:

"**Mitochondrial DNA transfer through exosomes during immune synapse primes antiviral innate immune response in dendritic cells**".

Revisado este trabajo, el que suscribe considera el trabajo realizado satisfactorio y autoriza su presentación para ser evaluado por el tribunal correspondiente.

Y para que así conste y a los efectos oportunos, firma el presente certificado en Madrid a 10 de Junio de 2019

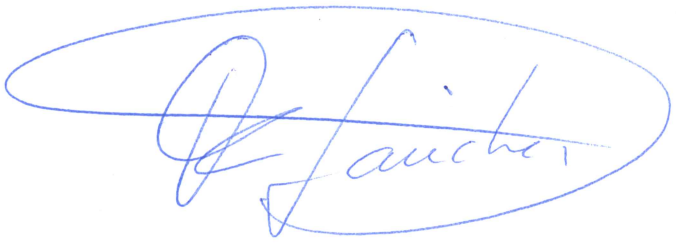

Fdo: Francisco Sánchez Madrid

A mis padres, a mi hermana

A mi mujer y mi hijo

*"**Un gran poder conlleva una gran responsabilidad**"*

Franklin D. Roosevelt/ Tío Ben

Agradecimientos

Agradecimientos

Dice el proverbio chino "*El leve aleteo de las alas de una mariposa se puede sentir al otro lado del mundo*". En un sistema dinámico complejo como es el de la vida, ligeras variaciones pueden amplificarse y desembocar en inmensos cambios. Es curioso cómo los pequeños actos de nuestra vida cotidiana tiene inmensas repercusiones completamente imprevisibles en nuestras vidas futuras. Creo que tener esto en mente puede ayudarnos a entender que tenemos un gran poder en todos nuestros actos diarios hacia los que nos rodean, pueden cambiar el destino de alguien por muy insignificantes que parezcan. Tenemos un gran poder y eso conlleva una gran responsabilidad.

Así que si hoy estoy aquí, concluyendo un gran hito académico, es gracias a muchas personas que a través de pequeños cambios me han hecho convertirme en quien soy hoy. Quizás no tenga otra oportunidad de agradecer formalmente a todos los que me rodean o me han rodeado en algún momento. Discúlpeme el lector por la extensión, la tesis comienza unas hojas más adelante. En primer lugar me gustaría darle las gracias al Dr. Sánchez-Madrid, conocido entre todos como Paco. Él fue mi profesor de Inmunología, probablemente la asignatura que más me fascinó durante la carrera. Esto definió mi destino en la investigación científica y en mi futuro profesional. Paco me aceptó en su laboratorio hace ya bastantes años para realizar mi proyecto de investigación de fin de carrera y finalmente la tesis doctoral. Gracias Paco por darme autonomía, espíritu crítico y perseverancia en los proyectos.

En segundo lugar gracias a todos los profesores que han formado parte de mi educación, su labor es fundamental, ellos crean a los ciudadanos del mañana y no podemos olvidar su labor. Me gustaría mencionar algunos en concreto. Gracias a José Miguel Serrano, mi profesor de Biología de secundaria, él pensó que éramos capaces de saber más de lo que se nos exigía y nos enseñó los misterios de la bioquímica y la biología celular. El encendió la llama que años más tarde terminaría haciendo que estudiara Bioquímica. Gracias al profesor Mateo, él despertó mi pasión por las ciencias formales y la lógica. Consiguió que pasara de odiar las matemáticas a amarlas, y lo hizo consiguiendo que las entendiera y no las memorizase. Este evento cambió mi perspectiva de la educación y mi desempeño a lo largo de toda la carrera y tesis.

He de hacer una mención a la ayuda de la Fundación La Caixa, su programa de becas me ha permitido centrarme en investigar y en estudiar sin preocuparme de la financiación. Sin duda esto es indispensable para poder desarrollarse a nivel profesional y personal. Gracias.

Para ser un buen científico creo que hay que desarrollar una buena imaginación. No me corresponde juzgar si soy un buen científico pero sin duda si alguien me ha ayudado a desarrollar esta habilidad han sido mis inseparables amigos Mario, Miguel, Ignacio y Jose. Pero esto no es el único regalo que he recibido de su parte, en ellos encuentro los mejores valores del ser humano y ellos han tenido una tremenda influencia en quien soy yo hoy. Gracias Mario por entrenarme en mi incansable empeño por discutir y traer sentido a todo lo que me rodea, quizás una de las razones por las que me dediqué a la ciencia. Gracias también por todos los buenos consejos que me has dado y por tu paciencia. Gracias Miguel por ser un ejemplo de voluntad y perseverancia luchando por un sueño, hay que ser muy valiente para dar un giro tan radical a tu vida. Gracias por estar siempre cerca y apoyarme en el camino. Gracias Ignacio por ser un ejemplo de lealtad, amistad y bondad. Una persona en la que se puede depositar una confianza absoluta porque nunca te fallará. Gracias Jose por tu buen sentido del humor y tu asertividad. Me habéis enseñado mucho. Gracias a los cuatro por estar a mi lado siempre.

En el colegio conocí a mucha gente y ese periodo definió en gran medida la personalidad que terminaría moldeando en los años venideros. Gracias a Juan Luis por tantos recreos de última hora, y por tan buenos ratos que vivimos y seguimos viviendo. También me gustaría agradecerle a Victoria por todas esas explicaciones y tanta ayuda que me dio, gracias por las confidencias y tu cariño. Gracias por último a David que ha sido un gran compañero y amigo desde el cole hasta hoy.

De mi etapa universitaria sin duda tengo que agradecer a mis amigos de Biología de la UAM, personas que permanecerán siempre cerca y que hicieron que mis años en la universidad pasaran como un suspiro y que guardé en mis recuerdos como una de las mejores etapas de mi vida. Dicen que un científico debe ser guiado por su curiosidad, y, ¿quién tiene más curiosidad que un niño? Sin duda alguna ellos me han hecho mantener a mi niño interior activo, de disfrutar de las pequeñas cosas y de valorar cada momento. Muchas gracias Barrio por la amistad y el apoyo a lo largo de estos años (a tu manera). Sin duda eres un ejemplo de lealtad y fidelidad hacia tus amigos. Él me enseñó que las cosas inolvidables son las que nunca se olvidan. Gracias por toda la morralla de YouTube que me ha hecho pasar tantas horas haciendo y diciendo tonterías. Si hablamos de niños grandes el premio se lo lleva Petrini, gracias por hacernos reír tanto y por todas las aventuras en las que nos has metido. Siempre apoyado por Cogollos que nunca defrauda para tener una nueva historia que contar. A veces la vida nos trae sorpresas, y cuál fue la mía cuando encontré a mi amigo de la infancia del colegio en mi clase de Biología, Miguel ese chico silencioso que siempre era nuevo en el colegio y que también fue nuevo en la Universidad logró ganarse nuestros corazones. Muchas gracias por

compartir conmigo tu humildad y buen corazón. Gracias a David, por retarme y hacerme querer llegar más lejos, un poco de competencia sana siempre puede alentarnos a ser mejores cada día, aunque probablemente el único que competía era yo… Gracias por ayudarme tan desinteresadamente y por resolver mis histéricas dudas de última hora antes del examen. Gracias a Hurtado por enseñarme como el esfuerzo y las ganas de conocer pueden llevarte a sitios maravillosos. Gracias a Didi, ella fue mi confidente durante los años de Universidad, gracias por tantos pequeños momentos y por darle alas a mi sentido del humor en la cafetería. Sobre todo muchas gracias por preocuparte tanto por mí y por todo el cariño que me has dado. Otro punto de inflexión en mi vida y mi carrera fue cuando Marina me invitó a hacerle una visita a su cabaña flotante en el Amazonas, mi forma de tomarme la vida dio un giro de 360 grados, muchas gracias por haberme dado esa oportunidad y por empujarme a ir a por la que a día de hoy es mi mujer. Por último gracias a Marta, Varela y Velilla por hacerme sentir en familia y porque gracias a vosotras cada día en la Uni era más divertido. En conjunto todos vosotros habéis tenido una tremenda influencia en quien soy hoy y a donde he llegado. No podré nunca agradecéroslo lo suficiente.

En mi época universitaria también entro en mi vida Alma, no lo sabía aun pero terminaría siendo parte de mi familia. Gracias por todo el cariño que nos has dado a mí y a Mery a lo largo de estos años. Gracias por estar siempre ahí sin importar que pasara y muchas gracias por aguantar mis chinches que tanto disfruto y que tanto te desesperan.

Victor y Fran, dos grandes amigos que me llevo de mi etapa predoctoral. Probablemente son de las personas con más capacidad que he conocido y de las que más admiro. Fran, creativo y trabajador donde los haya (aun siendo de Graná) y Victor, experto networker y proactivo a más no poder. Ambos con un excepcional sentido del humor. Gracias por tantas meriendas y por tantas discusiones científicas. Gracias por escuchar mis hipótesis por apoyarme en mis momentos de dudas. Sé que llegareis donde os propongáis

También me gustaría darle las gracias a Charlie, hablar con él es siempre un reto intelectual, gracias por esas reuniones para arreglar el mundo que ha permitido que mi imaginación volase. Una persona que sin duda sabe escuchar y siempre aporta sentido y lógica a la vida.

Tengo que hacer un agradecimiento especial a todos laboratorios que me han acogido antes de llegar al laboratorio de Paco. Muchas gracias Guada por darme la oportunidad de hacer el CICERONE contigo, fue una de las mejores experiencias que tengo de mis veranos en la Universidad, de allí me llevo a grandes personas: Lucho, Eli, Edgar y sobretodo Toñi.

Toñi me ha enseñado a “salir de la caja”, a pensar más allá de lo establecido y a que un científico tiene que ser flexible en el pensamiento puesto que debemos estar dispuestos a enfrentarnos a lo desconocido sin prejuicios. Que no debemos rechazar una idea por muy loca que sea. Probablemente al entrar en el laboratorio mi cabeza era lo contrario a esto, dogmático e inflexible, gracias a ella me he acercado un poco más a la ciencia de verdad. Gracias por ser mi mentora de esta etapa y por guiarme en este camino que a veces me ha resultado tan difícil.

Otro verano que recuerdo con especial cariño es el que pasé en el laboratorio de Mercedes Rincón en Vermont. Fue una experiencia que me ayudó a superar momentos complicados y que disfruté a más no poder. Gracias Mercedes por enseñarme lo que significa la verdadera vocación y a vivir la ciencia con pasión.

Durante estos años de laboratorio he tenido la oportunidad de conocer a mucha gente fuera del laboratorio. Muchas gracias a los “Sanchos”, en conjunto un ejemplo de dedicación y perseverancia. Gracias Salva por tan buenos consejos científicos y por las charlas informales en cualquier esquinita. Gracias Mary, Ruth, Sarai y Sofía por compartir esos ratitos de cultivos diciendo tonterías y amenizando esos largos ratos muertos.

En los 5 años de tesis en el laboratorio de Paco he podido compartir poyata con grandes personas. Gracias a los Jurásicos, grandes noches y momentos. Gracias Norman por enseñarme a encontrar la felicidad en pequeñas cosas. A Rafa por su sencillez y su capacidad de sacar un buen momento de cualquier situación. A Eu por su humor y por todas las conversaciones científicas y no tan científicas que hemos sacado. A Álvaro y Javi, gracias a vosotros y las conversaciones frikis me habéis hecho sentir siempre como en casa. Lo he pasado muy bien. Muchas gracias chicos.

Gracias a Noe tu simpatía y por montar planes tan divertidos fuera del laboratorio en los que he podido conocer a mis compañeros más a fondo. Gracias a Ana, con esa templanza que le caracteriza siempre ha conseguido que fuese capaz de verle el lado bueno a todas las cosas. Gracias por tus ánimos constantes. Gracias a Irene, que empezó como mi estudiante de CICERONE y ahora soy yo quien tiene que consultarle todo a ella. Una persona metódica y ordenada de la que tengo mucho que aprender. Gracias por crear tan buen ambiente en el laboratorio y por ayudarme cuando lo he necesitado. Gracias a Marta, la que podría ser nuestra hermana mayor del lab, ella nos guía y ayuda en todo, siempre tiene unas palabras para animarte. Gracias a Laurín, que siempre sacaba una sonrisa e intentaba animarte aunque el panorama estuviese negro. Eres una gran persona. Gracias también a Olga por haber

compartido tantos momentos y poyata, aunque mi desorden te pusiese nerviosilla. Gracias a Lola por estar siempre dispuesta a sacar una conversación interesante y por su contagiosa risa. Gracias a Raquel por ser un ejemplo de esfuerzo, me habéis enseñado mucho. Gracias a Nieves por su simpatía y buen rollo. Para que un laboratorio funcione hacen falta personas como vosotras. También es necesario que haya personas que hagan girar los engranajes del lab y ahí se encuentra La Secre María Ángeles. Muchas gracias por toda tu ayuda para resolver cualquier asuntillo. Gracias Jose María por tus chistes malos y por amenizarme tanto las horas de laboratorio. Gracias a Danay por ser un ejemplo de voluntad, vocación y focalización. Para mi eres una referencia del esfuerzo que debe hacer un científico para tener éxito. Gracias por todas las lecciones que me has enseñado. Gracias a Fran Baixauli, sin el cual claramente esta tesis sido tal y como es. Gracias por guiarme por el tortuoso camino de la tesis y por tu generosidad. Gracias a Noa, que sobre todo en esta última etapa me ha ayudado sobremanera, consiguió tirar para que el paper pudiera ser publicado. Gracias por tus consejos que me has dado. Gracias a Raúl y a Vicky, que me habéis tenido que soportar con diligencia en vuestros veranos, gracias por recordarme lo que es la pasión por aprender. También tengo que agradecer a todos los integrantes de las unidades de citometría y microscopía en las que he pasado tantas horas, gracias a todos los que habéis hecho que mi trabajo fuera un poco más sencillo.

Siempre guardaré en el corazón a todas las personas que he conocido en el laboratorio, ha sido una etapa dura y ellos han estado siempre ahí. Mi personalidad y mis objetivos en la vida han cambiado mucho desde el primer día que entré en el CNIC, ellos me han acompañado en este cambio y me han apoyado cuando me ha hecho falta. Gracias de vedad.

Hace unos años al casarme empecé una nueva familia y extendí la que ya tenía. Ellos me han acogido como si fuera un hijo y un hermano desde el principio. Gracias por darme tanto cariño y por dejarme formar parte de vuestras vidas. Sois una familia transparente y humilde y me encanta formar parte de ella. Gracias Juan padre por transmitirme tu sentido de la responsabilidad y por tu empeño y dedicación al trabajo. Gracias por valorarme y hacerme sentir parte de tu círculo. No puedo olvidar agradecerte que me invitaras aquel verano al barco, hoy no estaría aquí de no ser por eso. Muchas gracias Eleni, porque de verdad me he sentido como un hijo. Desprendes genialidad y felicidad, gracias por regalar tanta positividad y alegría, eres indispensable. Gracias a la Abuela por todo el cariño que me da y por toda la vitalidad y energía que trasmite cada día. Gracias a Juan hijo por hacerme sentir uno más, por

contar conmigo siempre, por valorarme y por hacérmelo pasar tan bien y conseguir sacarme una carcajada a la mínima de cambio.

Si alguien ha podido influir en mi sin duda alguna ha sido mi familia, ellos me han acompañado desde que tengo uso de razón y han forjado mi carácter. Gracias a mi tito Aure, posiblemente la persona más buena de corazón que conoceré, él lo daría todo por el resto, un ejemplo de amor y devoción por sus padres. Gracias a mi tío Jose, por confiar tanto en mí, él siempre dijo que yo sería un gran científico, espero que este logro académico le haga sentir que me acerqué un poco a sus predicciones. Gracias a mi abuelita María y a mi abuelo Antonio que tanto me han cuidado y querido, que me ha hecho querer ser alguien del que se pudieran sentir orgullosos. Siempre han sido pacientes conmigo y me han querido tal y como era. Gracias también a mi familia de Colombia, a mi Tia Upi por el amor que irradia al mundo, a mi tía Vicky por su carácter afable y cariñoso. Por supuesto a mi abuelo Hoover y a mi abuela Estrella, os he sentido muy cerca aunque tanto tiempo hayamos estado tan lejos. Si algo me ha enseñado mi abuelo, hombre de muchas virtudes, es el saber estar, la corrección y la elegancia. Gracias a mi abuela estrella por enseñarme a contar cuentos y el sentido de la actuación, hoy son de gran ayuda en mi vida profesional.

Dicen que el amor incondicional es el de una madre por su hijo, creo que puede extenderse al de unos abuelos por su nieto. Así lo he sentido de todos ellos, sé que a los que no pueden estar aquí hoy habrían sido felices viéndome delante del atril defendiendo mi tesis. A ellos se lo dedico.

Para acabar tengo que agradecer especialmente a mis padres y a mi hermana. Gracias a mi padre Antonio por ser un rol de vida, por ser un ejemplo de rectitud y bondad. Gracias por enseñarme a ser un hombre de bien y por darme los valores y principios morales que a día de hoy rigen mi vida. Gracias por enseñarme a llevar los problemas con estoicismo y valentía, siempre con una sonrisa y una buena actitud. También te agradezco profundamente haberme dado la oportunidad de elegir con total libertad lo que quería hacer en mi vida adulta. Sin duda esto es lo que me ha permitido estar hoy escribiendo una tesis doctoral.

Gracias a mi madre Cristina por enseñarme el valor de la ternura y el cuidado. Por escucharme incansablemente, por entenderme y por apoyarme sin condición en todos los proyectos que he tomado. Gracias por confiar en mí desde niño y por darme autonomía para tomar mis decisiones y equivocarme. Porque es desde el fallo desde donde se crea la experiencia y se crece. Gracias por enseñarme a no tener vergüenza y a hacer las cosas simplemente porque quiero sin preocuparme por los juicios de otras personas. Gracias por

inculcarme que para conseguir un objetivo hay que estar dispuesto a hacer sacrificios y que se requiere trabajo duro. Estas enseñanzas que todavía a día de hoy recibo me han ayudado a terminar este proyecto. Por último gracias por enseñarme junto a Papi la importancia de la familia. Ambos sois un ejemplo a seguir en todos los sentidos y siempre me he sentido muy orgulloso de vosotros. No me imagino una familia mejor en la que haber nacido.

Mencionaba en el inicio como pequeños cambios pueden transformar la vida de las personas, el día que mis padres decidieron tener a mi hermana Carol cambió mi mundo, ya nunca más iba a estar solo. No me imagino mi vida sin ella, ha estado siempre a mi lado y sé que estará hasta el último día, porque la familia es lo que siempre queda. Es difícil enumerar todas las razones por las que estoy agradecido, supongo que su mera existencia ya transformó para bien mi vida. En primer lugar gracias por ser mi mejor amiga, por todos los buenos momentos que hemos pasado juntos. Gracias por despertar mi vena sentimental y artística, gracias por enseñarme a no tener miedo a derramar lágrimas, pues más de una vez ha ocurrido durante esta tesis. Por supuesto un agradecimiento especial por haber diseñado la portada de la tesis donde como en el Renacimiento ciencia y arte han quedado integradas.

Como dice Paco, para ser un buen científico hay que ser primero una buena persona. Si hoy soy una buena persona es gracias a mis padres y mi hermana. Nunca podré agradecer suficiente todo lo que me habéis dado. Espero poder hacerlo tan bien con mis hijos como vosotros lo habéis hecho con nosotros.

En último lugar, no por casualidad, si no siguiendo el orden en las autorías de los trabajos científicos, está Mery, mi amiga, mi mujer y compañera de vida, mi mitad, mi aliento para seguir adelante y mi bastón cuando tropiezo. Ella es mi roca en medio de la tempestad, la única cosa que sé que no me fallará cuando todo el resto falle. Ella me ha levantado cada vez que me he caído con un simple: “Tu puedes, confío en ti”.

Si algo me ha enseñado Mery es que no podemos dejar de hacer cosas por lo que pueda ocurrir, a la gente le paraliza el miedo cuando tienen que tomar decisiones y arriesgar. Mery es un claro ejemplo de lo contrario. Ella me ha enseñado que solo cuando vamos más allá de nuestros límites del confort es cuando podemos desarrollarnos a nivel personal y crecer. Si nosotros no hubiéramos salido de esa zona de confort yo no sería el mismo y ella no estaría a mi lado. Como decía al principio son justo esas pequeñas acciones las que pueden cambiar por completo el transcurso de una o más vidas.

Mery me inspira a ser mejor en todos los ámbitos cada día, junto a ella aprendo cosas nuevas todos los días, quiero ayudar a los demás y ser mejor persona. Me contagia de felicidad y positividad. Me da energía y fuerzas para afrontar lo que sea, no importa que. Siento un profundo respeto y admiración por ti Mery. Sin ti no habría podido llegar al final gracias por regalarme tus fuerzas.

Por último ella me ha dado la oportunidad de crear una familia, uno de mis mayores deseos en la vida. Hace unos meses mi hijo Lucas, Luke para los amigos, llegó cual terremoto. Desde antes de nacer ha sido un gran motor de cambio y de crecimiento personal. El me inspira a querer ser mejor persona y padre cada día. Me conformaría con poder aportarle lo mismo que mi familia me ha dado a mí. Quizás en unos años lea esta tesis y espero que se sienta orgulloso de su padre. Muchas gracias hijo por adelantado por todo lo que me vas a dar.

Resumen

Las respuestas inmunitarias específicas frente a patógenos requieren de la interacción inicial de una célula T con una célula presentadora de antígeno (CPA), concretamente las células dendríticas (CD). El reconocimiento por parte de la célula T de un antígeno unido al complejo mayor de histocompatibilidad (CMH) conduce a la formación de una unión intercelular estable conocida como sinapsis inmune (SI). En las células T, la SI implica una importante redistribución del citoesqueleto y de los receptores asociados a membrana. También conlleva una polarización del tráfico intracelular y de los orgánulos secretores. La sinapsis inmune es una estructura adecuada para una comunicación intercelular eficiente. Durante este proceso las células T y las CD intercambian numerosas moléculas, incluyendo citoquinas, receptores de membrana aislados, moléculas de señalización y material genético. Las vesículas extracelulares (VE) son uno de los mecanismos que median la transferencia de información entre la célula T y las CD. Los cuerpos apoptóticos, los ectosomas y los exosomas son las principales vesículas extracelulares. Los exosomas se distinguen por su origen endocítico puesto que se forman por la invaginación de la membrana de los cuerpos multivesiculares (CMV) o endosomas tardíos. Cuando los CMV fusionan con la membrana liberan estas vesículas al medio. Los exosomas están particularmente enriquecidos en material genético; principalmente ARN, como los ARN pequeños y los ARN largos no codificantes, también se ha detectado presencia de ADN genómico. Esto los hace versátiles mediadores en la comunicación intercelular. No obstante, todavía queda mucho por explorar en los mecanismos de cómo el material genético contenido en los exosomas induce respuestas específicas en las células receptoras.

En este trabajo hemos demostrado que las células T secretan VE cargadas de proteínas y ADN mitocondrial (ADNmt) que pueden ser transferidas a las CD a través de la sinapsis inmune. Evidenciamos que algunas proteínas de origen mitocondrial y el ADNmt se encuentran en los cuerpos multivesiculares y que el bloqueo de la secreción de exosomas altera la función y morfología mitocondrial, lo que sugiere que la liberación de contenido mitocondrial mediado por los exosomas contribuye a la homeostasis mitocondrial. También demostramos que tanto las proteínas mitocondriales como el ADNmt se transfieren durante la SI de forma unidireccional desde la célula T a la CPA y que esta transferencia pre-activa a las células dendríticas protegiéndolas en infecciones virales posteriores. En conclusión, los datos resultantes ilustran un nuevo mecanismo por el cual las células T promueven un estado de alerta en las células dendríticas promovido por la transferencia exosomal de ADN. Estos hallazgos aportan información relevante sobre cómo la comunicación recíproca entre las células del sistema inmune innato y del sistema inmune adaptativo facilita respuestas más eficaces frente a patógenos.

Summary

The generation of a specific immune response against a pathogen requires the initial interaction of an antigen-specific T cell with antigen-presenting cells (APCs), specifically dendritic cells (DCs). T cell recognition of major histocompatibility complex (MHC) bound to antigens leads to the formation of a stable intercellular junction between the cells, the immune synapse (IS). In T cells the IS involves a redistribution of membrane-associated receptors, the cytoskeleton, and the polarization of intracellular trafficking and secretory organelles. The transfer of bioactive molecules from the T cell to the DC through the IS constitutes a main vehicle of intercellular communication. T cells and DCs exchange numerous molecules, including cytokines, membrane receptors, membrane patches, signaling molecules or genetic material (mainly functional microRNAs) during IS formation. Extracellular vesicles are one of the cellular mechanisms mediating information transfer between the T cell and the DCs. EVs comprise apoptotic bodies, ectosomes or microvesicles, and exosomes. Exosomes are distinguished by their unique endocytic origin. Exosomes form by invagination of the multivesicular body (MVB) membrane and are released to the extracellular medium upon the fusion of the MVB with the plasma membrane. Exosomes are particularly enriched in genetic material, mostly RNA species such as small RNAs and long non-coding RNAs, as well as DNA. This makes them attractive candidates to mediate cell-to-cell communication. However, the ability of the genetic material contained within exosomes to evoke immune signaling responses in recipient cells is largely unexplored.

Our data show that T cells secrete extracellular vesicles containing mitochondrial DNA (mtDNA) and mitochondrial proteins that can be transfer to the APC through cognate interactions. We provide evidence that mtDNA and related proteins segregate into MVB pathway. Blockage of exosome secretion alters mitochondrial function and morphology which suggests that release of mitochondrial content loaded into exosomes contributes to mitochondrial homeostasis. In addition, we demonstrate that both mitochondrial proteins and mtDNA are transferred during IS in a unidirectional way from the T cell to the APC.

Finally, our results show that T cells prime DCs through the transfer of exosomal DNA, supporting a specific role for antigen-dependent contacts in conferring protection to DCs against subsequent viral infections. In conclusion, our data illustrate a way by which T cells promote an alert state in DCs that protects them against posterior infection driven by the vesicular transfer of DNA. These findings shed new light on how the reciprocal communication between innate and adaptive immune cells allow efficacious responses to unknown threats.

Index

Index

List of Abbreviations

List of Abbreviations

8-OHdG	8-hydroxy-2' -deoxyguanosine
ADAP	adhesion and degranulation promoting adapter protein
APC	Antigen presenting cells
ATAD3	ATPase family AAA domain-containing protein 3
BCR	B Cell Receptor
BMDC	Bone marrow-derived dendritic cells
ChIP	Chromatin Immunoprecipitation
COX1	Human Complex IV subunit I
cSMAC	Central supramolecular activation cluster
CTVT	Transmissible canine venereal tumor
Cx43	Connexin 43
DAG	Diacylglycerol
DAMPs	Damage-associated molecular pattern
DC	Dendritic cells
EE	Early endosome
ER	Endoplasmic Reticulum
ESCRT	Endosomal sorting complex required for transport
EV	Extracellular Vesicles
FCCP	carbonilcyanide p-triflouromethoxyphenylhydrazone
GO	Gene Ontology
GTPase	guanosine triphosphate hydrolase
HGT	Horizontal gene transfer
Hrs	Hepatocyte growth factor-regulated tyrosine kinase substrate
ICAM-1	Intercellular Adhesion Molecule 1
IFNγ	Interferon gamma
ILV	Intraluminal vesicles
IP3	Inositol trisphosphate
IRF3	Interferon regulatory factor 3
IS	Immune Synapse
ISEV	International Society of Extracellular Vesicles
ISG	Interferon-stimulated gene
LBPA	Lysobisphosphatidic Acid
Lck	lymphocyte-specific protein tyrosine kinase
LE	Late endosome
LFA-1	Lymphocyte function-associated antigen 1
MDV	Mitochondrial derived vesicle
MERCs	Mitochondria and endoplasmic reticulum contact sites
MHC	Major histocompatibility complex
miRNA	micro RNA

MSC	Mesenchymal stem cells
mtDNA	mitochondrial DNA
mtExo	mitochondrial-containing extracellular vesicles
MTOC	Microtubule-organizing center
MVB	Multivesicular Bodies
NF-κB	nuclear factor κB
NFPs	N-formyl peptides
NMII	non-muscle myosin
nPKC	Protein kinase C isoforms
nSMase2	neutral sphingomyelinase 2
OXPHOS	oxidative phosphorylation
PA	Phosphatidic acid
PAMPs	Pathogen-associated molecular patterns
PC	Phosphatidylcholine
PCR	Polymerase chain reaction
PIP2	Phosphatidylinositol 4,5 bisphosphate
PKC- ε	Protein kinase C epsilon
PKC- η	Protein kinase C eta
PKC- θ	Protein kinase C theta
PLCγ1	Phospholipase C, gamma 1
PLD	Phospholipase D
PLP	Proteolipid
pMHC	peptide-bound MHC
pSMAC	Peripheral supramolecular activation cluster
RLC	Regulatory light chain
ROS	Reactive oxygen species
S1P	sphingosine 1-phosphate
SEE	Staphylococcal enterotoxin superantigen E
SMS2	Sphingomyelin Synthase 2
SphK2	sphingosine kinase 2
SSBP1	Single-stranded DNA-binding protein
StingGt/Gt	Sting deficient mice
TCR	T cell surface receptor
TEM	Tetraspanin-enriched domains
Tfam	Mitochondrial transcription Factor A
TIRF	Total internal reflection fluorescence
TLR	Toll-like receptor
TNTs	Tunneling nanotubes
Tsg101	tumor susceptibility gene
WB	Western Blot

Introduction

Introduction

The immune system is a highly specialized compartment that protects individuals against pathogens and external threats. Immune responses act through cell-based mechanisms to protect the organism against self and non-self menaces. When fighting against pathogens, two different branches of immune populations are involved: innate and adaptive. Innate and adaptive immunity components are independent and derive from different lineages. Innate subset is the first barrier of defense and it is specialized in responding against conserved types of molecules that are common to many pathogens, called pathogen-associated molecular patterns (PAMPs). The adaptive subset mounts a specific response to a particular antigen of a pathogen; by contrast with the innate response, the adaptive is slower and requires activation, clonal selection and expansion. Adaptive immunity is responsible for the generation of memory cells that will reactivate and respond faster upon reinfection. In order to trigger a strong and coordinated response against pathogens, the collaboration between both compartments is essential.

The adaptive compartment is formed mainly of B cells, mediators of the humoral immunity and T cells, mediators of the cellular immunity. Both cell types express cell surface receptors that allow them to recognize the antigens. B cells express the BCR (B Cell Receptor) and T cells express the TCR (T cell surface receptor). The TCR can recognize specific, processed peptides on the context of the major histocompatibility complex (pMHC) molecules. All nucleated cells express MHC class I (MHC-I) molecules bound to self-antigens on their surfaces and T cells are trained to tolerate them. In case of infection, cells present pathogenic antigens bound to MHC-I molecules and specialized cyototoxic CD8 T cells recognize with avidity the complex and terminate the presenting cell through cytolysis. On the other hand, professional antigen presenting cells (APC; such as dendritic cells) from the innate compartment express not only MHC-I but also MHC-II, which presents processed antigens from phagocyted proteins. CD4 T cells can recognize pathogenic peptides presented on the context of MHC-II and mount a specific response against them. Moreover, APCs are able to cross-present phagocyted antigens in MHC class I and activate CD8 responses [1].

In this context, the intercommunication between the adaptive and the innate compartments is evident. Adaptive T cells receive input from innate cells, e.g. dendritic cells, through well-delineated cell-cell contacts, appropriately known as Immune Synapses (IS).

1. The Immune Synapse

The cognate interaction between lymphocytes and APCs is performed through a highly specialized structure called the IS. The IS acts as a platform for intercellular communication; signals coming from this close interaction can modulate the final outcome of cells involved. Even though IS only covers around 20% of a T cell surface when stabilized, it involves an important rearrangement of proteins and organelles in both cell sides [2]. The formation of the IS requires the close contact of the T cell membrane and the APC membrane. Recognition of an antigenic peptide-bound MHC (pMHC) by the T cell receptor (TCR) induces IS stabilization. Other adhesive contacts contribute to the stabilization of the IS, e.g. integrin adhesion receptors and co-stimulatory receptors, such as CD2 or CD28 [3].

TCR receptors appear in the microvilli of resting T cells, enabling them to scan the surface of the APC in rapidly occurring cell contacts **(Figure I1 A)** [4,5]. Once the peptide is recognized, the area of contact is immediately enlarged, allowing firm adhesion through LFA-1 and ICAM-1 interaction. ICAM-1 rapidly accumulates at the interface between the T cell and the APC upon antigen recognition **(Figure I1 B)** [6]. This interaction and the conformation of LFA-1 is relevant to organize the actin cytoskeleton underneath the plasma membrane, which sustains cell-cell contacts[7,8].

The mechanisms that trigger TCR activation and accumulation at the IS include conformational changes in the αβTCR and associated CD3 complex (TCR/CD3); aggregation of receptors forming nano- and micro-clusters; and segregation by spatial constrictions through binding of partner receptors in cis and trans, cytoskeletal connections or by ectodomain-size spatial exclusion [9].

Receptors have been proposed to move through the T cell surface by passive lateral diffusion or directional actin dynamics once the TCR recognizes the pMHC. The ability of the actin cytoskeleton to cluster different receptors enables T cell activation upon engagement of low affinity TCRs by a few MHC complexes [10]. However, the possibility of TCR signaling without IS rearrangement makes clear that TCR signaling precedes the formation of the IS [11] **(Figure I1 B)**.

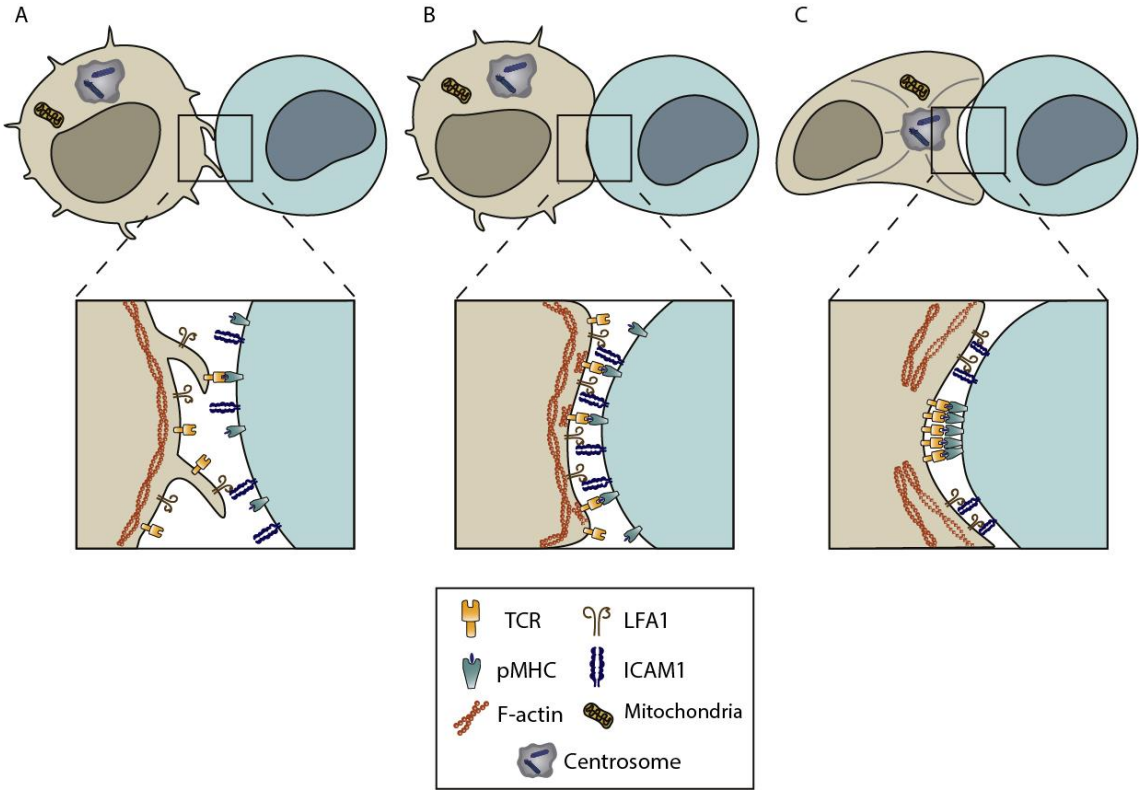

Figure I1. Establishment of an immune synapse. A) The initial interactions between a T cell (left) and an antigen-presenting cell (APC, right) involve the contact of microvilli formed on the surface of the T cell with the APC surface. Integrins such as LFA-1 may contact their ligands (mainly ICAM-1) on the APC. **B)** TCR complexes on the microvilli will engage with antigen-MHC complexes on the APC upon antigen is recognition; the contact expands through the surface of the T-APC. The interaction between LFA-1 and ICAM-1 will be reinforced by TCR signaling, apposing together the T cell and the APC. **C)** Mature immune synapse; receptors will reorganize in different regions directed by the cytoskeleton dynamics, which also shows a polarized distribution.

TCR/CD3 is translocated into specific lipid rafts where it is activated by Lck [12]. TCR in lipid rafts engage with pMHC complexes; if these interactions are productive, TCR microclusters and their associated molecules migrate from the periphery to the center of the IS [13], shaping the so-called central supramolecular activation cluster (cSMAC) where receptors are internalized and recycled [14,15]. This movement is coupled to the retrograde flow of the F-actin [15], the contraction of actomyosin-II arcs [16], and the presence of myosin IIA [17].

On the other hand, classic adhesion molecules maintain the interaction between cells forming the peripheral SMAC (pSMAC), which is highly enriched in integrins such as LFA-1 and ICAM-1 on the T cell and APC respectively **(Figure I1 C)** [3,18]. In this regard, the number of pMHC needed for TCR activation may be as small as one [19]. The formation of clusters of MHC-II and ICAM-1 on the APC helps the localization of TCR and LFA-1 at the T cell side of the IS, respectively, decreasing by 100-fold the threshold of TCR activation and shaping the IS properly [20–22].

The minimal duration of interactions to elicit a proper T cell response is still under debate; however, the establishment of a classical immune synapse does not seem to be essential for a durable interaction, as a dynamic kinapse would be sufficient to activate the T cell [23]. Formation of the SMACs is not specifically needed to observe full T cell activation, but the organized shape of the IS improves signaling by positioning properly the different components at the IS, such as receptors, cytoskeleton and organelles [24,25].

1.1 Organelle polarization in T cell during the Immune Synapse

The reorganization of the cytoskeleton is essential to control the dynamic polarity of organelles and the cell shape at the IS. Actin and Tubulin cytoskeleton act coordinately in order to distribute properly organelles and receptors[25]. Actin cytoskeleton rearranges sequentially underneath the immunological synapse upon TCR activation. It includes the whole cell cytoskeleton and not only the cortical actin beneath the membranes [26]. F-actin plays a role in the distribution of receptors and integrins, and it also controls the proper fusion and secretion of the vesicles at the cSMAC [27]. On the other hand, microtubules relocate the required cellular compartments to the immune synapse, therefore guiding vesicles and organelle movement. Tubulin cytoskeleton rearrangement relies on the polarization of the T cell centrosome, a microtubule-organizing center (MTOC) [28].

The polarization of the MTOC to the immune synapse enables the translocation of specific organelles and the directional secretion towards the antigen-presenting cell [29–31].

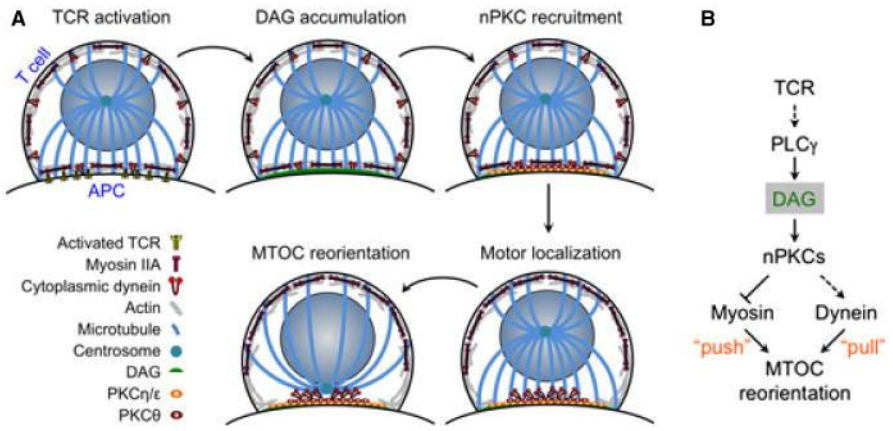

Figure I2. Mechanisms of MTOC reorientation to the IS. A) Upon TCR activation, DAG accumulates at the synaptic surface. DAG recruits nPKC which leads to the polarization of the MTOC through Myosin and Dynein motors. **B)** Schematic diagram of MTOC polarization towards the IS surface, solid arrows denote direct connections, and dotted arrows denote either indirect or multistep connections. Figure from Huse et al. 2015 [32].

CD3 phosphorylation by Lck, activates a downstream cascade[33,34] that ends in the recruitment of PLCγ1 into the cSMAC [25,35]. PLCγ1 hydrolyzes phosphatidylinositol 4,5 bisphosphate (PIP2) into inositol trisphosphate (IP3) and diacylglycerol (DAG). DAG accumulates preferentially at the center of the immune synapse [36]. Centrosomal movement is thus guided by a gradient of diacylglycerol at the IS **(Figure I2)** [37]. MTOC translocation by a DAG gradient is partially explained by the recruitment of different PKC isoforms containing DAG-specific C1 domains. Specifically, PKC-ε and PKC-η, which have redundant recruitment functions, accumulate in a broad area of the membrane. PKC-θ is also required for MTOC reorientation and is synergistically recruited with DAG [38]. Motor proteins are involved in MTOC reorientation. Hence, dynein reorients the MTOC during cognate interaction as it moves along the microtubules from the plus end to the minus end. It accumulates at the immune synapse together with ADAP, therefore connecting the motor to LFA-1 clusters [39]. Impairment of dynein-dynactin complex activity inhibits MTOC translocation after TCR antigen priming [28]. PKC isoenzymes also shape the positioning of non-muscle myosin (NMII) through direct phosphorylation of the regulatory light chain (RLC), which forms clusters behind the MTOC and probably pushes it from behind while dynein would pull from the center of the synaptic region, to move the MTOC [40].

The secretory machinery orientates towards the immune synapse in the T cell. Two main intracellular pathways have been described: the Golgi apparatus-Endoplasmic Reticulum (ER) secretory pathway and the endolysosomal system **(Figure I3)**.

1.2 Polarization of secretory machinery: the Golgi-ER pathway

The Golgi-ER secretory pathway is guided towards the synaptic cleft [28,29,41–44], providing directionality to the secretion of some cytokines and signaling mediators. Specifically, IL4 is preferentially secreted by CD4 T cells towards the site of activation [45] and it accumulates at the site of T-B cell synapse together with IL5, IL2 and Interferon γ (IFNγ) after 24 h **(Figure I3-1)** [31]. In the Golgi-ER secretory pathway, the CD3-TCR complexes are synthetized and retained, which conforms a TCR reservoir ready to be released and engaged to induce activation. These complexes assemble properly and progress through the secretory pathway; the vesicles containing these complexes fuse with the plasma membrane and TCR/CD3 complexes form microclusters and traffic continuously between plasma membrane and endosomes in rapid cycles and can be eventually degraded by lysosomal fusion **(Figure I3-2)** [46] .

As previously mentioned the second secretory pathway polarized towards the immune synapse is the endolysosomal system; specifically, receptors and proteins from the membrane are endocytosed and recycled. TCR signaling and function not only depend on its expression but also on its membrane localization and the dynamics of TCR-CD3 complex, including its recycling into vesicles. The degradation of the TCR is important for synapse termination and its downstream signaling. Upon TCR engagement, endosomal trafficking is redirected towards the immune synapse by microtubules and endosomal traffic regulators such as vesicle transport proteins, docking proteins, and fusion regulatory molecules [47–51]. TCR activation triggers its rapid uptake through a clathrin-dependent pathway, and it is then incorporated into a flotillin-positive endocytic network, which is essential for the correct recycling of the TCR to the membrane again [52]. A complex framework of endosomal vesicles fine-tunes the T cell response beneath the synaptic cleft membrane, by exposing, hiding or degrading receptors and signaling molecules **(Figure I3-3)**.

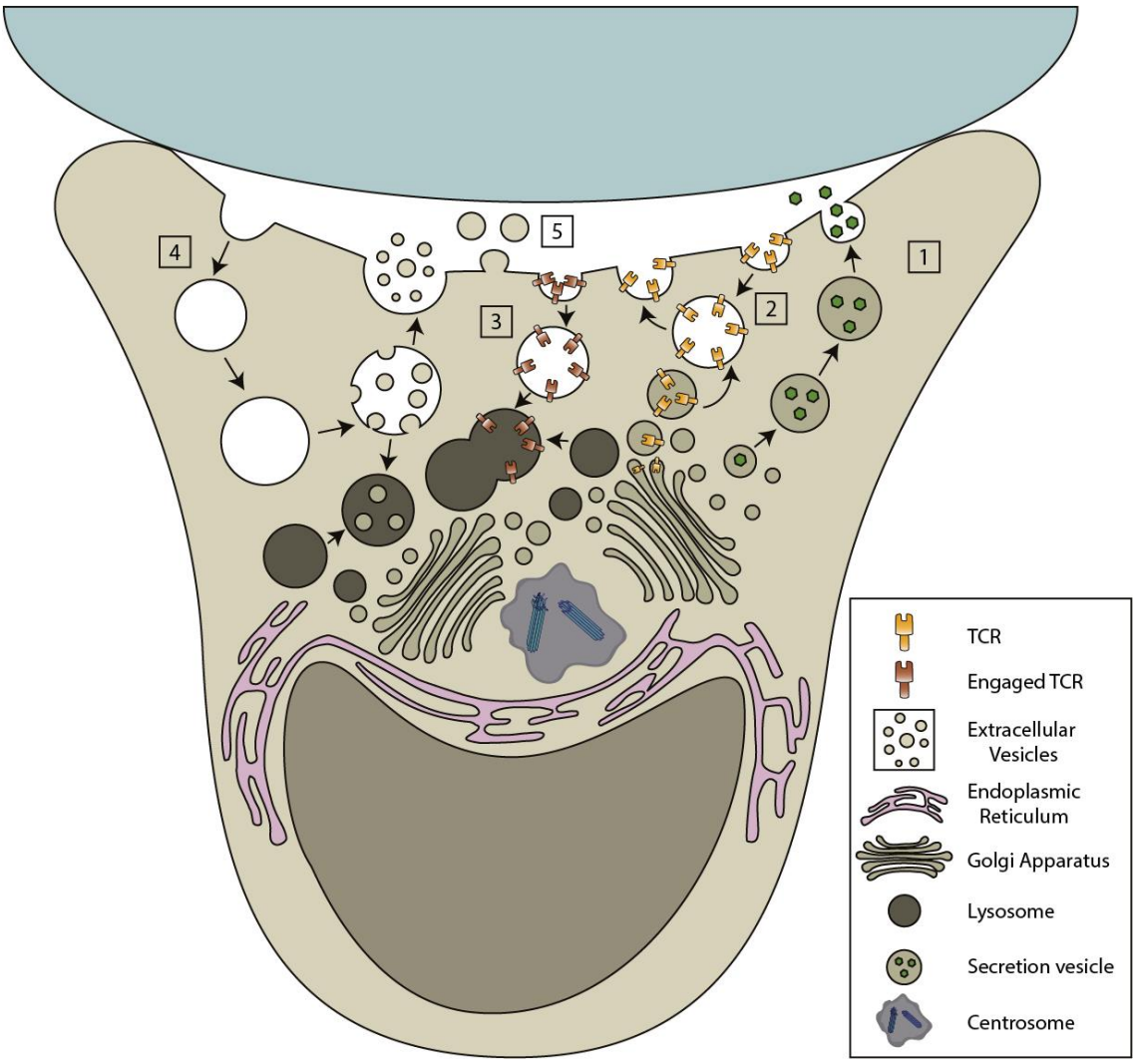

Figure I3. The secretory and recycling pathways at the Immune Synapse. The secretory machinery of the T cell is actively polarized towards the T cell-APC contact by the movement of the centrosome and the coordinated action of molecular motors. (1) The ER-Golgi dependent pathways direct their vesicles towards the immune synapse to deliver newly synthetized adhesion and signaling receptors and soluble mediators such as chemokines and cytokines. (2) TCR-CD3 complexes (orange) cycle between membrane and endosomes in a steadystate loop. Some CD3-TCR complexes are synthetized in excess and retained in the Golgi (3) T Cell Receptor molecules (red) are internalized at the central area of the T cell-APC contact; they can be degraded or recycled through the endolysosomal pathway. (4) Multivesicular bodies (MVB) are formed from the endosomes, through specific sorting of their components. MVB can deliver their content into the immune synapse cleft, as extracellular vesicles (i.e.: exosomes) or soluble components. Viruses can use this pathway to spread into APCs. (5) Ectosomes can be formed, excised and released from the plasma membrane to the IS cleft.

1.3 Polarization of multivesicular bodies and exosomes biogenesis

Another level of complexity includes the role of late endosomes (LE), also called multivesicular bodies (MVB). These organelles are enriched in specific proteins and may form part of the cell recycling system by fusing with lysosomes to degrade their content. On the other hand, they can also serve as secretory organelles, by fusing with the plasma membrane and releasing its content to the extracellular media [53,54]. In T cells, MVB reorient towards the immune synapse and release there their content [55,56].

MVB are part of the endolysosomal system. Upon endocytosis early endosomes (EE) are formed and these vesicles can be recycled back to the plasma membrane either by direct fusion or through the recycling of the endosome compartment. Proteins from EE can also be sorted into vesicles that maturate into MVB/LE [57]. There is a specific selection of proteins that progress through the maturation of the endosomes and protein cargo composition can vary along the maturation process. Cytosolic proteins associate with endosomes and define its function and destiny. Rab5 associates in the first steps of EE formation[58] and it is the main regulator of the conversion to LE. A crucial step for endosome maturation is the Rab5/Rab7 switch; Rab5 recruits Rab7 to the EE and it is replaced by this GTPase which assumes its functions of protein recruitment and fusion with other LE[59]. Absence of Rab7 activity results in loss of lysosomal acidification and functionality, dispersal of endosomes and a block in cargo trafficking to the lysosomes [60]. On the other hand, Rab7 constitutively active mutant (Rab7Q67L) expression leads to the fusion of LE and the formation of larger vesicles that are not restricted to the perinuclear area [61].

Endosomes are motile organelles that change their subcellular localization along its maturation process and function. The number, size and intracellular position of endosomes are not determined randomly but are tightly regulated [62]. The flux of maturation is a centripetal movement; it goes from the cell periphery to the perinuclear area, where the majority of lysosomes are localized **(Figure I4)**. The motor proteins responsible for endosomal trafficking along microtubules are dynein and kinesin [63–67]. Endosomes can directly interact with motor proteins or by its indirect binding mediated by dynactin acting as a scaffold which depends on Rab7 activity[68,69].

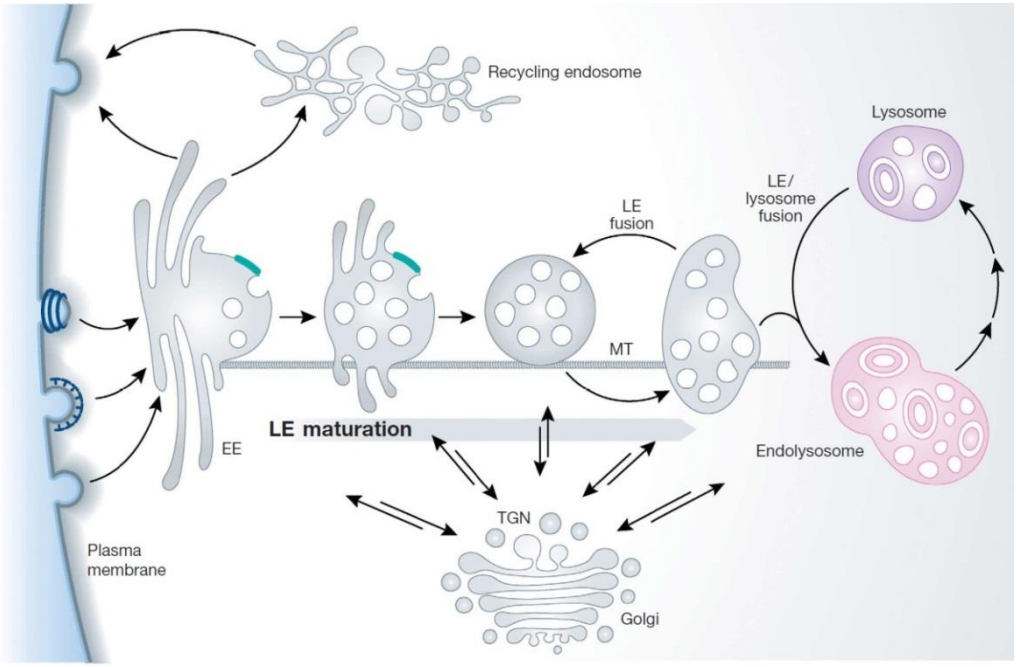

Figure I4. Endolysosomal system. Early endosomes (EE) are formed by the invagination of the plasma membrane. Proteins from EE can cycle back directly to the plasma membrane or through recycling endosomes. Early endosome maturate into late endosomes (LE)/MVB. These vesicles move towards the perinuclear space along microtubules (MT). This compartment combines endocytosed cargo with newly synthetized proteins from the Trans Golgi Network (TGN). They also load proteins from the cytoplasm through the ESCRT complex. Finally LE/MVB can either fuse with lysosomes and degrade their content or fuse back with the plasma membrane and release their content to the extracellular media. Figure from Houtari and Helenius 2011 [57].

During the process of endosome maturation there is bidirectional traffic between the endosomes and the Golgi apparatus, newly synthetized proteins such as hydrolases feeds the system and end up in the lysosomes maintaining their activity, function and localization **(Figure I4)** [60,70]. In addition, cytoplasmic material can be selectively incorporated into endosomes through the invagination of the endosomal membrane, generating intraluminal vesicles (ILV)[71]. ILVs are small vesicles that are confined inside of MVB, that range between 50-100nm of diameter and that are enriched in proteins and genetic material. It has been proposed that ILV can be formed by different mechanisms, therefore coexisting in the same MVB compartment ILV coming from different origins with different protein and lipid composition. There are three models proposed for endosomal membrane invagination and ILV constitution: the Endosomal Sorting Complex for Transport (ESCRT) proteins machinery, the lipid dependent invagination and the tetraspanin mediated mechanism **(Figure I5)** [72].

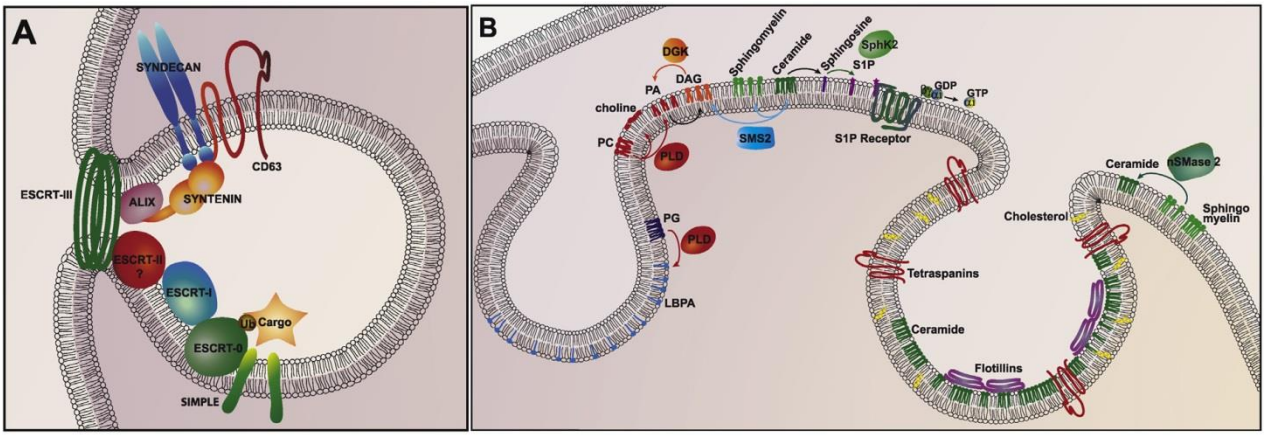

Figure I5. Proposed mechanisms for endosomal membrane invagination. A) ESCRT proteins control the sorting of ubiquitinated proteins into ILV. Syntenin and syndecan are also involved in the ESCRT dependent mechanism [73]. B) Tetraspanin dependent mechanism; CD81, CD9 and CD63 are involved in the formation of ESCRT independent formation of ILV. Lipid-mediated ILV synthesis depends on lipid composition (DAG, S1P, PA, PC, LBPA) and lipid-related enzymes (nSMase2, S1P receptors, SphK2, SMS2, PLD). Modified from Villarroya et al 2014 [72].

The ESCRT recruit other ubiquitinated partner proteins during this process and determine the sorting of different components to ILVs [74]. ESCRT machinery consists in four different protein complexes; ESCRT-0, ESCRT-I, ESCRT-II, ESCRT-III and the Vps4 AAA-ATPase complex [72,75]. Early-endosome-associated proteins such as Hrs (ESCRT-0) recruits ESCRT-I proteins [76] and ubiquitinated proteins [77] to clathrin-coated microdomains of EE which leads to ILV formation. Nevertheless, it is in the late endosome where most of the ILV are formed. Tsg101 is an ESCRT-I protein that has a central role in LE endosome structure, maturation and ILV generation. ESCRT-0/I proteins recruit ESCRT II which in turn recruits and activates ESCRT-III together with the adaptor protein Alix which stabilizes the complex. The energy for bud abscission is provided by the ATPase Vps4 **(Figure I5A)** [78,79].

Membrane-lipid composition is also important for the proper formation of MVB and ILV. Proteolipid (PLP)-containing exosomes are enriched in ceramide and their secretion is not dependent on Hrs, Alix or Tsg101 expression. Ceramide synthesis is mediated by the membrane associated protein neutral sphingomyelinase 2 (nSMase2) which controls exosomes secretion in multiple cell models [55,80–82]. Ceramide-mediated membrane bending and ILV formation is explained by the spontaneous aggregation of lipid microdomains. The coalescence of domains induces a negative curvature in the membrane, probably promoted by the cone-shaped structure of ceramide [80]. Lipid composition can also influence the sorting of ILV cargo and MVB maturation in an ESCRT-independent manner. Gi-coupled sphingosine 1-phosphate

(S1P) receptor is present on endosomal membranes and its sustained activation controls exosomal maturation and cargo sorting through the formation of F-actin networks [83,84]. In addition, sphingosine kinase 2 (SphK2) absence decreases exosomes secretion and cargo loading [83,85] **(Figure I5B)**.

Tetraspanins are highly enriched in ILV membranes, in contrast with other proteins from the MVB such as Lamp1 and Lamp2 [86]. The differential distribution of membrane proteins indicates that it has to be driven by active protein sorting. Tetraspanins form tetraspanin-enriched domains (TEM) and organized membrane dynamics through its association with other transmembrane and cytosolic proteins and lipids[87]. Therefore, tetraspanins are able to influence the cargo sorting; CD9 tetraspanin controls the loading of CD10 metalloproteinase in exososomes by the interaction with its cytoplasmic domain. CD63 tetraspanin controls in melanosomes the loading of PMEL into ILV in an ESCRT independent manner [88,89] **(Figure I5B)**.

Some of these mechanisms described as independent, under physiological conditions, are likely to interact and cooperate producing a mixed population of ILV [72]. For example the deficiency in ESCRT proteins Hrs and Tsg101 decreases the secretion of exosomes containing CD63 and CD81 [90], but still allows MVB to be formed [91]. In addition, the secretion of CD63-positive exosomes from T cells is ceramide-dependent; therefore nSMase2 activity directly affects tetraspanin-containing exosome synthesis [55]. Finally, blockage of an ILV formation pathway usually does not completely abrogate the secretion of exosomes [89]. This piece of evidence points out the existence of heterogeneous populations of MVB and ILV and the complexity of studying these vesicles.

As mentioned above, MVB can either fuse with lysosomes and degrade their content or fuse with the plasma membrane and release its content to the extracellular media; released ILV are better known as exosomes. The mechanisms through which MVB take the degradative pathway or the secretory pathway are still elusive, however there are some molecules described essential for MVB secretion. Rab27 is a small GTPase required for the docking of MVB at the plasma membrane. There are two isoforms, Rab27a and Rab27b, that control different steps of MVB localization, docking and fusion, which are therefore crucial in the exosome secretion pathway [92]. ISGylation, an ubiquitin-like modification, has been proposed as regulatory signal for MVB´s fate. Tsg101 ISGylation promotes MVB fusion with lysosomes and subsequent degradation, impairing exosome secretion [93,94]. Likewise, acetylation also impairs protein sorting into ILV competing for Lysines with the ubiquitination [95]. In B lymphocytes, two pools of MVB can be distinguished and only MVB with high cholesterol levels are able to fuse

with the plasma membrane and release exosomes [96]. In polarized cells, exosomes secreted from the apical and basolateral side contain different cargo and composition implying the existence of distinct MVB pools and secretion mechanisms [97–99]. Transport of MVB to the plasma membrane is dependent on cytoskeleton interactions. Cortactin promotes exosome secretion by stabilizing cortical actin-rich MVB docking sites [100]. In the context of the IS, upon antigen recognition the MTOC relocates close to the interacting area. Dynein/dynactin motor proteins move MVB to the minus-end bringing these organelles near to the plasma membrane, therefore facilitating their fusion and release of its ILV to the synaptic cleft [55].

1.3.1 Exosome cargo

Exosomes contain proteins involved in their biogenesis, vesicle trafficking, lipid membrane organization, as well as proteins and adhesion receptors specific of the producing cell. ESCRT proteins and tetraspanins such as CD63, CD9 and CD81 are found in exosomal fractions [74]. ILV lipids are also different from the limiting membrane of the endosome. ILV contain more cholesterol, sphingolipids and BMP/LBPA, therefore, exosomal lipid content differs from that of the secreting cell [101]. Exosomes are particularly enriched in genetic material, mostly RNA species such as small RNAs and long non-coding RNAs, as well as genomic DNA **(Figure I6)** [102–105]. In addition, it has been reported that some cell lines, such as astrocytes, release exosomes containing mitochondrial DNA [106]. This makes them attractive candidates to mediate cell-to-cell communication. However, the ability of the genetic material contained within exosomes to evoke immune signaling responses in recipient cells is largely unexplored.

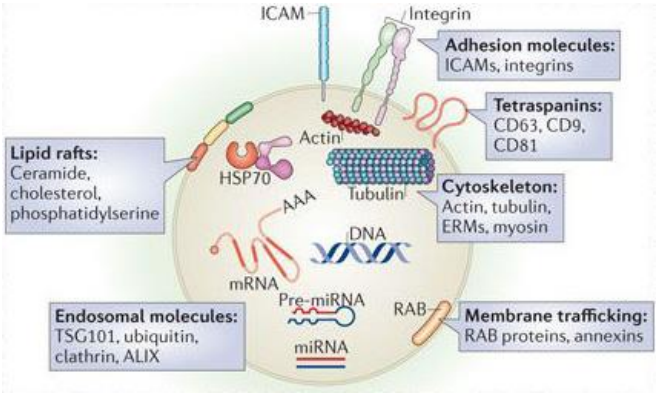

Figure I6. Exosomal components. Lipids present in exosomes include ceramide, cholesterol and phosphatidylserine. Heat shock proteins, actin, tubulin, tetraspanins and proteins from ESCRT complex are usually found in exosomes. Specific repertoires of miRNA and DNA are also loaded in these extracellular vesicles. Figure modified from Mittelbrunn et al 2012 [56]

The specific repertoire of proteins and genetic content in exosomes and its differences in composition with the secreting cell imply the existence of sorting mechanisms that regulate the specific transport of selected RNAs and proteins into the exosomes. Posttranslational modifications are responsible for part of the specificity in cargo sorting [107]. The ESCRT complex is the responsible of sorting ubiquitinated proteins to MVB [108], however, de-ubiquitination is essential for packaging the cargo into the ILV [109]. On the other hand ISGylation tags the proteins for lysosomal degradation and prevents them for being sorted into ILV [94]. Sumoylation also target protein to exosomes [110]. In addition, some miRNA can be sorted into ILV when they are bound to post-translational modified proteins such as sumoylated hnRNPA2B1, which binds specific RNA sequences also called exo-motifs, and transport miRNA to the MVB [111]. Other sequences also target miRNA to MVB. Hence, it has been described an exo-motif that allows the binding of SYNCRIP to the miRNA and sorts it to the MVB in hepatocytes [112]. In addition, miRNA sorting change depending on the cell state proved by exosomal miRNA content variation along cell differentiation and maturation [113]. Another mechanism that could explain miRNA loading is the association of components of miRNA effector complexes and MVB [114], however it is more intriguing the mechanisms of exosomal loading of genomic and mitochondrial DNA since those organelles are separated by several membranes from MVB. It has been proposed that cytosolic DNA could be loaded due to its interaction with DNA binding motifs of connexin43 (Cx43) present in exosomes [115,116]. Although some of the mechanisms for genetic material sorting into exosomes have been reported, this is still an area boasting many outstanding questions to be solved.

Proteins, RNA and DNA contained in exosomes vary depending on cell status and it can provide information about the pathophysiological status of the secreting cell when exosomes were released. In addition, exosomes can be isolated from body fluids such as blood, urine, saliva, etc. Due to the easiness of exosome purification and the great amount of information that researchers can obtain from these extracellular vesicles (EV), exosomes are potentially regarded as non-invasive biomarkers for early diagnostics and prognostic of certain diseases [117–122].

1.3.2 Extracellular vesicle secretion at the Immune Synapse

Almost every cell type secretes a heterogeneous population of vesicles to the extracellular medium in a constitutive manner although cellular stress or activation signals modulate their secretion [72]. The size of those vesicles range from 40-1000 nm, thus the taxonomy and nomenclature of these extracellular vesicles (EV) is still under debate [123].

Nonetheless, they are classically divided into microvesicles, exosomes and apoptotic bodies, depending on their origin, size and molecular composition **(Figure I7)** [124,125].

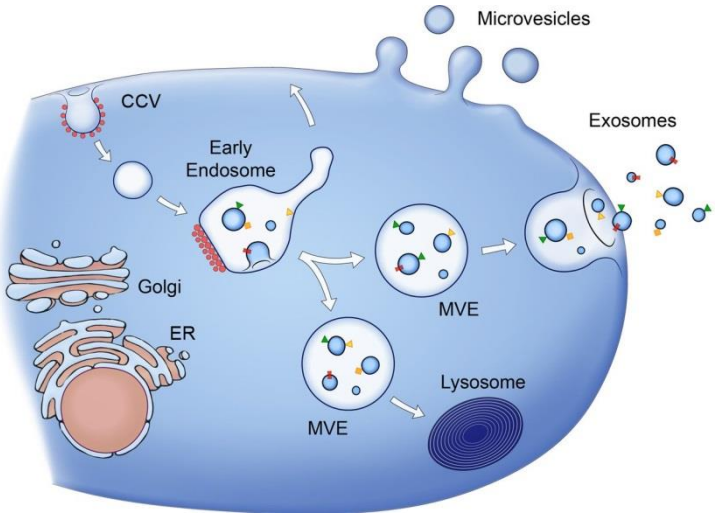

Figure I7. Extracellular vesicle populations. Microvesicles bud directly from the plasma membrane, whereas exosomes have an endocytic origin and are released by fusion of MVBs with the plasma membrane. Figure from Raposo et al 2013 [124]

Immune cells secrete a variety of EVs to the extracellular milieu that can exert diverse immune functions, including antigen presentation, immune activation, induction of tolerance, or suppression of immune responses [126].

At the IS, the MVB external membrane fuses with the plasma membrane to release the ILVs into the synaptic cleft, which are then called exosomes **(Figure I3-4)**. TCR activation can induce the secretion of TCR-TSG101-containing exosomes [127] and lead to proliferation in autologous resting CD8 T cells, acting synergistically with IL2 [128].

These EVs carry proteins and genetic material that are then transferred to recipient cells by using the IS as a focal point for polarized secretion. The uptake of these exosomes facilitates the release of their content into the recipient cells that may modify their behavior. Specifically, the uptake of exosomes loaded with miRNA that are secreted by CD4 T cells in the context of a synapse causes the downregulation of SOX4 in B cells [55]. Viruses (i.e. HIV) are able to hijack the polarized secretory machinery and spread across cells through immune synapses [129,130]. Apart from HIV, other viruses use the exosomal secretory machinery to disseminate [131]. The secretion of larger vesicles that bud directly from plasma membrane, usually called microvesicles or ectosomes has also been described. Upon antigen cognate recognition with the APC, membranes from CD4 T cells start to bud from the cSMAC of the synapse [132] **(Figure I3-5)**. TSG101, located at the cSMAC [133] is the responsible for the sorting of TCR into those EVs, while VPS4, which also belongs to the ESCRT machinery, is the responsible of the scission of the microvesicles from the plasma membrane.

After activation, T cells secrete microvesicles that are loaded with transmembrane-CTLA-4 negative regulator [134]. However, the functional roles of microvesicles containing CTLA-4 needs further investigation.

1.4 Mitochondria reorganization at the Immune Synapse

Mitochondria are dynamic organelles that drive many different functions in cells. They are involved in energy production, constituting a metabolic hub that centralizes the synthesis of many intermediate metabolites [135]. They also play a role in apoptosis, calcium homeostasis and in cell signaling, mediated by ROS production and mtDNA release [136,137]. In T cells, mitochondria are also involved in migration and class differentiation through asymmetric division [138]. Mitochondria also control lysosomal function during inflammatory T cell responses [139]. During IS mitochondria polarize towards the T cell-APC contact and it happens in the T cell [140] and the APC side [141]. In T cells, mitochondria specifically localize around the MTOC at the cSMAC/pSMAC area [41] and once there fuels the IS with local ATP and calcium for proper T cell activation. Mitochondrial enrichment at the IS favors local calcium entry and control the $Ca2^{+}$-dependent activation of transcription factors [140,142,143]. Conceivably, mitochondria move in two phases when polarizing towards the IS: in a first step mitochondria get closer to the IS contact site and in a second one they get distributed and anchored. Although not experimentally proven, mitochondria may follow an initial calcium gradient in a Miro1-dynein dependent manner and accumulate around the polarized MTOC [143–145], which would be a plausible mechanism for mitochondria transport to the IS. TCR engagement is not absolutely required to observe mitochondria accumulation at the T cell-APC area; the initial LFA1-ICAM1 interaction underlies this effect, facilitated by microtubule integrity [146]. Therefore, the increase of calcium flow upon TCR engagement would increase and sustain mitochondria polarization at the IS area, as a second step. This can be achieved through proteins like Miro-1, which links the tubulin and actin cytoskeletons and fine-tunes the mitochondria movement and docking [147]. Miro-1 is a scaffold protein for Myo19, which regulates the subcellular distribution of mitochondria through regulation of long-walks on microtubules and short-walks and anchoring to actin [148]. In this sense, the localization of the centrosome at the IS is prior to mitochondria recruitment, which requires fragmentation by drp1 [41]. The de-localization of the centrosome from the IS through inhibition of dynein/dynactin tubulin-based molecular motor by p50-dynamitin over-expression [28], also prevents mitochondria polarization at the IS [41].

2. Mitochondria horizontal transfer

According to the endosymbiotic theory, mitochondria are derived from eubacteria that engaged in a symbiotic relationship with primitive host cells. They have maintained some of their ancestral bacterial characteristics, such as a double membrane, a proteome similar to the α-proteobacteria, and the ability to generate the majority of ATP from cells in the process of aerobic respiration or oxidative phosphorylation (OXPHOS) [135]. Mitochondria are endowed with their own circular genome, which is 16.6 kb in length in mammalian cells. This mitochondrial DNA (mtDNA) encodes 13 subunits that are essential components of the electron transport chain, and a translational system made of two ribosomal RNAs and 22 tRNAs, required for the translation of these proteins [149]. A typical mammalian cell contains thousands of copies of the mitochondrial genome, which are organized in mtDNA-protein complexes. Tfam protein coats and bends mtDNA in a compact structure known as nucleoid [150]. In mammals, mitochondria and its genome are transmitted to subsequent generations mainly through the maternal lineage. Specific mechanisms regulate the stability and transmission of mitochondria and their genome during germline transmission and somatic cell proliferation [151].

Mitochondria have been recently shown to be horizontally transferred between mammalian cells, challenging current concepts of mitochondria and mtDNA segregation and inheritance. This transfer promotes the incorporation of mitochondria into the endogenous mitochondrial network of recipient cells, contributing to changes in the bioenergetic profile and in other functional properties of recipient cells, not only *in vitro* but also *in vivo*. Moreover, intercellular transfer of mitochondria involves the horizontal transfer of mitochondrial genes, which has important implications in the physiopathology of mitochondrial dysfunction. The intercellular transfer of mitochondria or their components may also result in the initiation of stem cell differentiation, reprogramming of differentiated cells, or activation of inflammatory signaling pathways. The first evidence of functional mitochondrial transfer involved healthy mitochondria from human stem cells rescuing mitochondrial respiration in mitochondria-depleted recipient cells [152]. Cells devoid of intrinsic mitochondrial function by mtDNA depletion through long-term ethidium bromide treatment, do not survive in standard media. However, when these cells were co-cultured with mesenchymal stem cells (MSC) or fibroblasts that donated functional mitochondria, they acquired mitochondria and re-established aerobic respiration. The careful examination of mitochondrial and nuclear DNA polymorphisms in the rescued clones excluded cell fusion as the main mechanism of mitochondrial transfer, also confirming the stem cell origin of the transferred mtDNA [152]. Transfer did not occur through

the passive uptake of mitochondrial fragments or isolated organelles, but rather involved active processes such as the formation of tunneling nanotubes (TNTs) and/or the vesicular transfer of mtDNA or mitochondrial fragments.

Recent evidence strongly supports that mitochondrial transfer does occur in vivo and may be involved in diverse pathophysiological situations, such as tissue injury and cancer progression [153–157]. Mitochondrial transfer from stem cells to lung epithelial cells and endothelial cells is an important mechanism by which MSC exert their protective effects in several animal models of lung diseases. A study demonstrated that transfer of intact mitochondria can contribute to tissue repair in vivo by a mechanism involving connexins and/or extracellular vesicles **(Figure I8).** [155].

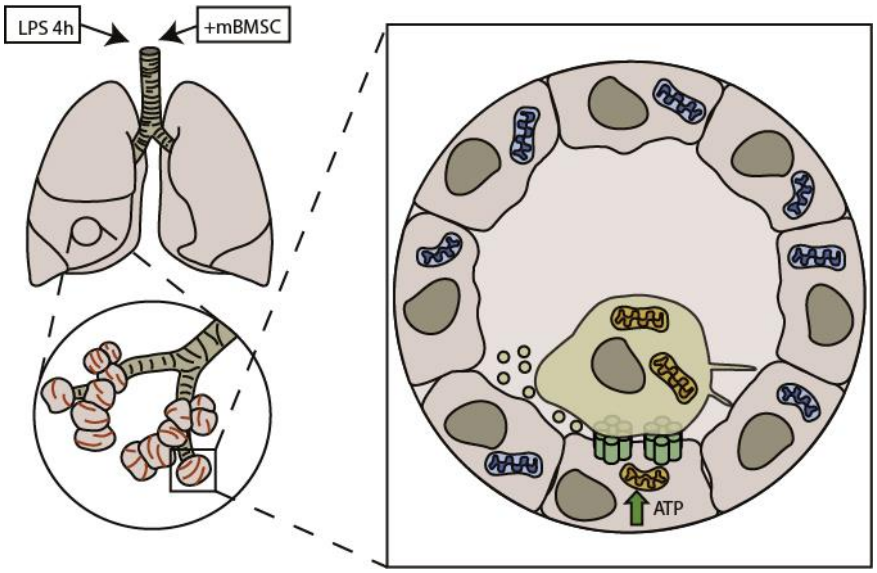

Figure I8. Mitochondrial transfer in a lung disease model. Bone marrow-derived stem cells (BMSC) infused to the trachea of lipopolysaccharides (LPS)-treated mice attached to injured alveolar epithelial cells transfer mitochondria and rescue damaged cells by a mechanism involving connexins and/or extracellular vesicles. Mitochondria acquisition by the alveolar cells triggered the restoration of ATP levels and increased the secretion of pulmonary surfactant. In blue damaged mitochondria, in orange healthy mitochondria.

Cell stress has been proposed as organelle transfer initiator. Mitochondrial transfer is triggered by an almost complete absence of mitochondrial function, such in the case of mtDNA depletion or treatment with mitochondrial inhibitors. Severe damage is necessary to trigger transfer since it is not detected in cells harboring pathogenic mutations that only partially

affect mitochondrial function [158,159]. An intriguing question pertains to the degree of cellular damage required to initiate intercellular transfer of functional mitochondria.

Cells likely possess mechanisms to trigger organelle exchange in response to injury signals emanating from the recipient cell. However, the molecular cues that initiate such crosstalk are still unidentified. Cellular structures that mediate intercellular mitochondrial transfer include TNTs, extracellular vesicles, cell fusion or mitochondrial ejection. Transfer through these diverse structures may result in different functional outcomes for the recipient cells i.e. functional mitochondrial acquisition, immune activation or transmitophagy. The molecular and signaling mechanisms by which cells containing dysfunctional mitochondria acquire mitochondria from other cells and how this process is regulated remain unclear.

Mitochondrial components have been detected in EVs, although the mechanisms by which mitochondrial proteins and mtDNA are loaded in the diverse EVs are still unknown. Exosomes, with a size ranging 40-150 nm, contain genetic material, mostly small RNAs [72], but genomic and mitochondrial DNA have also been detected [103,106,160,161]. Larger EVs can contain entire mitochondrial particles and mtDNA, as observed in mesenchymal stem cells and astrocytes [154,162]. These cells produce EVs with regenerative potential in several tissues under damaging conditions [163–165]. Whether mitochondrial material contained in these vesicles participates in the regenerative potential of stem cells is yet to be shown **(Figure I9)**.

The release of mitochondria or mitochondrial components into the extracellular space has important immune consequences. After an episode of acute injury, release of mitochondrial components into the extracellular medium and bloodstream may trigger potent pro-inflammatory responses. In fact, mitochondrial components can be recognized by cells of the immune system as damage-associated molecular patterns (DAMPs) [166–168]. Different mitochondrial proteins such as TFAM, together with other mitochondrial DAMPs like N-formyl peptides, mtDNA, cardiolipin or extracellular ATP, robustly activate the inflammatory response [169].

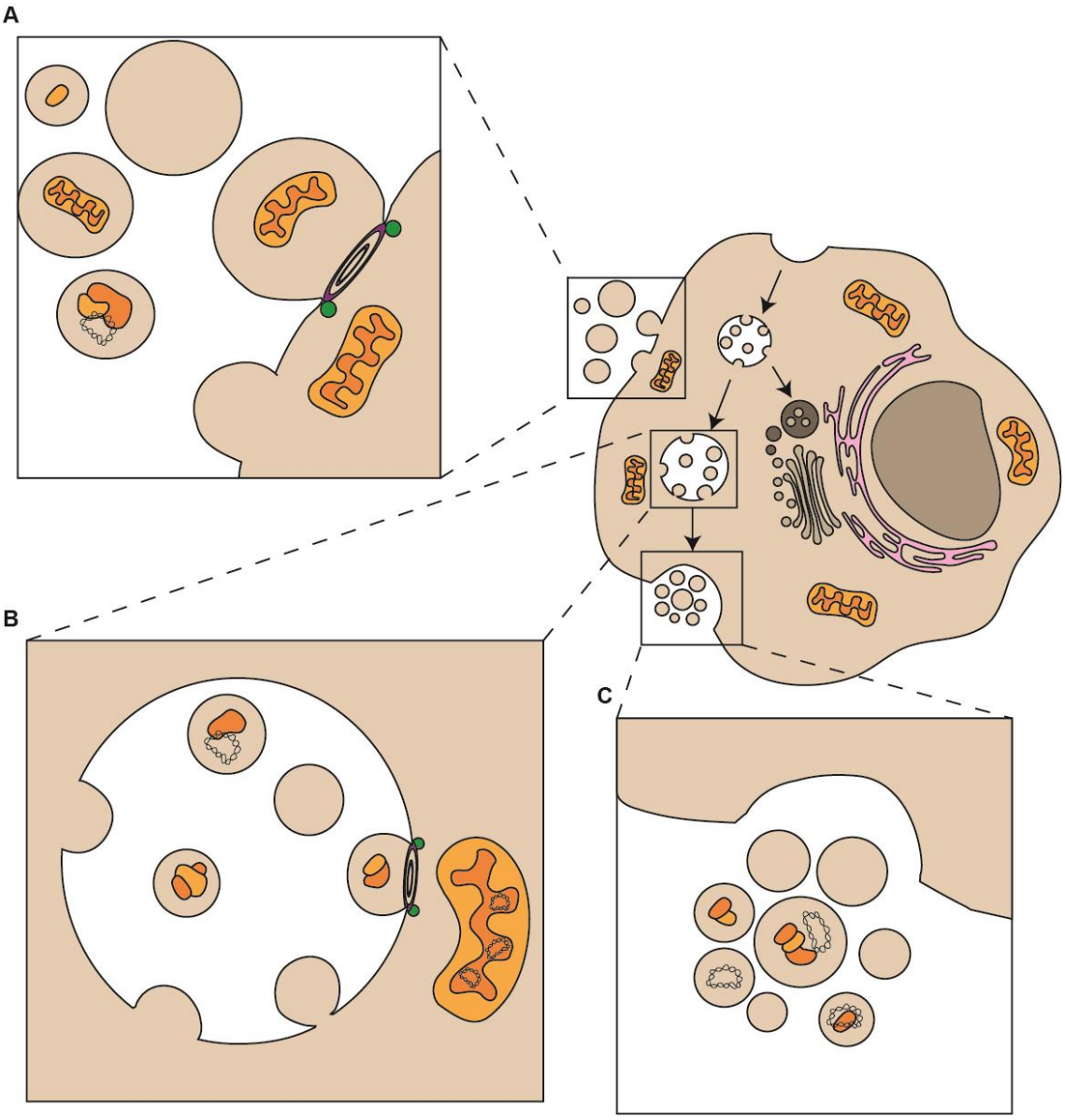

Figure I9. Loading of mitochondrial components in Extracellular Vesicles. A) Microvesicles that shed directly from plasma membrane are very heterogeneous in size and composition. B) The inward budding of MVB forms intraluminal vesicles that are released into the extracellular environment as exosomes, small vesicles from 50-150nm with an endocytic origin. C) Exosome release is achieved through the fusion of the MVB with the plasma membrane. Extracellular vesicles can contain mitochondrial components which include mitochondrial proteins and mtDNA (depicted in yellow and orange). Bigger particles such as microvesicles can be loaded with full functional mitochondria [162].

Mitochondrial DNA induces inflammation when found beyond mitochondrial membrane boundaries [168]. Mitochondrial DNA injected directly into mice joints causes inflammation and arthritis [170]. Moreover, mitochondrial DNA that escapes autophagy leads to Toll-like receptor (TLR) 9-mediated inflammatory responses in a cell-autonomous manner [171]. When abnormally found in the cytosol, mtDNA triggers NRLP3-inflammasome activation and STING-dependent antiviral signaling [167,172], which ultimately leads to cell death. Neutrophils release to the extracellular environment oxidized mitochondrial nucleoids that activate the interferon response in pathological situations such as human systemic lupus erythematosus [173], whereas activated platelets release into the bloodstream entire mitochondria or mitochondria encapsulated in microparticles to boost the inflammatory response [174]. Interestingly, mtDNA released by eosinophils or basophils contribute to inflammatory responses creating DNA net traps to fight against invading pathogens [175,176].

Mitochondria-dependent activation of the inflammatory response is relevant to understand intercellular mitochondrial transfer. In this regard, innate immune cells target cells containing allogenic mtDNA [177]. Such recognition mechanism, displayed by natural killer cells and dendritic cells, is not yet understood, but it is likely to control the extent of intercellular mitochondrial transfer in pathophysiological conditions. As a consequence, careful modulation of immune surveillance mechanisms in recipient cells could be a potential strategy to boost exogenous mitochondrial donation for therapeutic purposes.

Objectives

Objectives

Previous studies have shown that extracellular vesicles, specifically exosomes, are transferred during Immune synapse. T cells secrete exosomes that contain genetic material that can be transferred to the antigen presenting cell. Both the secretory machinery and mitochondria are polarized towards the contact area of the immune synapse upon antigen specific interactions. In addition, whole mitochondria or mitochondrial components can be transferred between contacting cells. Based on this background knowledge we postulate the following hypothesis: *Mitochondrial constituents are transferred through extracellular vesicles during cognate interactions which induces a response in receptor cells*.

In order to challenge our hypothesis, we have addressed 3 main objectives:

1) Dissect the constituents of CD4 T lymphocyte exosomes transferred to dendritic cells during the immune synapse.
    - Analyze the exosomes secreted by CD4 T cells.
    - Study the exosomal proteome of CD4 T lymphocytes.
    - Identification of mitochondrial genome presence in CD4 T cells exosomes.
    - Understand the relation between mitochondrial and endolysosomal compartments.

2) Define the transfer of mitochondrial material during cognate interactions.
    - Analyze the mitochondrial protein constituents transfer from the CD4 T cell to the antigen presenting cell.
    - Elucidation of unidirectional transfer of mtDNA from T lymphocytes to dendritic cells during specific immune interactions.

3) Assess the effect in dendritic cells upon uptake of mitochondrial cargo carried in exosomes from T cells during during immune synapse.
    - Identification of the effects induced by T cell exosomes in dendritic cells
    - Determine the signaling pathway responsible for the antigen presenting cell response
    - Ascertain the effects of exosomal uptake during specific T-Dendritic cell interactions.

Material and Methods

Materials and Methods

Reagents and antibodies

Antibodies used are indicated in the table below:

Antibody	Manufacturer	Catalog number	Application and dilution
anti-human CD63	Calbiochem	OP171	WB (1:1000)
anti-human CD81 5A6	Santa Cruz	sc-23962	WB (1:500)
anti-human TSG101	Abcam	Ab83	WB (1:1000)
anti-GFP	Clontech	632381	WB (1:2000)
anti-TFAM	Abcam	ab47517	WB (1:500)
anti-HRS	Abcam	ab72053	WB (1:500)
anti-COX1	Invitrogen	459600	WB (1:1000)
anti-VDAC1	Abcam	ab14734	WB (1:1000)
anti-Cyt C	Abcam	ab110325	WB (1:1000)
anti-LC3	Cell Signaling	2775S	WB (1:1000)
anti-MnSOD	Enzo Life Sciences	ADI-SOD-110	WB (1:1000)
anti-ATAD3	Abnova	H00055210-D01	WB (1:1000)
anti-Tubulin	Sigma	T6199	WB (1:2000)
anti-nSMase2	RD System	MAB7184	WB (1:1000)
anti-Rab27a	RD System	AF7245	WB (1:1000)

Secondary antibodies used are indicated in the table below:

Antibody	Manufacturer	Catalog number	Application and dilution
anti-mouse peroxidase	Thermo Scientific	31430	WB (1:5000)
anti-rabbit peroxidase	Thermo Scientific	31460	WB (1:5000)

For immunofluorescence and flow cytometry the following antibodies were used:

Antibody	Manufacturer	Catalog number	Application and dilution
anti-CD63 Tea 3/18	Generated in the laboratory		IF (1µg/ml)
anti-HRS	Abcam	ab72053	IF (1:200)
anti-EE1A	Santa Cruz	sc-137130	IF (1:200)
anti-LBPA	Tebu-Bio	ML062915-21	IF (1:200)
anti-Ceramide	Sigma	C8104-50TST	IF (1:200)
anti-8 hydroxyguanosine	Abcam	ab62623	IF & Cyt (1:500)
anti-DNA AC-30-10	Progen	61014	IF & Cyt (1:50)
anti-Tmem173/Sting	Proteintech	19851-1-AP	IF (1:100)
anti-SSBP1	Novus Bio	NBP1-80720	IF (1:200)
anti-CD69	BD Pharmigen	552879	IF & Cyt (1:200)

Secondary antibodies used are indicated in the table below:

Antibody	Manufacturer	Catalog number	Application and dilution
GAM-488/568/647	Invitrogen	# A-11001	IF & Cyt (1:500)
GAR-488/568/647	Invitrogen	# A-11034	IF & Cyt (1:500)
DAG-488/568/647	Invitrogen	# A-11055	IF & Cyt (1:500)

Cells

Human cells

Human T lymphoblasts were isolated from buffy coats obtained from healthy donors by separation on a biocoll gradient (Biochrom). After 30 min of adhesion at 37 °C, non-adherent cells were cultured in RPMI (Gibco) for 2 days in the presence of 5 µg/ml phytohemagglutinin (PHA) to induce lymphocyte proliferation. T lymphoblasts were maintained by addition of IL-2 (50 U/ml) to the medium every 2 days over 8-10 days. For T lymphoblast restimulation, cells were incubated overnight with 50 ng/ml PMA and 750 ng/ml ionomycin.

Human peripheral blood mononuclear cells (PBMC) were isolated from buffy coats obtained from healthy donors by separation on a Lymphoprep gradient (Nycomed, Oslo, Norway) according to standard procedures. Buffy coats of healthy donors were received from the Blood Transfusion Center of Comunidad de Madrid, and all donors signed their consent for the use of samples for research purposes. All the procedures using primary human cells were approved by the Ethics Committee of the Hospital Universitario de la Princesa. Monocytes were purified from PBMC by a 30 min adherence step at 37°C in RPMI supplemented with 10% fetal calf serum. Non-adherent cells were washed off and the adhered monocytes were cultured in RPMI, 10% FCS containing IL-4 (10 ng/ml, R&D Systems Inc, Minneapolis, MN USA) and GM-CSF (200 ng/ml, Schering-Plough, Madrid, Spain). Cells were cultured for 6 days, with cytokine re-addition every other day, to obtain a population of immature hDC.

The human Jurkat-derived T cell line J77 E6.1 (TCR Vαl. 2 Vβ8) (from NIH AIDS reagent program) and the lymphoblastoid B cell line Raji (Burkitt lymphoma) (from ATCC, CCL-86™) were cultured in RPMI (Gibco) containing 10% FBS. Stable cell line clones overexpressing CD63-GFP were generated by transfection and selection with G418 (1 mg/ml, Sigma).

HEK293T cells (from ATCC, CRL-3216™), were cultured in DMEM (Gibco) containing 10% FBS. For colocalization experiments HEK293T cells were treated with 1µM FCCP 4 h (low dose), then washed and immediately fixed with PFA 6%. HEK923T cells were used as a bona-fide cell factory for exogenous protein synthesis and organelle compartmentalization.

Cells were regularly tested for mycoplasma contamination by PCR.

Mouse strains

Mice were housed under specific pathogen-free conditions at the Centro Nacional de Investigaciones Cardiovasculares Carlos III (CNIC), and experiments were approved by the CNIC Ethical Committee for Animal Welfare and by the Spanish Ministry of Agriculture, Food, and the Environment. Animal care and animal procedures license were reviewed and approved by the local Ethics Committee for Basic research at the CNIC Ethical Committee for Animal Welfare and the Organo Encargado del Bienestar Animal (OEBA) del Gabinete Veterinario de la Universidad Autonoma de Madrid (UAM). C57BL/6JOlaHsd (or C57BL/6), C57BL/6 OT-II, C57BL/6JOlaHsd with NZB mtDNA (or C57BL/6 NZB) and C57BL/6NZB OT-II mice were bred under specific pathogen-free conditions at the CNIC (Madrid, Spain) in accordance with European Union recommendations. The C57BL/6JOlaHsd strain does not harbour the nicotinamide nucleotide transhydrogenase (NNT) spontaneous mutation that renders the encoded enzyme undetectable, and which is characteristic of the C57BL/6J strain provided directly by Jackson Laboratories. C57BL/6 NZB OT-II mice were obtained by backcrossing C57BL/6 OT-II transgenic males with C57BL/6 NZB females. *Sting*$^{Gt/Gt}$ (STING-deficient) mice were provided by Dr. Gloria González Aseguinolaza, Gene Therapy and Regulation of Gene Expression Program, Center for Applied Medical Research, Health Research Institute of Navarra (IdisNA), Pamplona, Spain. These mice have a single nucleotide variant (T596A) which is a null mutation resulting in failure to produce STING protein[178]. *Irf3*$^{-/-}$ mice were kindly provided by Prof. Adolfo García Sastre, Icahn School of Medicine at Mount Sinai, New York, USA.

Mouse cell isolation, differentiation and activation

CD4^{+} T cells were obtained from spleen-cell suspensions obtained from C57BL/6 OT-II transgenic mice. Splenic cells were incubated for 30 min at 4ºC with a biotinylated anti-CD4 antibody (BD Pharmingen) followed by extensive washing with PBS, 1% BSA, 5 mM EDTA. Cell suspensions were then incubated for 20 min at 4ºC with streptavidin microbeads (MACS; Miltenyi Biotec) and washed with PBS, 1% BSA, 5 mM EDTA. CD4^{+} T cells were obtained by positive selection using the auto-MACS Pro Separator (Miltenyi Biotec).

Bone marrow-derived dendritic cells (BMDCs) were obtained either from C57BL/6, C57BL/6^{NZB}, Sting$^{Gt/Gt}$ or *Irf3*$^{-/-}$ mice by incubating primary bone marrow cells for 9-10 days in RPMI (Gibco) supplemented with 20 ng/ml recombinant GM-CSF (ImmunoTools) and 1% sodium pyruvate, 50 U/ml penicillin, 50 µg/ml streptomycin, 5×10^{-5} M 2-mercaptoethanol, and 10% FBS (all from Invitrogen).

For T cell blasting, naive $CD4^+$ T cells were isolated from spleen and lymph nodes and cultured for 48 h with 2 ug ml^{-1} concanavalin A (Sigma). Cells were then incubated with 50 U/ml human recombinant IL-2 (Glaxo) every 2 days for at least 7 days to obtain differentiated T lymphoblasts. For antigen-specific restimulation, T lymphoblasts were conjugated with BMDCs and stimulated overnight *in vitro* with 100 ng/ml lipopolysaccharide (LPS) in the presence or absence of 10 µg/ml ovalbumin (OVA) peptide.

Plasmids, interference RNA and cell transfection

The following plasmids were used: mitoDsRed and mitoYFP, (kindly provided by Prof. L. Scorrano, Venetian Institute for Molecular Medicine, Italy), TFAM-GFP and TFAM-DsRED (generated by inserting the human TFAM cDNA into the pEGFP and DsRED plasmids), EGFP-Rab7A Q67L, LC3-GFP and ATG5-GFP (obtained from Addgene: plasmids 28049, 24920 and 22952, respectively), shRNA pLKO control plasmid, shnSMase2 and shRab27a shRNAs (obtained from Open Biosystems), and CD63-GFP [55].

Construct of DNase II with CD63 intraluminal domain: Following Gibson Assembly Protocol (New England Biolabs) hDNaseII (Human DNase II Gene ORF cDNA clone in cloning vector, HG16372-G, Sino Biological inc) was inserted in CD63-GFP plasmid in the intraluminal domain. CD63-GFP plasmid was cut with EcoRI. The following primers were used to amplify insert: Fw_DNaseII-EcoRI: CGAGCTCAAGCTTCGATGATCCCGCTGCTGCT Rv_DNaseII-EcoRI:TACCGTCGACTGCAGGGATCTTATAAGCTCTGCTGG GC

T-cell lines and human T lymphoblasts were transfected with a specific double stranded siRNA targeting human LC3 (GGUGCCUGUAGGUGAUCAA) or negative control siRNA (Eurogentec), using the Gene Pulser II electroporation system (Bio-Rad Laboratories) or the Nucleofector system (Amaxa Biosystems). When indicated, at 24 h post transfection, cells were cultured in exosome-depleted medium for 20 h and exosomes were isolated from supernatants.

For transfection, J77 T cells were transfected with the corresponding plasmids by electroporation; 20×10^6 cells were resuspended in Opti-MEM (Gibco; 5×10^7 cells per ml) with 20 µg of plasmid DNA and electroporated with a Gene Pulser Xcell electroporator (Bio-Rad) at 1200 µFa, 240 mV, 30 ms in 4 mm Bio-Rad cuvettes (Bio-Rad). Fluorescence-positive cells were FACS sorted, cloned, and cultured in RPMI containing 2 mg/ml G418 (Invitrogen). HEK293T cells were transfected using Lipofectamine 2000 (Invitrogen) according to the manufacturer's instructions.

Lentiviral infection

J77 cells with downregulated nSMase2 and Rab27a expression were generated by infection with lentiviral vectors expressing specific shRNAs. HEK293T cells were co-transfected using the Lipofectamine2000 system (Invitrogen) with pCMV-ΔR8.91-(Delta 8.9), pMD2.G-VSV-G, and plasmids encoding shRNAs targeting nSMase2, Rab27a or the corresponding shRNA pLKO control plasmids (Open Biosystems). Supernatants were collected after 48–72 h, filtered (0.45 µm), and added to J77 or HEK293 cell cultures. Cells were centrifuged (2000 x g, 2 h) and incubated for 4 h at 37 °C. Medium was replaced with RPMI containing puromycin (4 µg/ml).

Conjugate formation and assessment of mtDNA transfer

To assess mtDNA transfer during immune cognate interactions we used two mice strains (C57BL/6 and C57BL/6^{NZB}) that differ by 12 missense mutations in their mitochondrial DNA. Differentiated C57BL/6^{NZB} BMDCs were loaded with calcein (37°C, 20 min), extensively washed, and then co-cultured in the presence of ovalbumin (OVA) peptide (10 µg/ml) with C57BL/6 CD4^{+} OT-II T cells (5:1 T cell/DC ratio; 16 h). To assess mtDNA transfer from CD4^{+} OT-II cells to BMDCs, C57BL/6 OT-II CD4^{+} T cells and C57BL/6^{NZB} BMDCs were conjugated (1:5 T cell/DC ratio; 16h). Conjugates were blocked with Fc-block (CD16/CD32, BD Pharmingen), washed in PBS, 1% BSA, and incubated with antibodies against MHCII and CD3 (BD Pharmingen) diluted in PBS, 1% BSA. Viable cells were identified by propidium iodide exclusion. Singlet cells were discerned with a stringent multiparametric gating strategy based on FSC and SSC (pulse width and height). CD4^{+} T cells and BMDCs were distinguished by calcein staining and MHCII and CD3 fluorescence, and sorted on a FACSAria flow cytometer (BD Biosciences). DNA was extracted, and C57BL/6 and NZB mtDNAs were detected by restriction fragment length polymorphism (RFLP) analysis as follows. DNA (50 ng) was PCR-amplified using the RED Extract-N-Amp PCR Ready Mix Kit (Sigma Aldrich) with the oligonucleotides 5’ AAGCTATCGGGCCCATACCCCG 3’ (Fw) and 5’ GTTGAGTAGAGTGAGGGATGGG 3’ (Rv) at a concentration of 250 nM (Tm: 58º). After PCR amplification, samples were digested with BamH1 (10 units) for 2 h. Digested samples were loaded on a 2% agarose gel. C57^{C57} haplotype includes a BamHI restriction site; enzyme digestion results in two smaller fragments of 414 pb and 250 pb. Digestion of PCR products from C57BL/6^{NZB} haplotype results in a single band of 664 pb corresponding to the full length PCR product.

Conjugate formation of cell lines and mitoDsRed transfer

To distinguish Raji B cells from T cells, Raji cells were loaded with the cell tracer CMAC (7-amino-4-chloromethylcoumarin, Invitrogen). For antigen stimulation and IS formation, Raji cells were pulsed for 30 min with 0.5-1 µg/ml of *Staphylococcus enterotoxin superantigen* (SEE, Toxin Technology) and mixed with Jurkat cells expressing CD63-GFP, TFAM-dsRED, or mitoYFP at a ratio of 1:5 for 18-24 h at 37º C. Cell conjugates were analyzed by FACS in a FACS LSRFortessa Cell Analyzer (BD Biosciences) and data were analyzed with FACSDiva software (BD Biosciences).

To assess gene expression after IS formation, stable J77 CD63-GFP cells and CMAC-stained Raji cells were conjugated as described. After 16 h, cells were sorted according to CMAC staining and CD63 green fluorescence. The Raji population was split into 2 groups according to CD63-GFP uptake: Raji GFP+ Low (cells acquiring low amounts of CD63) and Raji GFP+ High (acquiring high amounts of CD63). After sorting, total RNA was isolated and qPCR performed to analyze antiviral response genes.

Exosome purification and sucrose-gradient purification

Cells were cultured in medium supplemented with 10% exosome-depleted fetal bovine serum (FBS, Invitrogen; FBS was depleted of bovine exosomes by overnight centrifugation at 100 000 x g for at least 16-20 h. Exosomes were obtained by serial centrifugation as described [179]. Briefly, cells were pelleted (300 x g for 10 min) and the supernatant was centrifuged at 2000 x g for 20 min to remove debris and dead cells. The collected supernatant was then ultracentrifuged at 10 000 x g for 40 min at 4 ºC (Beckman Coulter Optima L-100 XP, Beckman Coulter) to remove debris, apoptotic bodies, and shedding vesicles. Exosomes were pelleted by ultracentrifugation at 100 000 x g for 70 min at 4 °C, washed in PBS, and collected by ultracentrifugation at 100 000 x g for 70 min. DNase treatment was performed with RQ1 RNase-Free DNase (Promega) according to the manufacturer's instructions.

Exosomes were isolated by sucrose density gradient . Briefly, exosomes were obtained by serial centrifugation of 200 ml cell culture supernatant. Isolated exosomes were layered on top of a discontinuous sucrose gradient, ranging from 2.5 M sucrose at the bottom to 0.4 M sucrose at the top, in an SW40 centrifuge tube (14 x 95 mm; Beckman Coulter). Tubes were centrifuged overnight (18-20 h) in a SW40 rotor at 192 000 x g at 4 °C. One ml fractions were collected from the top of the gradient and were resuspended in an equal volume of acetone for protein precipitation and Western blot analysis or were treated as indicated for DNA isolation and PCR analysis.

Exosome adsorption to aldehyde-sulfate beads and detection

Exosomes were obtained as described above, resuspended in PBS, and coupled to 4 µm aldehyde-sulfate beads (Invitrogen) 15 min in rotation at room temperature. Then, coupled beads where incubated in overnight rotation in PBS containing 0.1% BSA and 0.01% sodium azide. Beads were washed twice with PBS, 0.1% BSA, 0,01% sodium azide. For surface staining, beads were washed and incubated with the indicated primary antibodies for 30-45 min on ice. For intraluminal staining, beads were fixed and permeabilized in PBS containing 1% Paraformaldehyde and 0.01% Triton X-100 for 20 min on ice, washed, and incubated with primary antibodies for 1 hour on ice. Beads were then washed and incubated with the appropriate secondary antibodies for 30 min on ice. Beads were analyzed with a FACS LSRFortessa Cell Analyzer (BD Biosciences) and data were analyzed with FACSDiva software (BD Biosciences). Negative controls were obtained with permeabilized and non-permeabilized exosome-coupled beads incubated with the indicated secondary antibodies.

Nanoparticle tracking analysis

Exosome numbers and size distribution were measured from the rate of Brownian motion in a NanoSight LM10 system, which is equipped with fast video capture and particle-tracking software (NanoSight, Amesbury, U.K.). Briefly, 0.5 mL of diluted exosome fraction was loaded into the sample chamber of an LM10 unit (Nanosight, Amesbury, UK) and three 30-second videos were recorded of each sample. Data were analyzed with NTA 2.1 software (Nanosight). Samples were analyzed using manual shutter and gain adjustments, which resulted in shutter speeds of 15 or 30 ms, with camera gains between 280 and 560. The detection threshold was kept above 4; blur: auto; minimum expected particle size: 50 nm. Samples were diluted before analysis to concentrations between 2×10^8 and 20×10^8 particles/ml.

Deep sequencing analysis

Total RNA was extracted with the RNeasy kit (Qiagen). Contaminating genomic DNA was removed using the specific column from the kit. RNA integrity and quantity were determined in an Agilent 2100 Bioanalyzer. Equal RNA amounts from 4 individual samples per group were analyzed in the Illumina Genome Analyzer IIx. Sequencing reads were pre-processed by means of a pipeline that used FastQC to assess read quality and Cutadapt to trim sequencing reads, eliminate Illumina adaptor remains, and discard reads shorter than 30 bp. The resulting reads were mapped against the mouse transcriptome (GRCm38, release 76; aug2014 archive) and quantified using RSEM v1.17. Data were then processed with a pipeline that used the EdgeR Bioconductor package for normalization and differential expression analysis in a paired strategy.

The number of reads obtained per sample was in the range of 12 to 17 million. The percentage of reads eliminated in the pre-processing step was below 1%. Genes with at least 1 count per million in at least 4 samples (11 383 genes) were considered for further analysis. Fold change and log(ratio) values were calculated to represent gene expression differences between conditions. Sets of genes differentially expressed across conditions were analyzed for functional associations using the Ingenuity Knowledge Database (IPA, http://www.ingenuity.com).

Exosome proteomic analysis

Exosomes from mouse T lymphoblasts were isolated by serial ultracentrifugation, and protein extracts (200 µg) were digested using the FASP method as previously described[180]. After digestion, the resulting peptides were desalted onto C18 OMIX tips (Agilent Technologies). Peptides were separated into 4 fractions by cation exchange chromatography with MCX cartridges (Waters) using graded concentrations of ammonium formate, pH 3.0 in acetonitrile (ACN), and desalted again before analysis by liquid chromatography–tandem mass spectrometry (LC-MS/MS).

Analyses were performed using a nano-HPLC Easy nLC 1000 chromatograph coupled to a Q-Exactive hybrid quadrupole orbitrap mass spectrometer (Thermo Scientific). Peptides were loaded in an analytical C18 nano-column (EASY-Spray column PepMap RSLC C18, 75 µm internal diameter, 3 µm particle size, and 50 cm length, Thermo Scientific) and separated in a continuous gradient consisting of 8-30% B for 60 min and 30-90% B for 2 min (B = 90% ACN, 0.1% formic acid) at 200 nL/min. The chromatographic run acquired an FT-resolution spectrum of 140 000 ions in the mass range of m/z 390–1600 followed by data-dependent MS/MS spectra of the 15 most intense parent ions. Normalized HCD collision energy was set to 28% and the parent ion mass isolation width was 2-Da.

Peptides were identified from MS/MS spectra using the SEQUEST HT algorithm integrated in Proteome Discoverer 2.1 (Thermo Scientific). MS/MS scans were matched against a mouse protein database (UniProt 2016_07 Release) and the parameters were selected as follows: a maximum of 2 missed trypsin cleavages, a precursor mass tolerance of 800 ppm, and a fragment mass tolerance of 0.02 ppm. Cysteine carbamidomethylation was chosen as the fixed modification and methionine oxidation as the dynamic modification. The same MS/MS spectra collections were searched against inverted databases constructed from the same target databases. SEQUEST results were analyzed by the probability ratio method. False discovery

rate (FDR) was calculated for peptides identified in the inverted database search results using the refined method [181].

Detection of oxidized DNA by chromatin immunoprecipitation

T lymphoblast exosomes were purified by differential ultracentrifugation and lysed in buffer containing 25 mM Tris-HCl, 150 mM NaCl, 2 mM MgCl, 0.5%, NP40, 5 mM DTT. Protein G-coupled magnetic beads (Protein G Dynabeads, Invitrogen) were washed and incubated for 2-3 h with 5 µg anti-8 hydroxyguanosine (8-OHdG) antibody [15A3] (Abcam), 5 µg of anti-DNA AC-30-10 (Progen) or with 5 µg of the isotype control (SantaCruz, sc-2015). Lysates were precleared with Protein G Dynabeads and then incubated overnight at 4ºC with antibody-coupled beads. Samples were washed 5 times with lysis buffer and eluted with 50 mM Tris-HCl pH 8.0, 10 mM EDTA, and 1% SDS for 1 hour at 65ºC. DNA was purified with the ChIP DNA Clean & Concentration kit (D5205-Zymo Research). qPCR was performed on whole samples with technical duplicates.

Mitochondrial enriched fraction was obtained from T lymphoblasts by resuspending them in mitochondrial extraction buffer (1mM EDTA ph8, 1mM DTT, 10mM NaCl, 3mM MgCl2, 5mM Tris-HCl ph8) during 15 min at 4ºC (Osmotic Lysis). Then, lysates were subjected to three freeze/thaw cycles with 5 min liquid nitrogen exposition and 10 min immersion in a water bath at 37ºC. Following lysis the tubes were centrifuged at 500*g* for 10 min at 4ºC. Supernatants were collected and spun down at 12000*g* for 20 min at 4ºC. The final pellets (mitochondria enriched fraction) were resuspended in lysis buffer and treated as exosomal fractions.

Analysis of antiviral response induction by exosomes

BMDCs were cultured and differentiated in vitro. After culture for 9-11 days, BMDCs were plated in p12 plates at 3×10^5 per well. Exosomes from T lymphoblasts were isolated by differential ultracentrifugation and 10-15 µg added to BMDCs for 6 h. BMDCs were then washed and frozen for RNA extraction.

Vaccinia infection

The recombinant vaccinia virus VACV-GFP was a gift from J. Yewdell (National Institutes of Health, Bethesda, MD). For analysis of exosome-mediated viral protection, BMDCs were cultured as previously described. After 9-11 days, cells were plated in p96 plates at 1×10^5 per well. T lymphoblast exosomes were purified by differential ultracentrifugation and 5-10 µg were added to BMDCs for 4-6 h. Vaccinia-GFP was added to cells at the indicated BMDC:virus ratios. After incubation for 4 h, cells were harvested, fixed for 10 min with BD

Cytofix/Cytoperm (BD Biosciences), and analyzed by flow cytometry. Viability was assessed with the LIVE/DEAD® Fixable Aqua Dead Cell Stain Kit (Molecular Probes).

For the analysis of antiviral protection during IS formation, BMDCs were cultured for 9-11 days and then plated in p24 plates at 2×10^5 per well. Receptor BMDCs were primed with 100 ng/ml LPS overnight, extensively washed, and co-cultured in the presence of ovalbumin (OVA) peptide (5 µg/ml) with C57BL/6 $CD4^+$ OT-II T cells (5:1 T cell/DC ratio). After conjugate formation for 4 h, vaccinia-GFP was added at a 1:1 ratio (total number of cells in the well) for 4h. Cells were harvested, blocked with Fc-block (CD16/CD32, BD Pharmingen), and stained with CD4 PE-Cy7 and CD11c PE. Viability was assessed with the LIVE/DEAD® Fixable Aqua Dead Cell Stain Kit (Molecular Probes). Cells were fixed for 10 min with BD Cytofix/Cytoperm (BD Biosciences) and analyzed by flow cytometry.

Cell viability Assay

In order to measure cell viability upon manumycin treatment and activation, $CD4^+$ OTII T lymphoblasts were incubated for 24h with increasing amounts of manumycin (0, 1 and 2,5 µM) and with anti-CD3 (10 µg/ml) and anti-CD28 (2 µg/ml). Cells were harvested and stained with anti-CD4 and DAPI to measure the percentage of DAPI negative (alive) CD4+ cells by flow cytometry.

To ascertain cell viability in the context of immune cognate interactions, CD4+ OTII T lymphoblasts were pre-treated for 2h with increasing amounts of manumycin (0, 1 and 2,5 µM) ,then CD4 T cells were conjugated with OVA-pulsed dendritic cells (5:1T cell/DC ratio; 4h). Cells were harvested and stained with anti-CD4 and DAPI to measure the percentage of DAPI negative (alive) CD4+ cells by flow cytometry.

Flow cytometry

For cytometry, adherent cells were harvested with 0.25% Trypsin-EDTA (Gibco), blocked with Fc-block (CD16/CD32, BD Biosciences), washed in PBS, 1% BSA, and incubated with primary antibodies diluted in PBS, 1% BSA. Viable cells were identified by HOECHST 58 exclusion. Singlet cells were discerned based on FSC and SSC (pulse width and height). For surface labeling, cells were stained with antibodies diluted in PBS, 0.5% BSA on ice.

For intracellular and surface staining, cells were fixed with 1% formaldehyde and permeabilized with 0.01% Triton X-100 (Sigma). After washing, cells were blocked with Fc-block (CD16/CD32, BD Biosciences), washed in PBS, 1% BSA, and incubated sequentially with primary and secondary antibodies (diluted 1:500) in PBS, 1% BSA. Cells were then analyzed by

FACS in a FACS LSRFortessa Cell Analyzer (BD Biosciences). Data were analyzed with FACSDiva software (BD Biosciences).

To detect intracellular ROS, HEK293T cells were incubated with 2',7'–dichlorofluorescin diacetate (DCDFA, Thermofisher), and to detect mitochondrial mass cells were loaded with mitotracker green (Invitrogen). Cells were analyzed in a FACS LSRFortessa Cell Analyzer (BD Biosciences) and data were analyzed with FACSDiva software (BD Biosciences).

Western blot

Cells or exosomes were lysed in RIPA buffer (50 mM Tris-HCl pH 8, 150 mM NaCl, 1% Triton X-100, 0.1% sodium deoxycholate, and 0.1% SDS) supplemented with a protease inhibitor cocktail (Complete, Roche). Proteins were separated on 10-12% acrylamide/bisacrylamide gels and transferred to nitrocellulose or methanol-pretreated PVDF membranes. Membranes were incubated with primary antibodies (1:1000) and peroxidase-conjugated secondary antibodies (1:5000), and proteins were visualized with LAS-3000.

Immunofluorescense

For immunofluorescence assays, cells were plated onto slides coated with fibronectin (50 µg/ml), incubated overnight, and fixed with 2% paraformaldehyde in PBS. Cells were permeabilized with PBS, 0.1% Triton X-100 (Sigma), washed and stained with the corresponding primary antibodies (1:100-1:200) followed by secondary antibodies (1:500) (Life Technologies). When indicated, cells were previously transfected with the indicated plasmids. Cells were fixed and stained with the indicated antibodies at 24 h post transfection. Samples were examined with a Leica SP5 confocal microscope fitted with a × 63 objective, and images were processed and assembled using Leica software. Quantification of images was done with Fiji software (ImageJ) using Manders' coefficient M2 as a marker for colocalization of mitochondrial markers (SSBP1) with endosomal markers (EEA1 and CD63)[182]. More than one hundred cells were quantified for experiment.

TIRFm analysis of isolated exosomal particles

Isolated exosomal particles (8x106 particles per coverslip) generated as described and quantified with Nanosight were spun in a sucrose cushion (10% in HBSS; 10000xg, 15 min, 25ºC. HS-4 rotor, Sorvall) over 13 mm diameter precision coverslips (thickness No. 1.5H; 0.170 mm ± 0.005 mm, 0117530 Marienfield) coated with 250 µg.ml-1 Poly-L-Lys (P6407 Sigma Aldrich) and fixed in 1% paraformaldehyde (HBSS, 5% sucrose; RT15710 Electron Microscopy Sciences) for 5 min, R/T. Coverslips were treated with Glycine 200 mM in Tris-HCL (pH 7.4) for 10 min, R/T and blocked (3% BSA, 20 µg.ml-1 human gamma-globulins in HBSS) for 1 h R/T.

Staining with anti-CD81 (rat anti-mouse clone MT81; 5 µg.ml-1, 4ºC, o/n) was followed by highly-cross-adsorbed Alexa-568-conjugated goat anti-rat Antibody (A-11077 Thermofisher Scientific 1:1000). Samples were then permeabilized with a 0.2% TX-100 solution (HBSS supplemented with 0.5% paraformaldehyde and 1.5% BSA), treated for autofluorescence and stained with anti-DNA (0.001 µg.ml-1) or anti-TSG101 (20 µg.ml-1, ab83 Abcam) mouse monoclonal antibodies for 3 h at 4ºC, followed by highly-Cross-absorbed Alexa-488-conjugated goat anti-mouse Antibody (A-11029 Thermofisher Scientific 1:1000). Samples were mounted on Prolong Gold antifade mountant (P36930 Thermofisher Scientifc). Coverslips were extensively washed with HBSS and a final wash with deionized water. Antibodies were diluted in 1.5% BSA in HBSS. Secondary antibodies were incubated for 1 h at R/T. All the solutions used for coverslip preparation and immunofluorescence were previously ultracentrifuged at 100000xg for 70 min (4ºC) in a swinging bucket rotor (Beckman Coulter) or for 30 min at 13200xg in a fixed-angle rotor (Eppendorf). Samples were imaged under a Leica AM TIRF MC M system mounted on a Leica DMI 6000B microscope fitted with a HCX PL APO 100×1.46 NA oil objective and coupled to an Andor-DU8285 VP-4094 camera. Penetration depth was 90 nm and 2x zoom was used to obtain an optical magnification of the samples. Equal experimental conditions for acquisition were used for the different coverslips. Brightness and Contrast adjustments were equal for all images. Processing of images was performed with Image J 1.51n (Wayne Rasband national Institutes of Health, USA. http://imagej.nih.gov/ij; Java 1.8.0_66; 64 bit).

Electron microscopy

Adherent HEK293 cells stably transfected with control shRNA, shRab27a, or shnMNase2 were washed in PBS and fixed for 1 h in 2.5% glutaraldehyde in 0.1 M phosphate buffer at room temperature. Cells were pelleted in 15ml Falcon tubes. Pellets were washed with phosphate buffer and incubated with 1% OsO_4 for 90 min at 4 °C. Samples were then dehydrated, embedded in Spurr, and sectioned on a Leica ultramicrotome (Leica Microsystems). Ultrathin sections (50–70 nm) were stained with 2% uranyl acetate for 10 min and with a lead-staining solution for 5 min and observed under a JEOL JEM-1010 transmission electron microscope fitted with a Gatan Orius SC1000 (model 832) digital camera.

For immunogold staining, cells were fixed in 4% PFA 0.5% glutaraldehyde in PBS at 4ºC. Samples were dehydrated, embedded and sectioned. Grids were rehydrated in TBS and treated with 0.01 M glycine to deactivate reactive aldehydes. Samples were blocked with goat blocking solution (Aurion) for 1h and incubated with primary antibodies; anti-Tfam (1:50) (Cell Signalling) and anti-DNA (1:15) (Promega) overnight in blocking solution. Grids were washed in

blocking solution and incubated with secondary antibodies conjugated to 12nm colloidal gold (1:75 for TFAM and 1:25 for DNA, Jackson ImmunoResearch) for 2h. Samples were washed in blocking solution and distilled water. Grids were air dried for 2h, stained with lead citrate and uranyl acetated and carbon coated for viewing under transmission electron microscope.

Extracellular Flux Analysis

Oxygen consumption rate was measured in a XF-96 Extracellular Flux Analyzer (Seahorse Bioscience) in equal numbers of shControl, shRab27a and shnSMase2 HEK293 cells incubated with XF medium. Three measurements were obtained under basal conditions and upon addition of oligomycin (1 mM), fluoro-carbonyl cyanide phenylhydrazone (FCCP; 1.5 mM), and rotenone (100 nM) + antimycin A (1 mM).

Quantitative PCR and assessment of mitochondrial DNA by PCR

Total RNA was isolated using the RNeasy kit (Qiagen). Genomic DNA was removed using the specific column from the kit. Reverse transcription was performed using the High Capacity cDNA Reverse Transcriptase kit (Applied Biosystems). Quantitative real-time PCR was performed in a 7900 HT Fast Real-Time PCR system (Life technologies) using SYBR green qPCR Master Mix (Promega). Data were normalized to the expression of beta-actin, beta-2-microglobulin, and/or ywhaz and analyzed with Biogazelle QBasePlus (Biogazelle). Primer sequences are specified below:

	Sequence	gene	Organism
Forward	CACCCAAGAACAGGGTTTGT	tRNA Leu	Human
Reverse	TGGCCATGGGTATGTTGTTA	tRNA Leu	Human
Forward	GCCTTCCCCCGTAAATGATA	16S RNA	Human
Reverse	TTATGCGATTACCGGGCTCT	16S RNA	Human
Forward	TGCTGTCTCCATGTTTGATGTATCT	B2 Microglob	Human
Reverse	TCTCTGCTCCCCACCTCTAAGT	B2 Microglob	Human
Forward	TTCGGCGCATGAGCTGGAGTCC	hCOX	Human
Reverse	TATGCGGGGAAACGCCATATCG	hCOX	Human
Forward	CTCACGGGAGCTCTCCATGC	HVRII	Human
Reverse	CTGTTAAAAGTGCATACCGCCA	HVRII	Human
Forward	ACCCCTTCTCTGTCTACCG	SDH	Mouse
Reverse	AATGCTCGCTTCTCCTTGTAG	SDH	Mouse
Forward	CCCAGATATAGCATTCCCACG	mtCOXI	Mouse
Reverse	ACTGTTCATCCTGTTCCTGC	mtCOXI	Mouse

Forward	TGCACCTACCCTATCACTCA	mtND1	Mouse
Reverse	GGCTCATCCTGATCATAGAATGG	mtND1	Mouse
Forward	TCCCAATCGTTGTAGCCATC	mtATP6	Mouse
Reverse	TGTTGGAAAGAATGGAGTCGG	mtATP6	Mouse

For the analysis of mitochondrial DNA contained in exosomes, DNA from T lymphoblast-derived exosomes was isolated with the Cell Lysis Solution and Protein Precipitation Solution from Qiagen. After DNA isolation, PCR was performed, primer sequences are specified in the table below:

	Sequence	gen	Organism
Forward	CCAGTGCTGCCGTCATTTTC	CXCL10	Mouse
Reverse	GGCTCGCAGGGATGATTTCAA	CXCL10	Mouse
Forward	CTAGAGCTAGAGCCTGCAG	ISG15	Mouse
Reverse	AGTTAGTCACGGACACCAG	ISG15	Mouse
Forward	GAGAGGACCATGAAGAGGA	USP18	Mouse
Reverse	TAAACCAACCAGACCATGAG	USP18	Mouse
Forward	TTCCCAGCAGCACAGAAAC	IFIT3	Mouse
Reverse	AAATTCCAGGTGAAATGGCA	IFIT3	Mouse
Forward	CAAGGCAGGTTTCTGAGGAG	IFIT1	Mouse
Reverse	GACCTGGTCACCATCAGCAT	IFIT1	Mouse
Forward	CGCGCATGCAACTGGCATATAACT	STAT1	Mouse
Reverse	ATGCTTCCGTTCCCACGTAGACTT	STAT1	Mouse
Forward	TAGTCCTTCCTACCCCAATTTCC	IL6	Mouse
Reverse	TTGGTCCTTAGCCACTCCTTC	IL6	Mouse
Forward	AGCAGAGGAACCTCCAGTCT	CXCL10	Human
Reverse	ATGCAGGTACAGCGTACAGT	CXCL10	Human

Statistical analysis

All values were expressed as the mean ± S.E.M. or mean with individual values included for data distribution. For in vitro experiments, statistical differences were evaluated with Student's *t* test and between group differences were evaluated with the Mann-Whitney U test for unpaired data (GraphPad Prism). Differences were considered significant when *$p < 0.05$, **$p < 0.01$, ***$p < 0.001$.

Data Availability

The authors declare that the data supporting the findings of this study are available within the article and its supplementary information files, or are available in a persistent repository or upon reasonable requests to the authors.

Deep sequencing analysis data supporting the findings of this study are deposited in GEO repository with the accession number: GSE110165

[https://www.ncbi.nlm.nih.gov/geo/query/acc.cgi?acc=GSE110165].

DNA seq data are deposited in BioSample repository: SRP148571 [https://www.ncbi.nlm.nih.gov/sra/SRP148571]

Raw data from RNAseq and DNAseq analysis are under a common umbrella project: Bioproject PRJNA472779 [https://www.ncbi.nlm.nih.gov/bioproject/PRJNA472779]:

PRJNA432987: Mouse RNA-seq data in GEO [https://www.ncbi.nlm.nih.gov/bioproject/PRJNA432987]

PRJNA472354: Human DNASeq data in SRA [https://www.ncbi.nlm.nih.gov/bioproject/PRJNA472354]

The mass spectrometry proteomics data are deposited to the ProteomeXchange Consortium via the PRIDE partner repository with the dataset identifier PXD008843 [http://www.ebi.ac.uk/pride/archive/projects/PXD008843]

Results

Results

Exosomes transferred from the T cell to the APC contain many different types of biologically active molecules, including proteins and genetic material [55,132]. To investigate the possible specific function of the different components of the biologic material transferred from the T cell to the DC, the protein and genetic content of EVs isolated from the culture supernatant of primary T lymphoblasts were characterized by differential ultracentrifugation [179] according to the current recommendations of the International Society of Extracellular Vesicles (ISEV) [183] **(Figure R1)**.

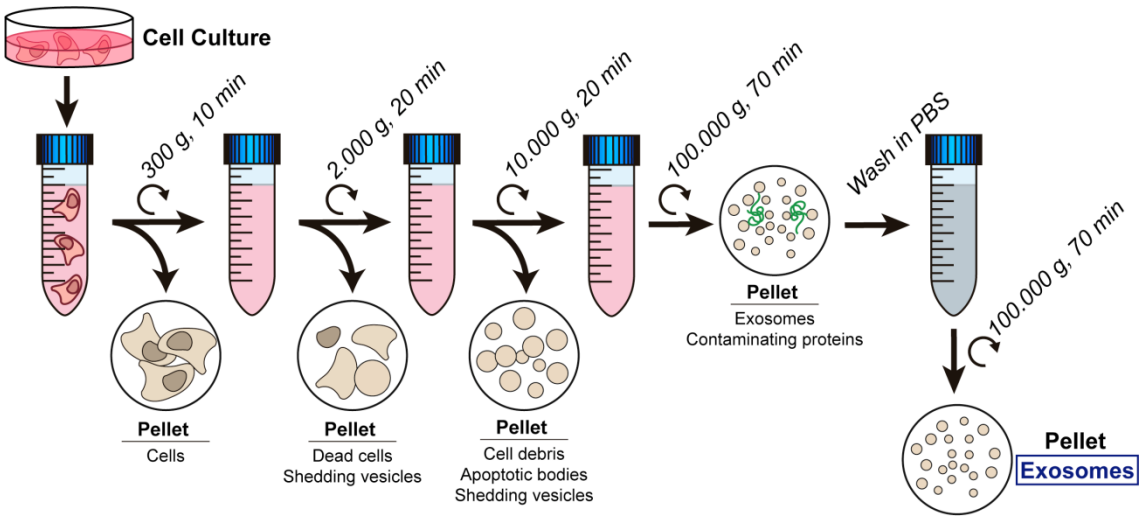

Figure R1. Differential centrifugation protocol for isolating exosomes from cell culture supernatants. Supernatants were centrifuged and pellets were consecutively discarded. After the 100.000g ultracentrifugation the supernatant was discarded and the pellet resuspended in PBS and centrifuged again in order to obtain a purified fraction of exosomes.

Diameters of exosomes obtained in the 100 000 ×g fraction ranged from 50 to 200 nm **(Figure R2a, R2b)**, in agreement with the reported size and shape of exosomes [124].

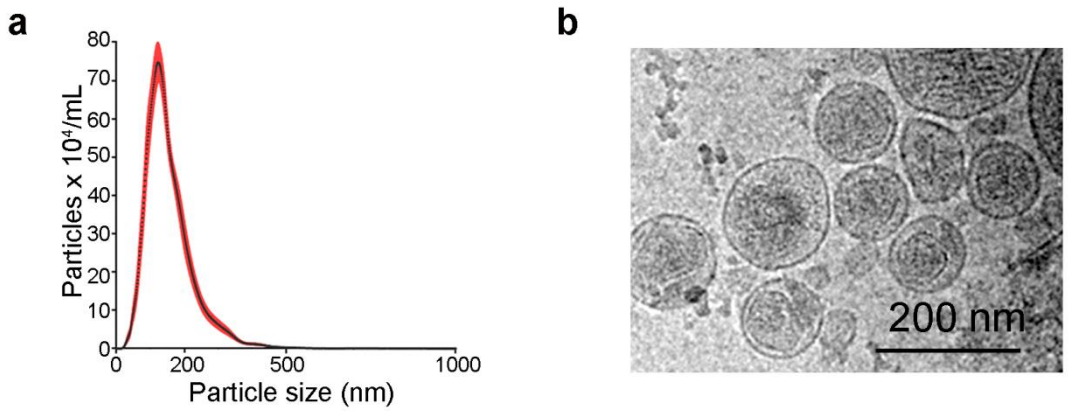

Figure R2. Size and shape of exosomes from T cell supernatants. (a) Size distribution analysis by Nanoparticle Tracking Analysis (NTA) of purified exosomes from primary human T lymphoblasts. **(b)** Electron microscopy of exosomal fraction from primary human T lymphoblasts. Bar 200nm.

1. T cells incorporate mitochondrial proteins in exosomes

Proteomic characterization of T cell Exosomes identified abundant peptides derived from canonical exosome components, including tetraspanins, endosomal proteins, cytoskeletal proteins, Rab-related trafficking proteins, heat-shock proteins and nucleotide-binding proteins. Gene Ontology (GO) term enrichment analysis revealed that a major fraction of the total number of identified peptides (>3000 peptides in 4 biological replicates) were significantly associated with the nuclear and mitochondrial fractions **(Figure R3a**). Mitochondrial peptides constituted 7.5 ± 0.3 % of the total exosome proteome, consistent with proteomic studies on exosomes isolated from other cell types, including immune cells [184,185]. Exosomes isolated from resting T lymphoblasts and cells activated with a polyclonal stimulus barely contained proteins of the mitochondrial matrix and the inner or outer mitochondrial membranes **(Figure R3b)**. Exosomes from activated T lymphoblasts contained significant amounts of mitochondrial transcription factor A (TFAM), a highly abundant mtDNA-binding protein, and the mitochondrial nucleoid-forming protein ATPase family AAA-Domain containing protein 3 (ATAD3) [186] **(Figure R3b)**. The presence of the canonical exosomal proteins CD81 and TSG101 in the purified 100.000 ×g fraction suggested an endosomal origin **(Figure R3b)**.

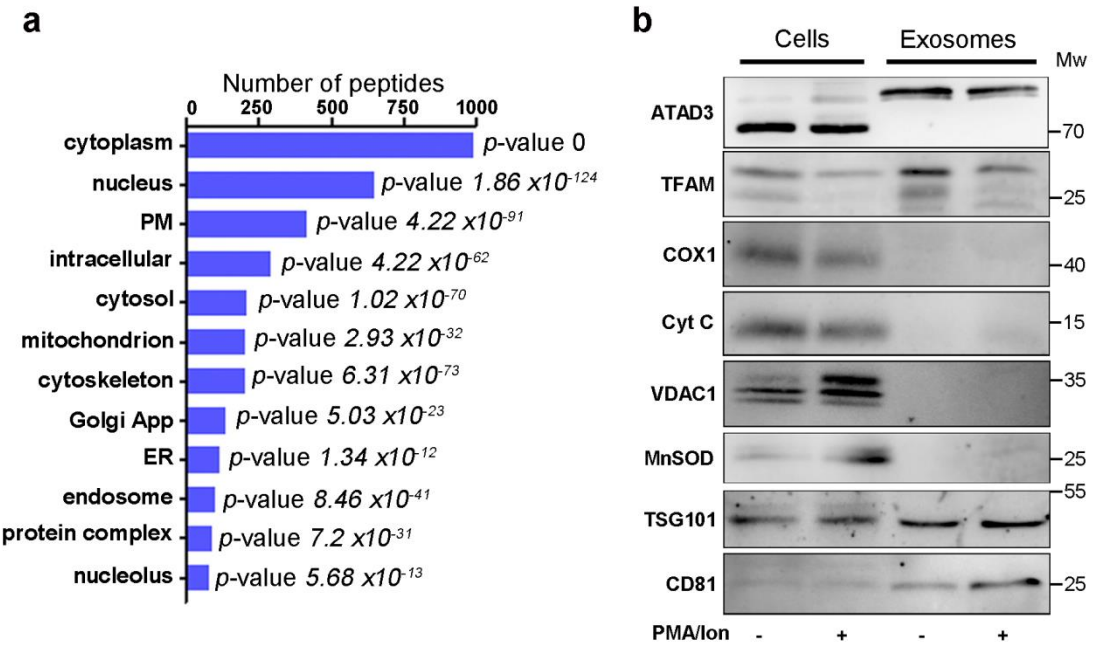

Figure R3. Cellular origin of protein content in T cell exosomes. (a) Gene ontology (GO) cellular component analysis of peptides identified in T cell exosomes. **(b)** Western Blot analysis of mitochondrial proteins in exosomes obtained from the culture supernatant of primary human T lymphoblast upon treatment with phorbol myristate acetate (PMA) together with Ionomycin to induce T cell activation.

TFAM and ATAD3 co-fractionated with the exosomal proteins CD81 and TSG101 in the 100.000×g EV fraction from sucrose-gradient isolation, **(Figure R4b and R4b)**, localizing mtDNA-binding proteins to exosomes.

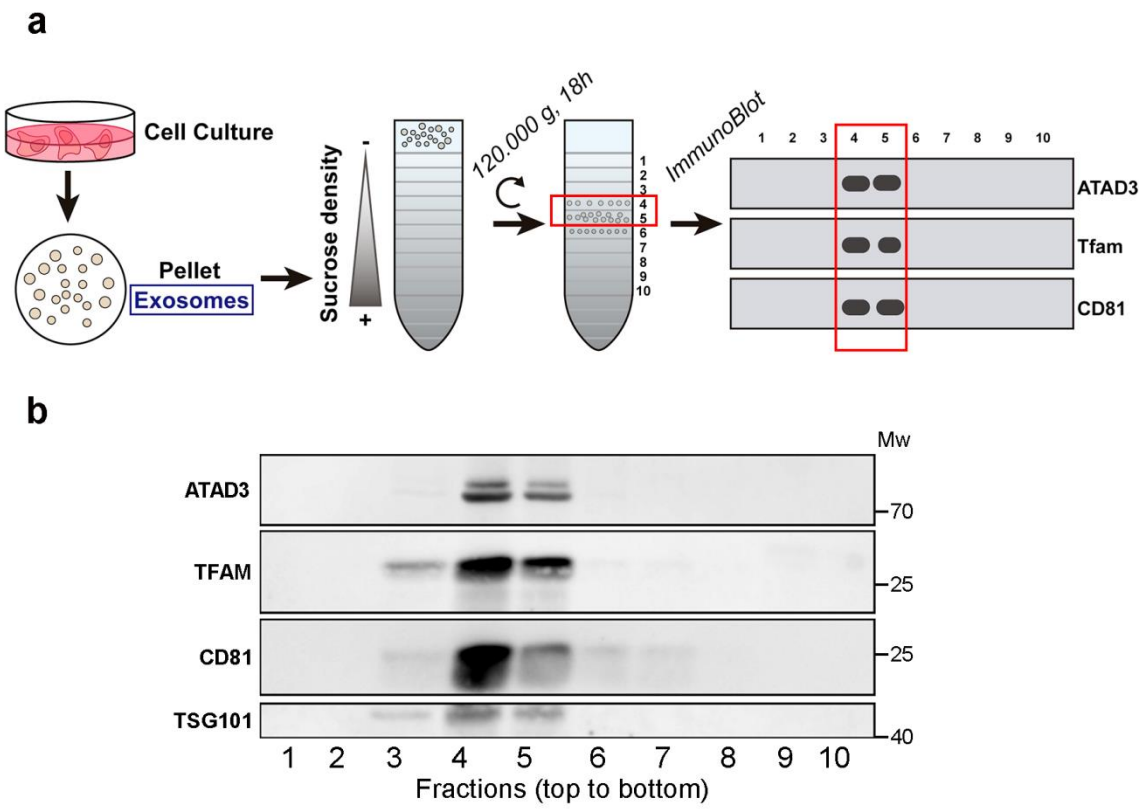

Figure R4. Sucrose gradient analysis of T cell exosomes (a) EVs obtained from the culture supernatant of human T lymphoblasts were laid on a discontinuous sucrose gradient and floated by overnight centrifugation. Gradient fractions were collected and analyzed by immunoblot to reveal the distribution of mtDNA-binding proteins and exosomal proteins in the sucrose fractions from lower to higher sucrose density (left to right). **(b)** Western blot analysis of ATAD3, TFAM, and the exosome markers CD81 and TSG101 in sucrose fractions. Gels shown are representative out of 3 independent experiments.

2. T cells incorporate genomic and mitochondrial DNA in exosomes

Among EVs, exosomes are enriched in genetic material, mostly non-coding RNAs [102,187]. Exosomes from cancer cell lines and patients contain DNA that reflects the mutational status of the parental tumor cells [103,105]. Deep-sequencing analysis of DNA in the EVs secreted by primary T lymphoblasts identified several reads that covered nuclear sequences and the entire mitochondrial genome **(Figure R5a)**. These results were confirmed by polymerase chain reaction (PCR) amplification of indicated regions of the mitochondrial genome and the B2M nuclear gene from the DNA obtained from the 100 000 ×g fraction **(Figure R5b)**.

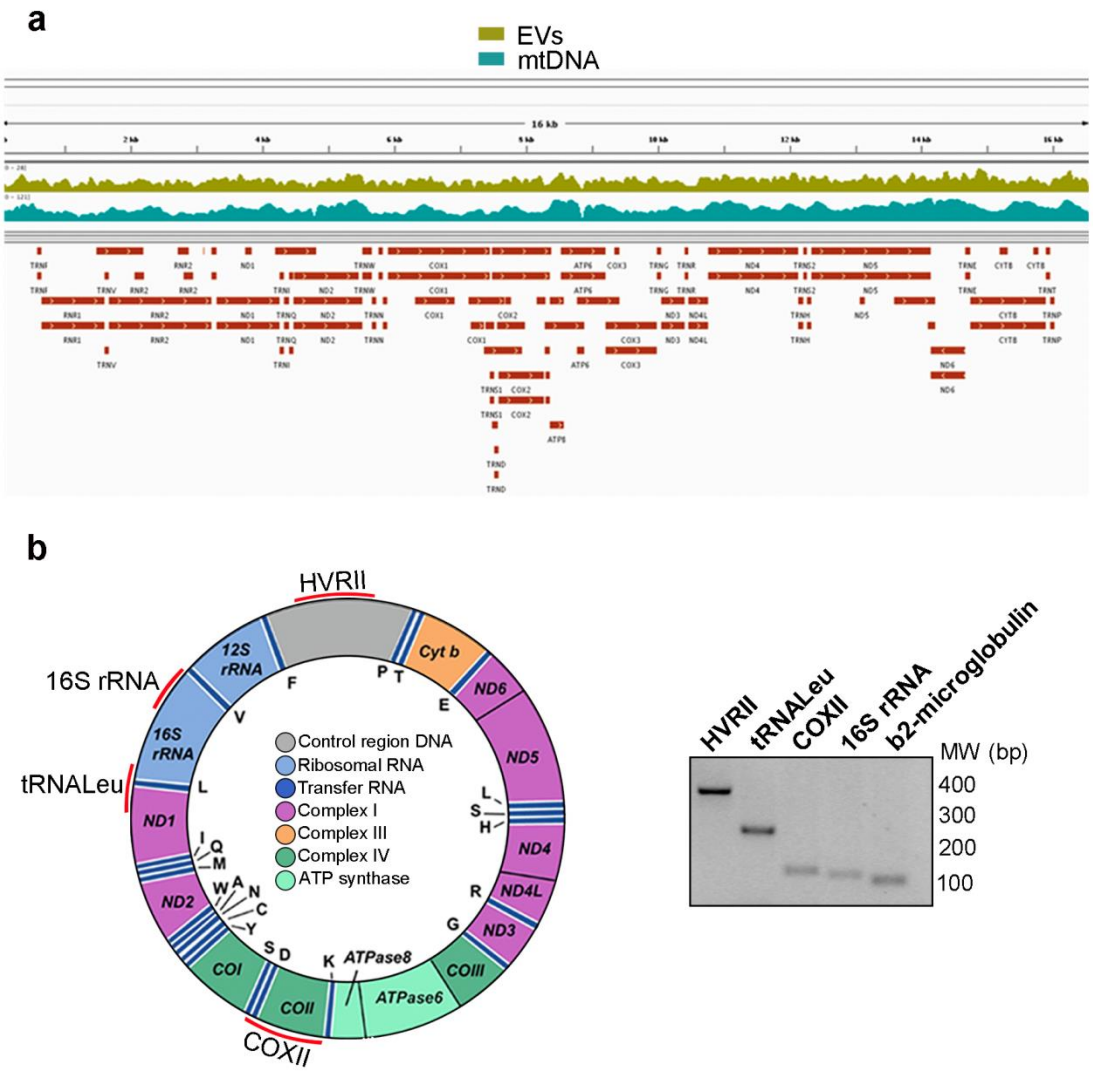

Figure R5. T cell exosomes shuttle mtDNA and genomic DNA. (a) Representation of the number of sequence reads aligned with the mitochondrial genome in EVs (EVs) and mitochondrial extracts (mtDNA) isolated from human primary T cells. **(b)** Left panel, Diagram of the mitochondrial genome, indicating the mtDNA regions analyzed by PCR (marked in red: HVRII, tRNALeu, COXII, and 16S rRNA). Right panel, Agarose gel showing the amplification products of the different mtDNA regions and the genomic DNA (β2-Microglobulin) analyzed in EVs purified from primary human T cells.

The DNA content of the isolated EVs was reduced by DNase treatment whereas a small fraction of the DNA remained protected unless vesicles were treated with DNase and a lipid destabilizing agent **(Figure R6a).** Two pools of DNA were present, one accessible (likely on the surface of the vesicle) and one inaccessible (likely in the lumen of the vesicle). The presence of mtDNA in the 100 000 ×g EV fraction was confirmed by the partial co-fractionation on sucrose gradients with the exosomal proteins CD63 and TSG101 **(Figure R6b)**.

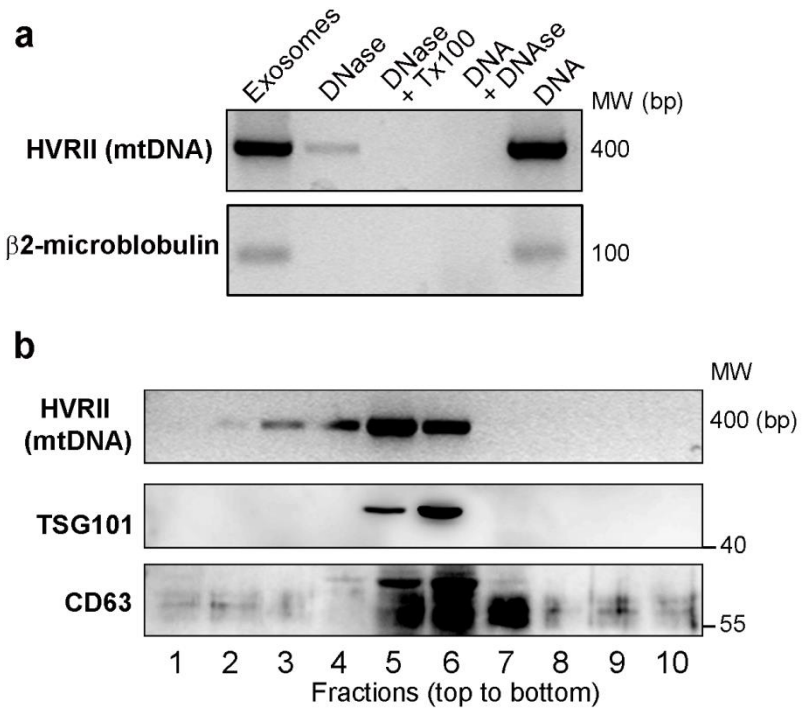

Figure R6. mtDNA is present both inside and outside of exosomes. (a) Agarose gel electrophoresis showing the detection of DNA in purified EVs. EVs obtained from the culture supernatant of J77 T were treated with DNase or DNase and Tx-100. Levels of mtDNA and genomic DNA were assessed by PCR amplification (HVRII and β2-MICROGLOBULIN, respectively). Isolated DNA from J77 T cells treated or not with DNase (DNA, DNA+DNase) is shown as control for DNase activity. **(b)** Distribution of mtDNA and TSG101 and CD63 in sucrose fractions. EVs from human Jurkat T cells were laid on a discontinuous sucrose gradient and floated by overnight centrifugation. DNA from gradient fractions was PCR-amplified for the HVRII mtDNA region. Proteins from gradient fractions were analyzed by immunoblot for TSG101 and CD63. A representative gel is shown (n=3).

3. mtDNA is partially oxidized and present only in a specific exosomal subpopulation

Flow cytometry analysis of EVs coupled to aldehyde sulfate beads reveals that the majority of beads were positive for both CD81 and DNA **(Figure R7a and R7b**). Total Internal Reflection Fluorescence (TIRF) microscopy-based analysis of the co-localization of exosomal marker CD81 with TSG101 or with DNA in isolated EVs showed that CD81 fully co-localized with TSG101, but only partly with DNA **(Figure R7c)**, suggesting the presence of DNA in a subset of $CD81^+$ exosomes in addition to other different populations of EVs.

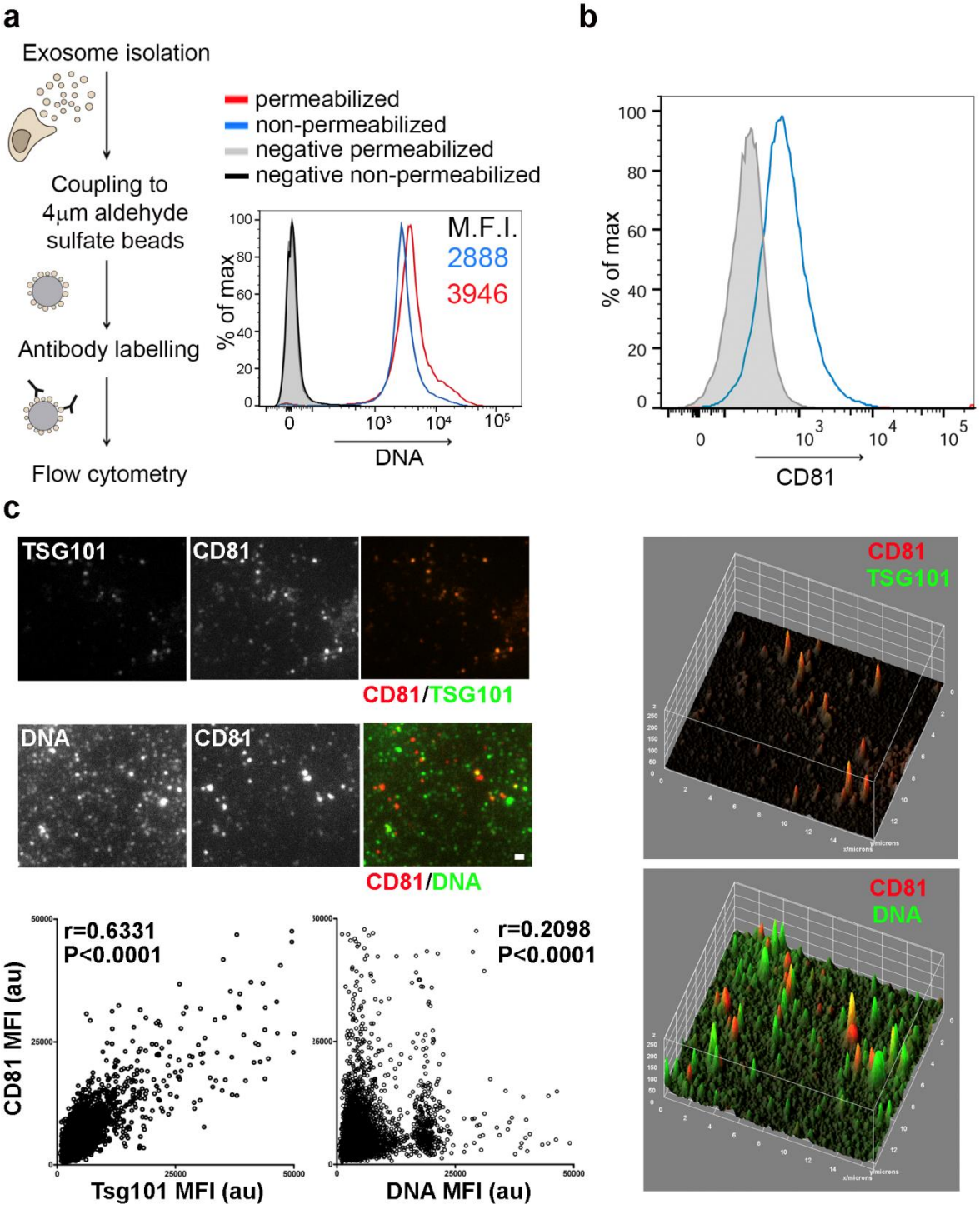

Figure R7. Characterization of the mtDNA containing vesicular subpopulation. Legend on the next page

Figure R7. Characterization of the mtDNA containing vesicular subpopulation.(a) Exosomes from primary mouse T lymphoblasts were purified, coupled to aldehyde sulfate beads, and analyzed by flow cytometry by staining with the anti-DNA Ab under permeabilizing and non-permeabilizing conditions. Histograms show DNA staining in exosomes. Numbers are mean fluorescence intensities of the positive population from a representative experiment (n=3). **(b)** Exosomes from primary mouse T lymphoblasts were purified, coupled to aldehyde sulfate beads and analyzed by flow cytometry by staining with the anti-CD81 Ab under non-permeabilizing conditions. Histograms show CD81 staining in exosomes coupled to aldehyde sulfate beads. **(c)** Images from isolated exosomal preparations stained for CD81 (red in merged images) and TSG101 or DNA (green in merged images). Exosomal preparations were spun on coverslips, fixed, processed for immunofluorescence and imaged in parallel. Permeabilization was performed upon CD81 staining. Imaging was performed with a TIRFm with a laser penetrance of 90 nm. Individual spots were detected. Scale bar, 1 µm. Graphs, Qualitative co-localization of fluorescence (yellow in merged images and graphs). The fluorescence intensity is plotted versus xy localization of the merged images showed. Scatter plots, correlation between mean fluorescence intensity from CD81:Tsg101 or CD81:DNA from TIRF images (r, Spearman coefficient for correlation; $P<0.001$, n=5937). Graphs were obtained with the Interactive 3D Surface Plot Plugging from Image J (https://imagej.nih.gov/ij/plugins/surface-plot-3d.html). Scatter plots correspond to the data from analysis with Image J from 20 different images from two different exosomal preparations from mouse T lymphoblasts. Images were normalized and processed in parallel.

DNA staining in non-permeabilized EVs increased upon permeabilization, confirming that DNA is present both outside and inside EVs. To examine the oxidative status of EV DNA, the 8-hydroxy deoxyguanosine (8-OHdG) DNA modification was evaluated as a hallmark of DNA oxidation. Staining with anti-oxidized-DNA antibody (Ab) is also detected in non-permeabilized EVs **(Figure R8a)**. In agreement with these results, chromatin immunoprecipitation of EV lysates with 8-OHdG Ab followed by DNA isolation and PCR analysis revealed the presence of several oxidized mtDNA and genomic DNA regions in EVs when compared with the control isotype Ab **(Figure R8b)**. To address the preferential localization of oxidized mtDNA, EVs and mitochondrial fractions of the corresponding cells were isolated and chromatin immunoprecipitation (ChIP) was performed with the 8-OHdG and total-DNA Abs. The enrichment in oxidized mtDNA at the EV fraction was demonstrated by qPCR analysis of mitochondrial genes in ChIP and quantification of the ratio between oxidized DNA vs total DNA **(Figure R8c)**. These results indicate that T cells release EVs carrying genomic DNA and mtDNA and associated mtDNA-binding proteins, and that the released DNA is partially oxidized.

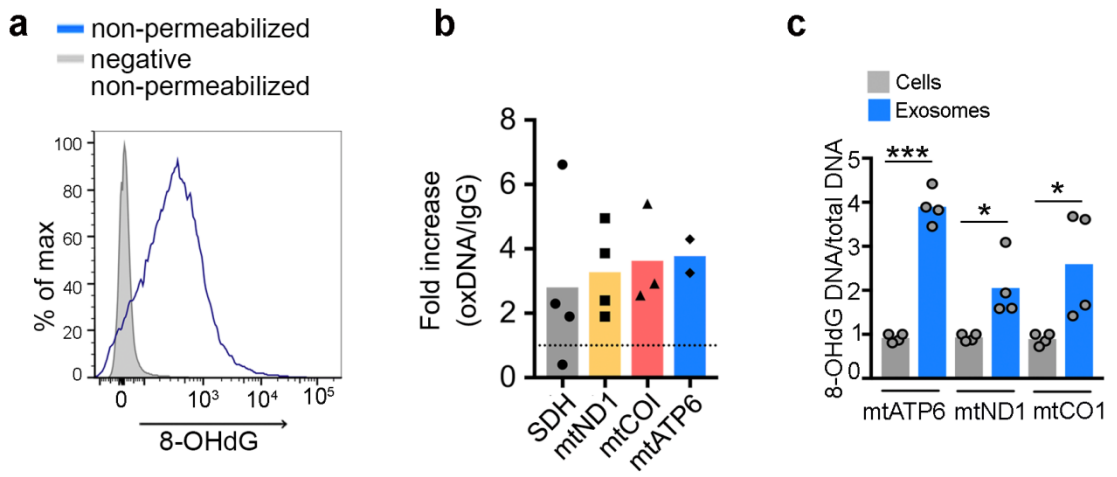

Figure R8. Analysis of oxidized state of mtDNA present in exosomes. (a) Histogram shows oxidized DNA staining in exosomes coupled to aldehyde sulfate beads with anti-8 hydroxydeoxyguanosine (8OHdG)Ab under non-permeabilizing conditions. **(b)** PCR analysis of the enrichment of the indicated mitochondrial (mtCO1, mtND1, mtATP6) or genomic (succinate dehydrogenase, SDH) genes in the DNA obtained from exosomes and immunoprecipitated with 8-OHdG Ab relative to isotype control IgG. Mean from quantification of 4 independent experiments. **(c)** qPCR analysis showing the enrichment of the indicated mitochondrial genes in the DNA obtained from exosomes and mitochondrial fractions from the same exosome-producing cells. DNA from both fractions was immunoprecipitated with 8-OHdG and total DNA Abs. Graph shows the ratio between oxidized DNA and total DNA in exosomes relative to their content in the mitochondrial fractions from the producing cells in duplicates from two independent experiments. t-test:*P-value<0.05, ***P-value<0.0001.

4. mtDNA and related proteins segregate into MVB pathway

The presence of mitochondrial components in EVs prompted us to investigate the molecular mechanisms controlling their extracellular release. We first co-transfected HEK-293 cells with TFAM-GFP and a mitochondria-targeted red fluorescent protein (mitoDsRed), then stained for endosomal markers. Confocal immunofluorescence analysis excluded co-localization of mitochondria and TFAM with the early endosome antigen 1 (EEA1), an early endosomal marker. Mitochondria and TFAM partially co-localized with components of maturing endosomal structures: HRS (hepatocyte growth factor regulated tyrosine kinase substrate), a component of the ESCRT machinery; lysobisphosphatidic acid (LBPA) and ceramide-positive structures, whose are markers of late endosomes and MVBs; and CD63, a highly abundant tetraspanin found in MVBs and exosomes **(Figure R9)**.

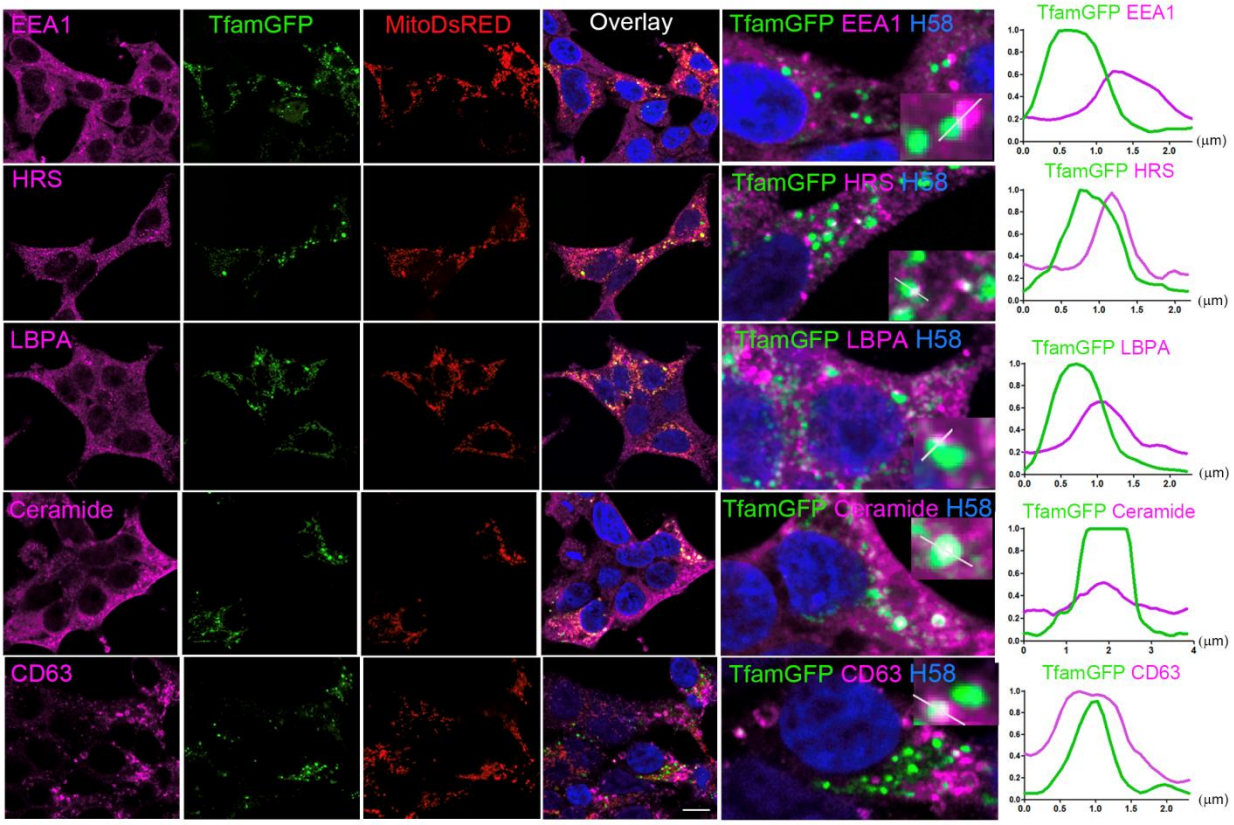

Figure R9. Mitochondrial components colocalize with markers from the endosomal pathway. Confocal co-localization analysis in HEK293 cells co-transfected with TFAM-GFP (green), nuclei with HOECHST 58 (blue) and a mitochondrial targeted fluorescent protein (mitoDsRed, red) and immunostained for endolysosomal compartment markers: the early endosome marker EEA1 and the ESCRT components HRS, LBPA, CD63, and ceramide (purple). Right images show high magnification views of co-localization between TFAM-GFP (green) and the various endolysosomal markers (purple). Charts show the fluorescence profiles along the corresponding white lines in the inset panels. Bar, 10 mm

To rule out potential analysis artifacts produced by the exogenous overexpression of TFAM-GFP, we measured the co-localization of endogenous mtDNA-binding protein single stranded DNA binding protein 1 (SSBP1) with EEA1 and CD63 in HEK-293 cells treated with low doses of FCCP, that promotes these events [188]. Increased co-localization of SSBP1 with CD63 indicates preferential localization in late endosomal structures **(Figure R10a)**.

The segregation of mitochondrial components into maturing endosomal structures was confirmed in HEK-293 cells transfected with constitutively active Rab7 (Q67L), which enhances endosomal trafficking, resulting in the formation of enlarged late endolysosomal structures [189].

Thus, Rab7 (Q67L) triggered the accumulation of endogenous TFAM within Rab7-positive endosomal structures, co-localizing with mitoDsRed **(Figure R10b)**. Also, immunogold labeling of TFAM and DNA revealed their appearance in canonical multivesicular body structures in electron microscopy studies **(Figure R10c)**, overall supporting the involvement of the endosomal pathway in the secretion of mitochondrial components in EVs.

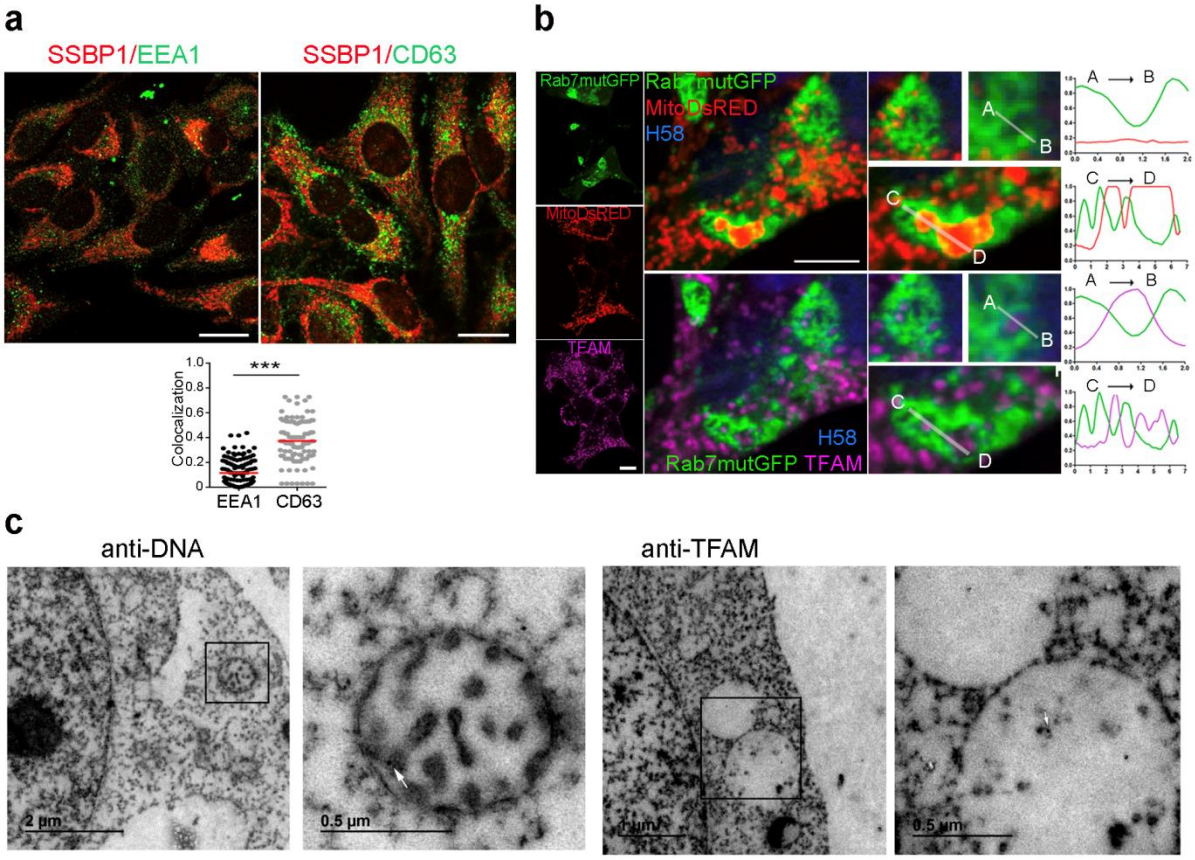

Figure R10. Mitochondrial components segregate into MVBs. (a) Confocal co-localization analysis in HEK293 cells treated with FCCP (4 h) and stained with SSBP1 (red), EEA1 and CD63 (green). Bar, 10 µm. Graph shows means for Mander's colocalization coefficient for SSBP1 and EEA1 or CD63 (n=3). t-test: ***P-value<0.0001. **(b)** Confocal co-localization analysis in HEK293 cells co-transfected with Rab7-Q67L-GFP (Rab7mutGFP, green) and mitoDsRed (red), and immunostained for TFAM (purple) and nuclei (HOECHST 58, blue). Center and right images show high magnification of left images (Rab7-Q67L-GFP and mitoDsRed in upper panels; Rab7-Q67L-GFP and TFAM in lower panels). Charts, Fluorescence profiles along the corresponding white lines. Bar, 10 µm. **(c)** Representative electron microscopy images showing DNA and TFAM immunogold staining in canonical multivesicular bodies from HEK293T cells transfected with the active mutant Rab7-Q67L-GFP.

5. Exosome secretion affects mitochondrial homeostasis

To further elucidate the nature of the vesicles containing mitochondrial components, we inhibited exosome biogenesis in T cells by targeting the neutral sphingomyelinase 2 (nSMase2, SMPD3) **(Figure R11a)**. This enzyme participates in exosome biogenesis by triggering the budding of intraluminal vesicles into MVBs [80]. These conditions reduced the recovery of exosomal proteins as well as mtDNA-binding proteins and mtDNA in the purified 100.000 ×g fraction **(Figure R11b)**, showing that mtDNA and mtDNA-binding proteins are released through canonical exosomal pathway and not in other EVs such as apoptotic bodies. The blocking of exosome biogenesis by silencing nSMase2 or MVB fusion with the plasma membrane by targeting Rab27a with specific shRNAs **(Figure R11a),** increased mitochondrial mass, intracellular TFAM levels, intracellular ROS, and DNA oxidative damage **(Figure R11c)**.

The suppression of nSMase2 or Rab27a altered mitochondrial morphology and cristae organization, with increased mitochondrial cristae width **(Figure R12a)**. Changes in mitochondrial cristae organization relate to changes in mitochondrial electron transport chain complex organization that in turn may result in functional changes in the respiration ability of cells. Specifically, tight cristae provide more efficient mitochondrial OXPHOS [190], whereas loose cristae appear in highly glycolytic cells [191]. Consistent with a loose organization of mitochondrial cristae, Rab27a and nSMase2 silencing significantly decreased mitochondrial respiration **(Figure R12b)**. These findings indicate that mitochondrial function is altered in the absence of proper exosome biogenesis and secretion and suggest that the release of mitochondrial content in exosomes contributes to mitochondrial homeostasis and mtDNA metabolism.

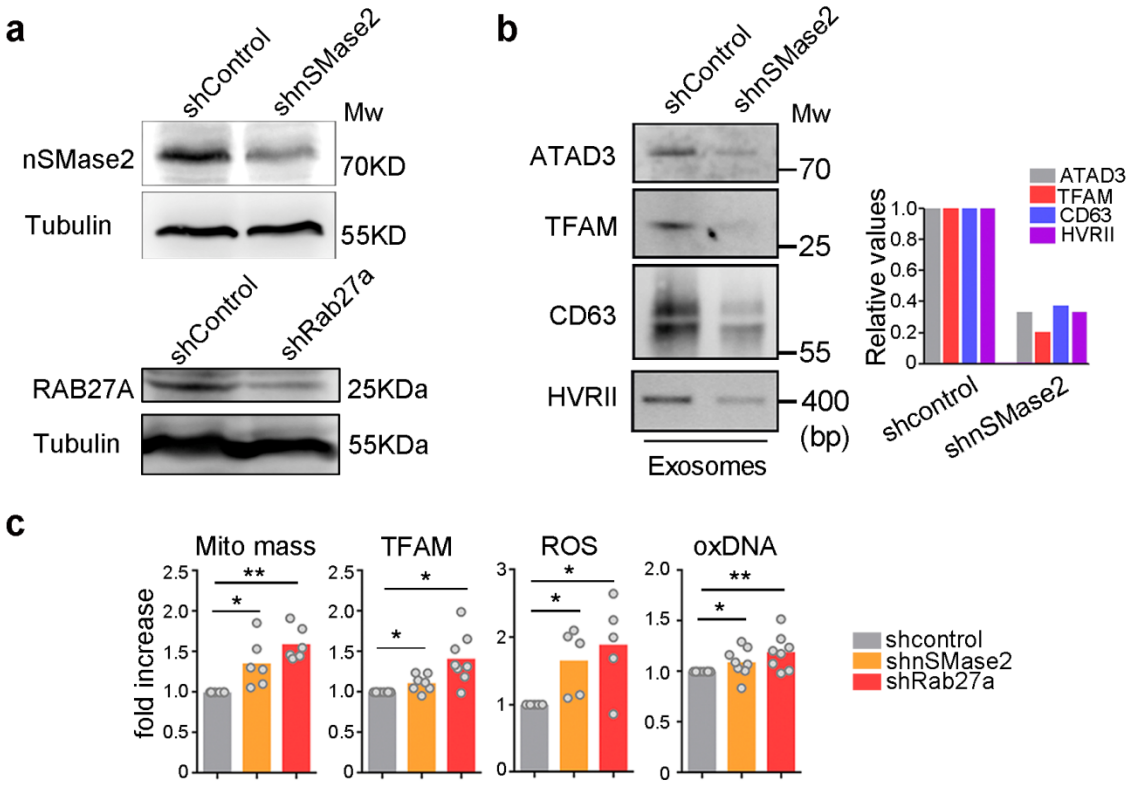

Figure R11. Exosomal secretion impairment affect mitochondrial parameters. (a) Up, Western blot analysis of nSMase 2 knockdown in J77 T cells infected with shControl or shnSMase2 shRNA. Down, Western blot analysis of Rab27a knockdown in HEK293 cells infected with specific shControl or shRab27a RNA. **(b)** Mitochondrial components in the exosome fraction obtained from equal numbers of shControl and shnSMase2 J77 T cells. ATAD3, TFAM, and CD63 were detected by immunoblot; mtDNA was detected by PCR for HVRII. Graph, Quantification of exosomal proteins and mtDNA in a representative experiment (n=3). **(c)** Flow cytometry analysis of mitochondrial mass (Mitotracker green), intracellular ROS levels (DCFDA staining), oxidized DNA (8-OHdG Ab staining), and endogenous TFAM in HEK293 cells knocked down for nSMase2 and Rab27a. Graphs, Quantification from 5-8 independent experiments (Mean). t-test *P-value<0.05; **P-value<0.001.

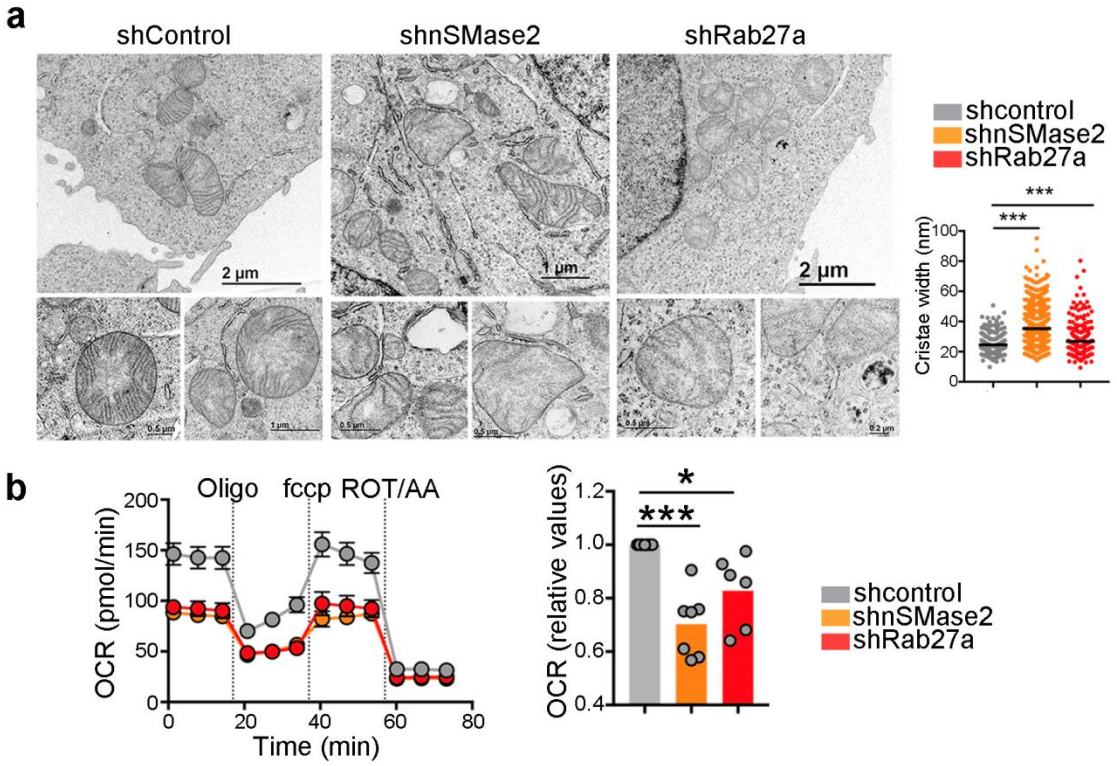

Figure R12. Exosomal secretion impairment affect mitochondrial organization and respiration. (a) Electron microscopy images show defects in mitochondrial ultrastructure and cristae organization in shnSMase2 and shRab27a HEK293 cells. Graph, Quantification of mitochondrial cristae width (Mean). t-test: ***P-value<0.0001 **(b)** Graph, Basal oxygen consumption rate (OCR) of control, shnSMase2 and shRab27a HEK293 cells. Dots represent mean from three independent experiments run in duplicate or triplicate. t-test, *P-value<0.05, ***P-value<0.0001. Chart, OCR from shControl, shnSMase2 and shRab27a HEK293 cells in response to oligomycin (Oligo), fccp, and rotenone plus antimycin A (Rot/AA). (n=2; mean ± S.E.M.)

We next investigated the contribution of mitochondrial turnover and degradation mechanisms to the secretion of mitochondrial components in EVs. Macroautophagy, from here on referred to as autophagy, is a self-degradation process that recycles cellular constituents, including misfolded or aggregated proteins and damaged organelles [192]. Confocal microscopy analysis did not reveal co-localization of autophagy proteins ATG5 and LC3 with MVBs or mitochondria **(Figure R13)**.

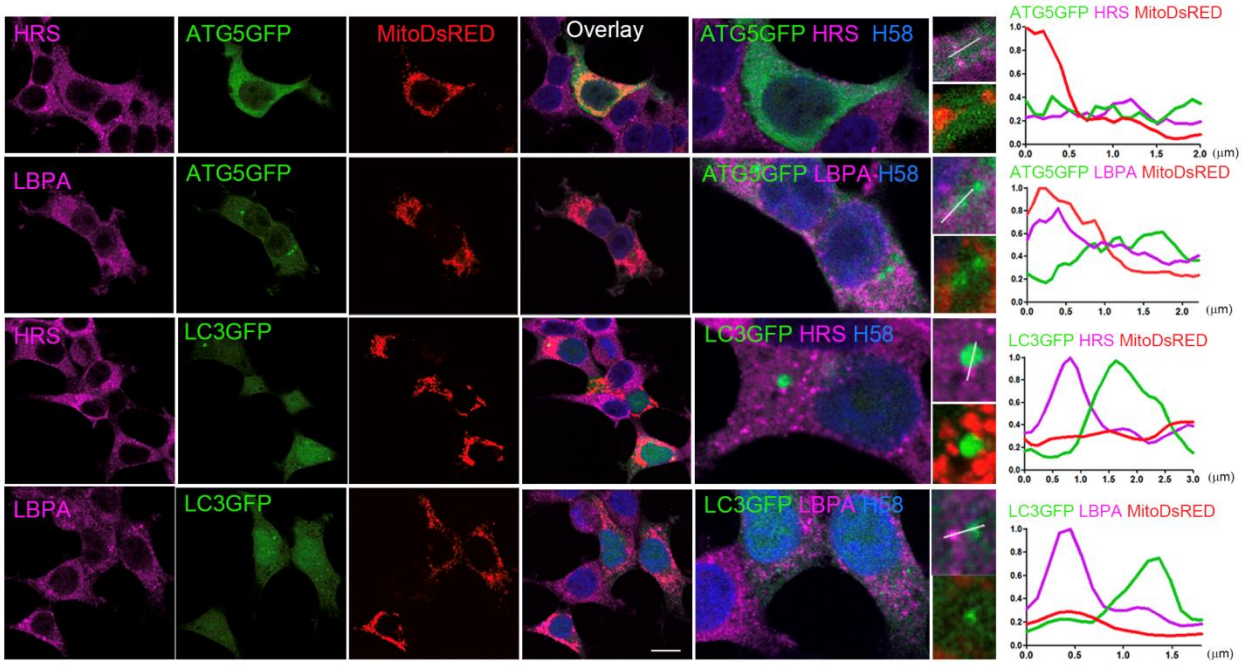

Figure R13. Colocalization of exosomal markers and autophagy proteins. Confocal co-localization analysis in HEK293 cells co-transfected with ATG5-GFP or LC3-GFP (green) and a mitochondria-targeted fluorescent protein (mitoDsRed, red) and stained with the endolysosomal compartment markers HRS and LBPA (purple) and nuclei with HOECHST 58 (blue). Right images show high magnification views of co-localization between ATG5/LC3 (green) and the various endolysosomal markers (purple). Charts show the fluorescence profiles along the corresponding white lines in the adjacent panels. Bar, 10 mm.

Serum deprivation, a reported autophagy stimulus, decreased exosome secretion concomitantly with reduced extracellular release of mitochondrial components **(Figure R14a)**, consistent with the autophagy-promoted specific degradation of MVBs [193]. Moreover, inhibition of autophagosome cargo degradation by bafilomycin-A1-mediated blockade of autophagosome-lysosome fusion did neither alter the detection of TFAM in the exosomal fraction nor the concentration and size of the purified EVs **(Figure R14a and R14b)**.

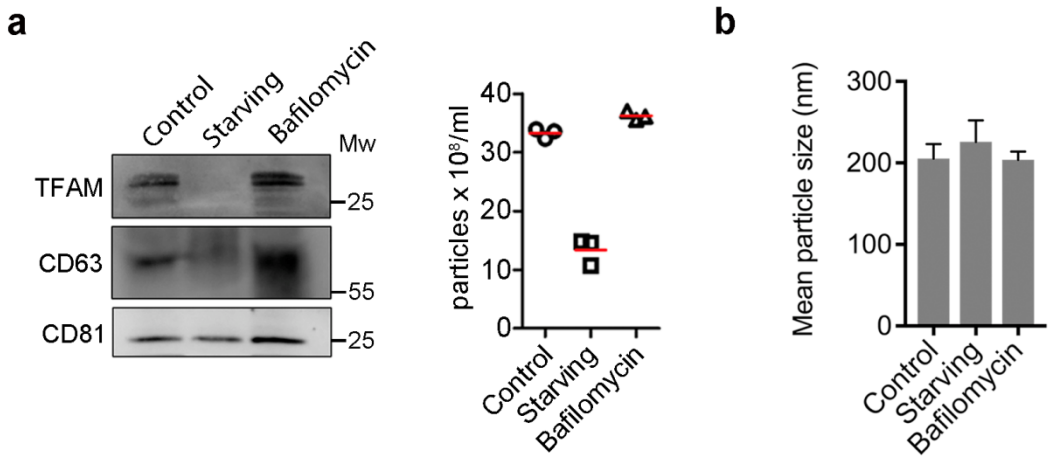

Figure R14. Autophagy is not responsible for the presence of mitochondrial content in exosomes (a) Western blot analysis of exosomes from Jurkat T cells left untreated, serum-starved overnight or treated with bafilomycin A. Membranes were blotted for TFAM, CD81 and CD63. Graph, Nanoparticle concentration in the exosomal fractions (mean, two independent experiments). **(b)** Size distribution analysis by Nanoparticle Tracking Analysis (NTA) of purified exosomes obtained from equal numbers of Jurkat T cells left untreated, serum-starved overnight, or treated with bafilomycin A.

This finding indicated that autophagosome secretion or content release upon bafilomycin-A1 treatment does not account for the presence of mitochondrial components in EVs. Additionally, specific siRNA silencing of the late autophagy mediator LC3 in J77 T cells did not alter exosome concentration and mitochondrial content **(Figure R15a and R15b)**. Together, these findings indicate that the loading and secretion of mitochondrial material in EVs occurs independently of general macroautophagy.

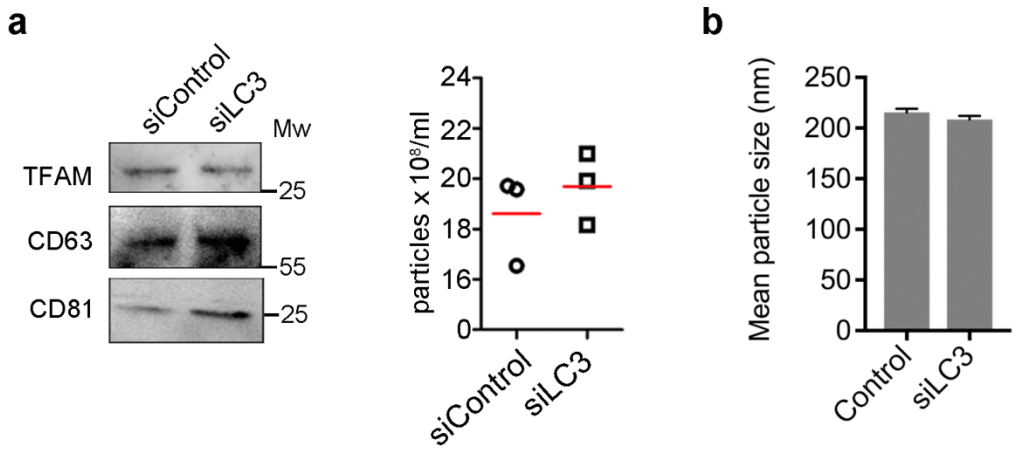

Figure R15. Autophagy is not related with mitochondrial containing exosomes secretion (a) Western blot analysis of exosomes obtained from Jurkat T cells transfected with control or LC3 siRNA. Graph, nanoparticle concentrations in the exosomal fractions (mean, n=2). Western blots are representative out of 3 independent experiments. **(b)** Size distribution analysis by Nanoparticle Tracking Analysis (NTA) of purified exosomes obtained from equal numbers of Jurkat T cells transfected with control siRNA or siRNA targeting LC3 from two independent experiments.

6. DNA and mitochondrial proteins are transferred at cognate immune contacts

The presence of mitochondrial constituents in exosomes led us to hypothesize that mitochondrial material could be transferred from the T cell to the APC during the formation of antigen-dependent contacts. To assess this, we first evaluated whether isolated exosomes shuttle mitochondrial components between cells. Purified exosomes from non-transfected J77 T cells or cells stably transfected with a mitochondria-targeted fluorescent protein, mitoDsRed, were added to Raji B lymphoblastoid cells, used as APCs. After incubation with exosomes from J77mitoDsRed cells, recipient cells exhibited mitoDsRed fluorescence **(Figure R16a)**.

We next assessed whether exosomes can mediate intercellular mtDNA transfer. Donor and acceptor cell mtDNAs were distinguished by the use of conplastic mice with the same nuclear genome (C57BL/6) but different mtDNA haplotypes, from the C57BL/6 mice strain ($C57^{C57}$) or from the NZB strain ($C57^{NZB}$) [194]. These two mtDNA haplotypes differ in 12 missense polymorphisms identifiable by restriction length fragment polymorphism (RFLP) analysis **(Figure R16b)**. Incubation of T cell-derived exosomes from $C57^{C57}$ mice with DCs differentiated

from the C57^{NZB} mice resulted in uptake of C57^{C57} mtDNA by recipient C57^{NZB} DCs, as shown by the acquisition of the C57^{C57} haplotype and the presence of C57^{C57} RFLP fragments in exosome-treated DCs **(Figure R16c)**, supporting the transfer of mitochondrial components and mtDNA between cells through exosomes.

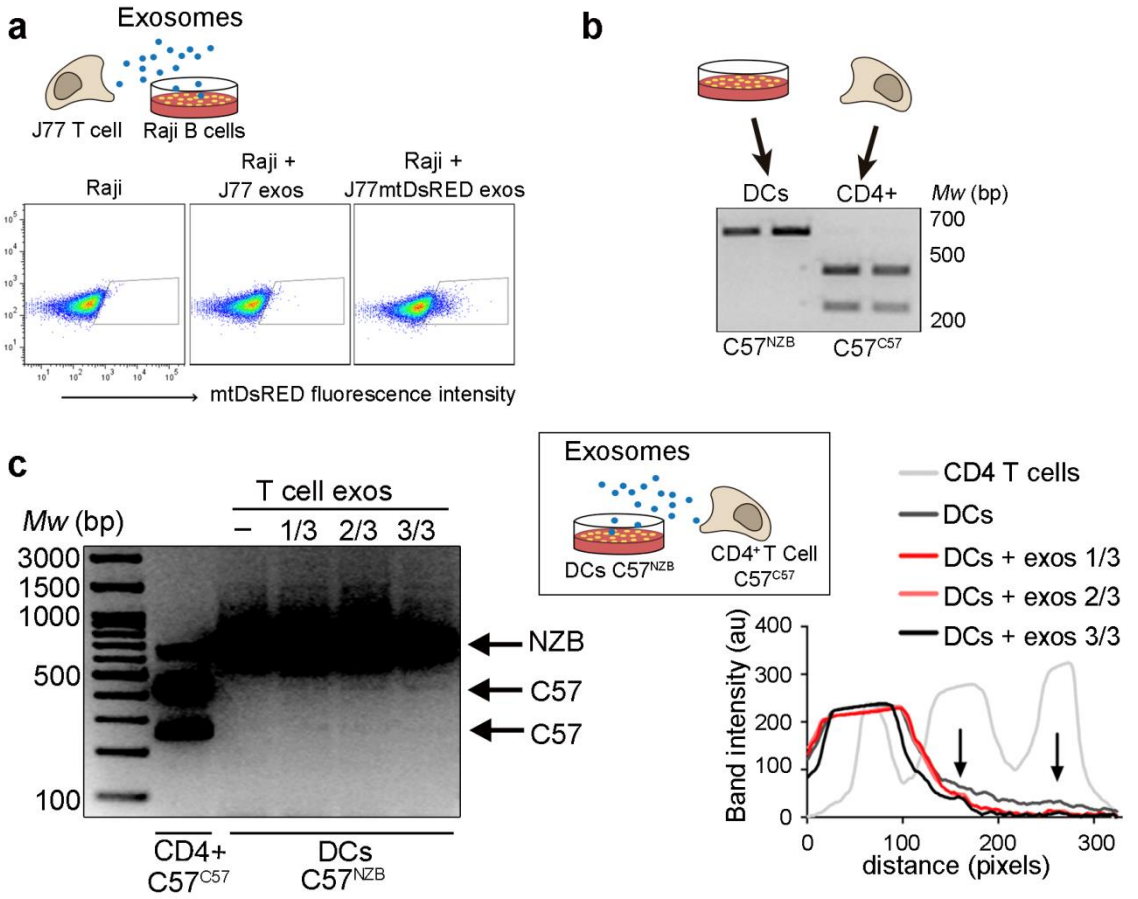

Figure R16. Mitochondrial proteins and DNA are transferred through exosomes to DC. (a) Flow cytometry analysis of Raji B cells incubated overnight with exosomes from J77 T cells control or stably expressing mitoDsRed (Representative experiment, n=3). **(b)** RFLP analysis of the mitochondrial genomes of C57^{C57} and C57^{NZB} mice. Total DNA is from C57^{C57} T lymphocytes and C57^{NZB} BMDCs. C57^{C57} haplotype results in 2 fragments. Digestion of PCR products from C57^{NZB} haplotype results in a single band. **(c)** RFLP detection of exogenous mtDNA in C57^{NZB} DCs incubated overnight with increasing amounts of exosomes from C57^{C57} CD4^{+} T lymphoblasts. 414 pb and 250 pb fragments appear in C57^{NZB} DCs upon addition of exosomes (lanes 1/3, 2/3 and 3/3). Chart, intensity profile of the RFLP analysis; arrows indicate the C57 mtDNA haplotype. C57^{C57} CD4^{+} lane displays a band of 664 pb which corresponds to an uncompleted digestion of the PCR product in the RFLP analysis and a high exposure of the image. Representative experiment (n= 3).

The mostly unidirectional nature of exosome transfer from T cells to DCs [55,132] suggested that the exchange of mitochondrial information between immune cells occurs upon antigen-dependent contacts. TCR Vβ8+ J77 T cells expressing a mitochondria-targeted fluorescent protein (mitoYFP) or a fluorescent version of TFAM (TFAM-DsRed) were co-cultured with Raji B cells preloaded with Staphylococcus enterotoxin superantigen-E (SEE), which mimics antigen recognition when confronted with TCR Vβ8+ T cells. Flow cytometry analysis revealed transfer of mitochondria (mitoYFP) and TFAM (TFAM-DsRED) from T cells to APCs during antigen-dependent interactions **(Figure R17)**.

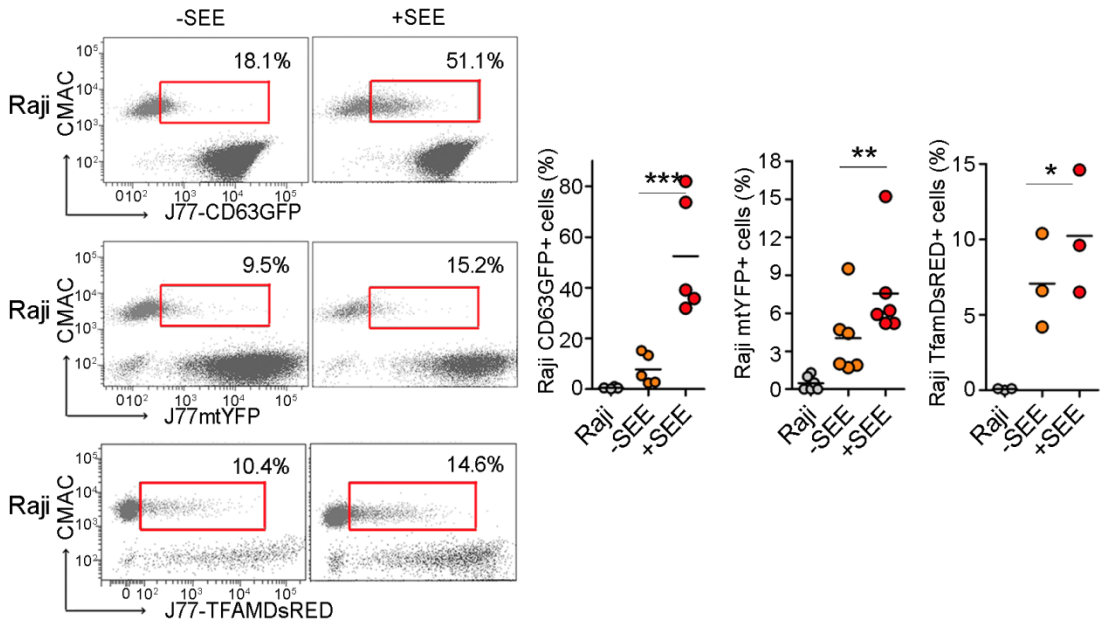

Figure R17. Exosomal and mitochondrial proteins are transferred upon cognate interactions. Exosome and mitochondrial transfer to unpulsed or SEE-pulsed Raji B cells (CMAC) from J77 T cells expressing the exosomal protein CD63GFP, the mitochondria-targeted mitoYFP or the mtDNA-binding protein TFAM-DsRED. Dot plots, cell populations after co-culture. Red boxes enclose Raji B cells that have acquired exosomal or mitochondrial fluorescent markers (percentage from total Raji cells). Graphs, percentage of Raji B cells acquiring fluorescence upon IS formation from 3-5 independent experiments; mean, t-test *P-value<0.05, **P-value<0.001, ***P-value<0.0001.

To address this in primary cells, we set up a model of antigenic presentation in which bone marrow-derived DC (BMDC) from $C57^{NZB}$ mice presented OVA peptide to CD4+ T cells from transgenic OT-II mice ($C57^{C57}$), which are specific for that antigen **(Figure R18a)** [194].

After 16h co-culture in the presence or absence of OVA peptide, we detected CD4+ T cell mtDNA only in recipient APCs from co-cultures including OVA peptide antigen **(Figure R18b)**, indicating that intercellular mtDNA transfer requires antigenic triggering. Using CD4+ T cells from OT-II $C57^{NZB}$ mice and BMDCs from the $C57^{C57}$ mice, we confirmed that mtDNA transfer occurred unidirectionally from T cells to BMDCs **(Figure R18c)**.

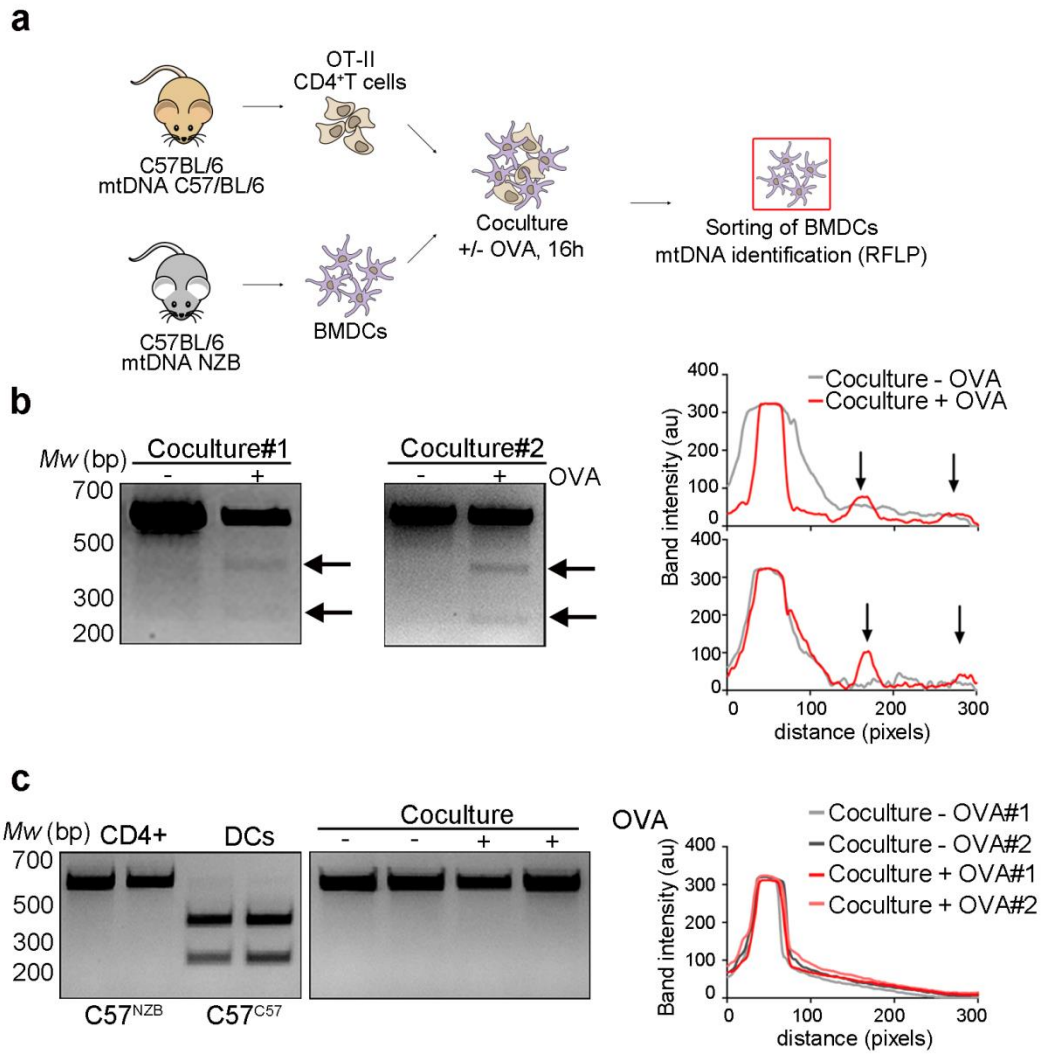

Figure R18. mtDNA is transfer during immune synapses. (a) Workflow for mtDNA transfer detection by RFLP during immune cognate interactions. **(b)** Detection of exogenous $C57^{C57}$ mtDNA from donor OT-II CD4+ T cells in recipient C57NZB DCs upon antigen stimulation (OVA). Gels, RFLP analysis of the mitochondrial genomes (n=2). Chart, intensity profile for RFLP. **(c)** RFLP analysis of the mitochondrial genomes of $C57^{C57}$ and $C57^{NZB}$ mice. Left gel shows RFLP analysis from $C57^{C57}$ T lymphocytes and C57NZB DCs. Right gel, lack of exogenous $C57^{C57}$ mtDNA from donor DCs in recipient $C57^{NZB}$ CD4+ T cells. Chart, intensity profile for RFLP analysis. Representative experiment (n=3).

7. Antiviral cGAS/STING-IRF3 pathway is activated upon exosome uptake

Mitochondrial components are a major source of danger-associated molecular patterns (DAMPs). They can trigger innate immune responses, likely due to their similarities to bacterial ancestors [195]. We hypothesized that the transfer of mitochondrial content and mtDNA during T cell-APC antigen-dependent contacts may represent a mode of cell-to-cell transmission of danger-associated messages. To examine this possibility, we interrogated which signaling pathways were controlled by T cell exosomes in recipient DCs. This was carried out by characterizing the changes to the gene profile of DCs upon incubation with T cell exosomes by RNA deep sequencing analysis **(Figure R19)**.

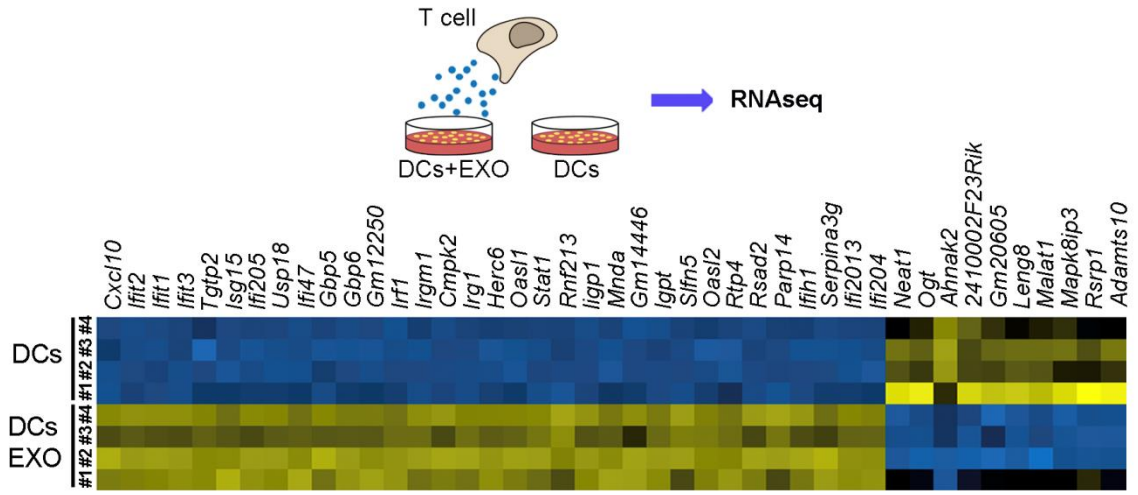

Figure R19. T cell exosomes prime DCs. Scheme explaining workflow for RNAseq analysis of DCs upon T cell exosome acquisition. Lower panel, RNAseq heat maps of 4 DC biological replicates with or without exosome uptake (DCs+EXO vs DCs). The panel shows upregulated (yellow) or downregulated (blue) genes with the highest significant fold changes.

Gene expression profiling identified more than 1600 significantly altered genes in recipient DCs exposed to T cell exosomes **(Figure R20a and R20b)**. Exosomes regulated the expression of a major set of genes involved in interferon (IFN) type I responses and antiviral activity, including IFN-stimulated genes (ISGs) Ifit1, Ifit2, Ifit3, Isg15, Usp18, and Cxcl10, and the antiviral signaling factors Gbp5 and Gbp6 **(Figure R19a)**. We validated the RNA sequencing results by quantitative PCR for the genes Cxcl10, Isg15, Ifit1, Ifit3, Usp18, and Stat1 **(Figure R20c)**.

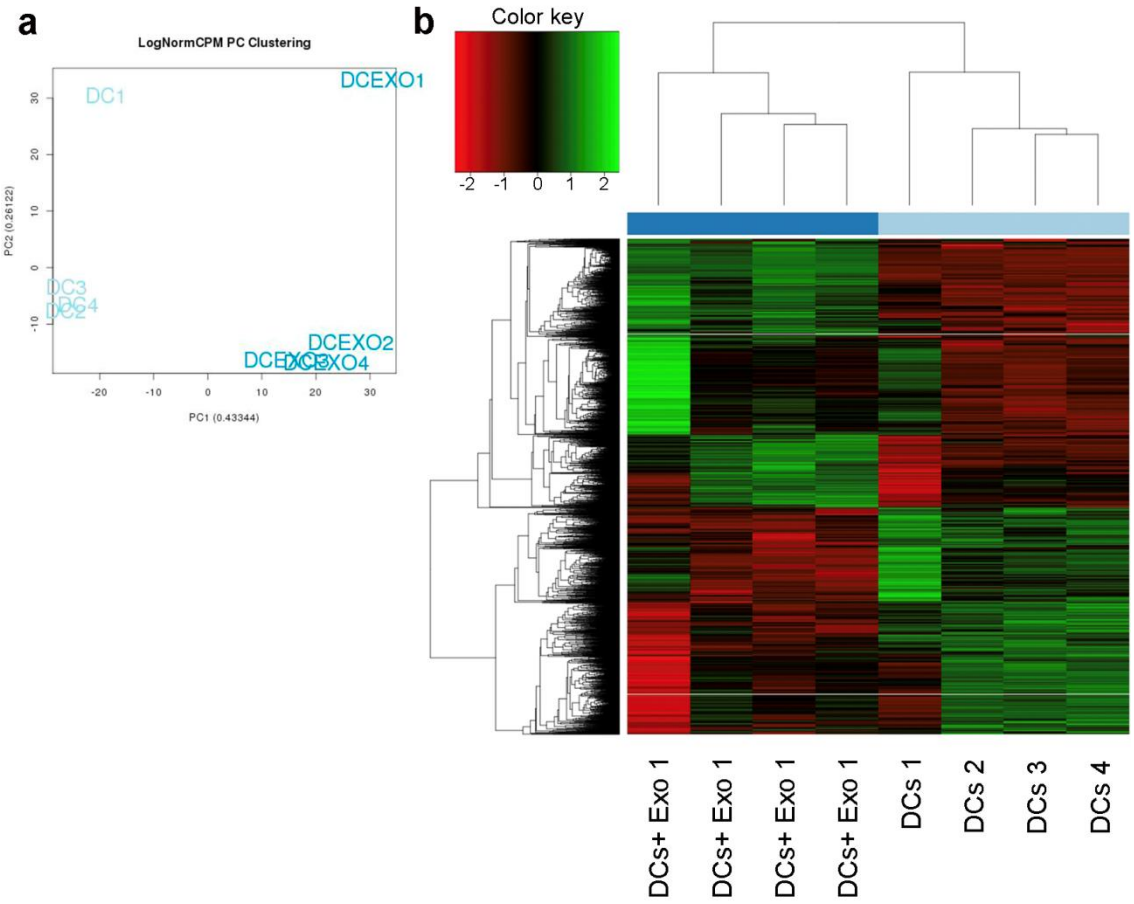

Figure R20. Bioinformatics analysis of the exosome-primed DC. (a) Principal Component Analysis (PCA) of the RNA samples obtained from 4 biological replicates of DCs and DCs incubated with exosomes. **(b)** Heatmap for the differently regulated genes in 4 biological replicates of DCs left untreated or treated with exosomes.

Analysis of the genes that changed their expression profile in response to T cell exosomes by Gene Ontology annotation indicated they were mainly involved in IFN signaling, exogenous DNA and RNA sensing, bacteria and viruses recognition, and crosstalk between innate and adaptive immune cells **(Figure R21a)**. These findings suggested that T cell exosomes prime the antiviral innate immune response in DCs, creating a gene signature that upregulates antiviral and antimicrobial responses to control pathogen infection and replication **(Figure R21b)**.

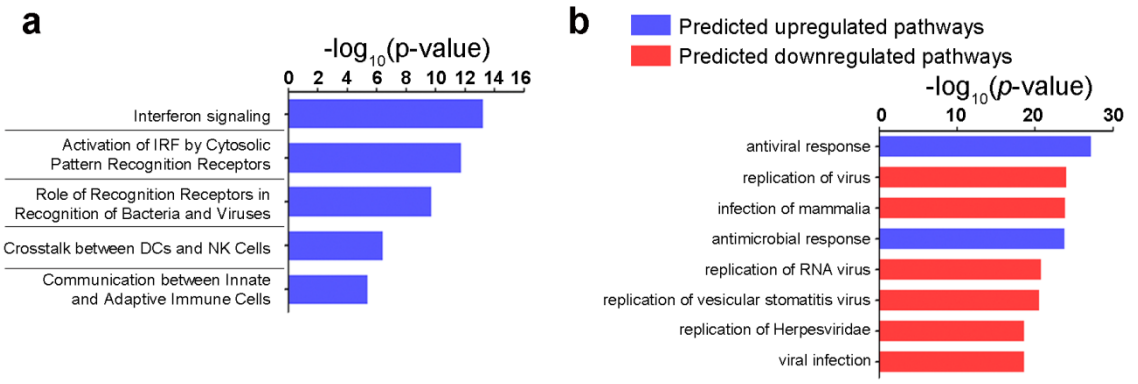

Figure R21. Pathogen defense pathways are upregulated in primed DC. (a) GO annotation of the biological processes differently regulated upon exosome addition; p-values are presented for the top-ranking biological processes. **(b)** Ingenuity analysis predictions of DC pathways upregulated or downregulated upon acquisition of T cell exosomes.

One of the most relevant pathways involved in ISG expression depends on cGAS/STING interaction upon cytoplasmic detection of endogenous or exogenous DNA [196]. cGAS functions as a main sensor of viral and bacterial DNA in the cytoplasm of infected cells. Upon its activation by DNA detection, it generates the second messenger cyclic dinucleotide cGAMP, which binds to and activates STING. STING in turn activates TANK-binding Kinase 1 (TBK1), which phosphorylates interferon regulatory factor 3 (IRF3) to promote its translocation to the nucleus, where it induces the expression of IFNγ and ISGs. Triggering of cytoplasmic DNA sensors is associated with intracellular clustering of STING [197]. Consistent with activation of the cGAS/STING DNA sensing pathway, exosomes induced a significant aggregation of STING in DCs **(Figure R22a)**. The expression of ISGs in response to exosomes was reduced in STING-deficient ($Sting^{Gt/Gt}$) DCs **(Figure R22b)**, and completely abrogated in Irf3-/- DCs **(Figure R22c)**.

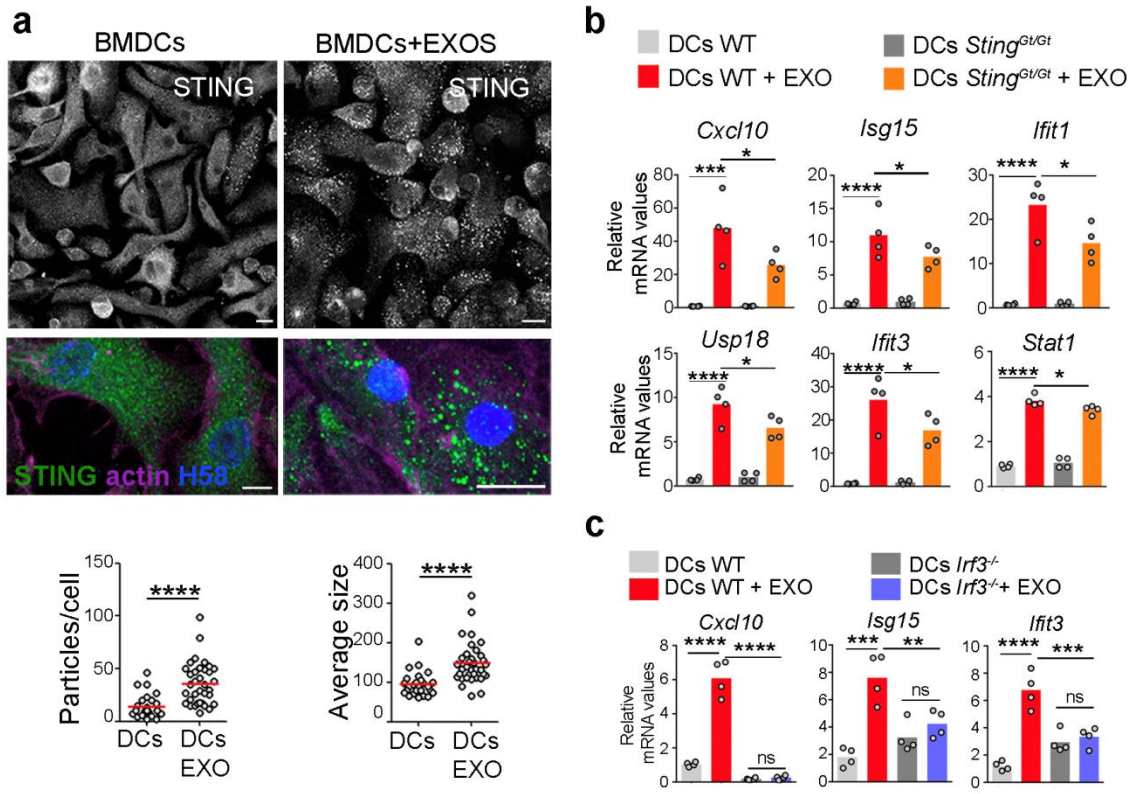

Figure R22. cGAS/STING DNA sensing pathway is partially responsible for the antiviral response signaling. (a) Upper panel, Immunofluorescence microscopy images showing STING aggregation (green) in DCs upon exosome addition. For clarity, DCs were stained for actin with phalloidin (purple) and for nuclei with HOECHST 58 (blue). Bar, 10 µm. Lower panel, Quantification of STING aggregate size and number upon exosome addition. Mean, n=26 (control), n=35 (STING), t-test ***P-value<0.0001 and ****P-value<0.00001 **(b)** Quantitative real-time PCR (qRT-PCR) of antiviral response genes in wild-type DCs and Sting$^{Gt/Gt}$ DCs upon exosome addition. **(c)** qRT-PCR analysis of antiviral response genes in wild-type DCs and Irf3$^{-/-}$ DCs upon exosome addition. Data (d,f) show quantification of mRNA levels of a representative experiment with four mice per genotype: t-test *P-value<0.05, **P-value<0.001, ***P-value<0.0001 and ****P-value<0.00001.

8. Antiviral signaling is triggered at least partially by DNA contained in exosomes

The role of exosomal DNA in triggering these responses was evaluated by treating exosomes with DNase. DNase treatment significantly reduced the ability of exosomes to trigger the activation of interferon-related genes in recipient WT DCs **(Figure R23a)**, suggesting that the DNA located in the outer surface of exosomes is important for full induction of antiviral responses in recipient cells.

To ascertain whether DNA located into the lumen of exosomes may also contribute to antiviral responses in recipient DCs, we genetically engineered a plasmid expressing DNase II fused to the intraluminal domain of the exosome-enriched protein CD63. qPCR analysis of isolated exosomes showed that exosomes from cells stably-expressing CD63-DNase II contain less mitochondrial DNA than exosomes from control cells stably-expressing wild-type CD63 (**Figure R23b)**. Exosomes from cells expressing CD63-DNase II triggered a lower antiviral response in recipient cells compared with exosomes obtained from CD63-expressing control cells **(Figure R23c)**. Overall, these results support that DNA on the surface and the inside of T cell exosomes can act transcellularly, i.e. in recipient DCs, to prime antiviral responses through activation of the STING-IRF3 DNA-sensing pathway.

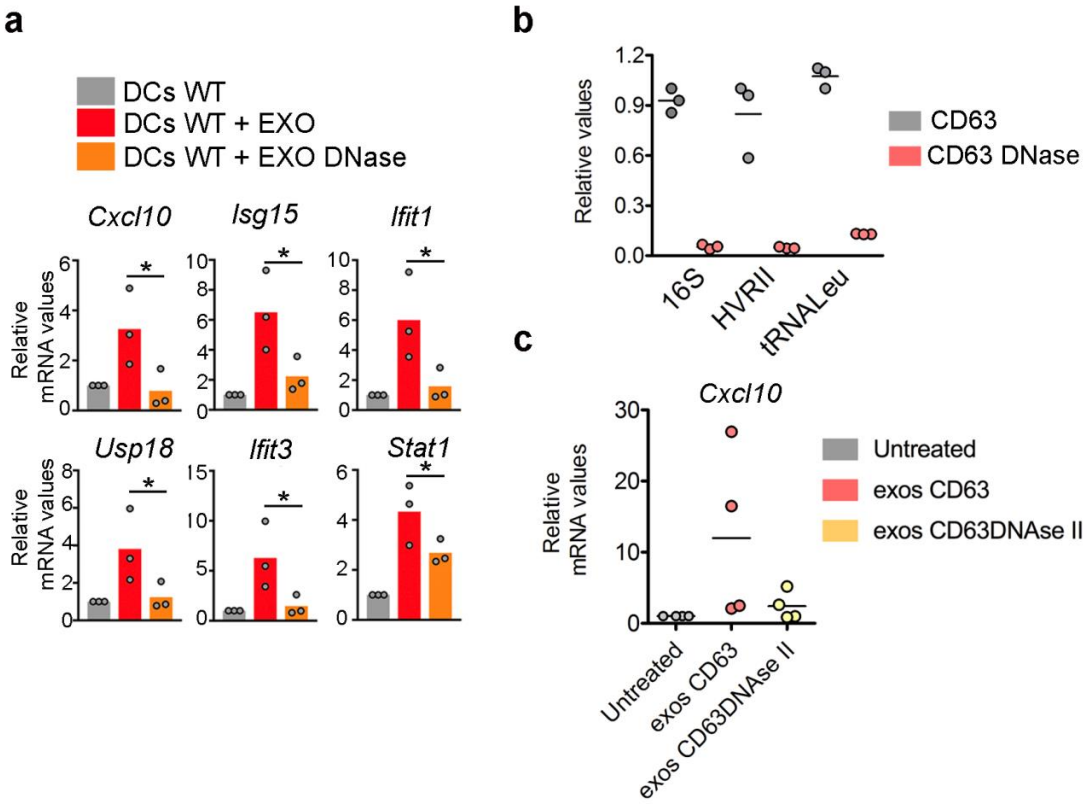

Figure R23. DNA is partially responsible for the antiviral response signaling. (a) qRT-PCR analysis of antiviral response genes in wild-type DCs upon addition of exosomes left untreated or pre-treated with DNase. Data shows mean from three independent experiments. t-test *P-value<0.05. **(b)** The level of mtDNA assessed by PCR amplification in EVs obtained from the culture supernatant of human HEK293 cells overexpressing CD63GFP or CD63 fused to DNase II. Mean. n=3. **(c)** qRT-PCR analysis of Cxcl10 in hDCs upon addition of exosomes from CD63GFP or CD63GFP-DNase II overexpressing HEK293 cells. Data show four independent experiments obtained from the culture supernatant of human HEK293 cells overexpressing CD63GFP or CD63 fused to DNase II. Mean. n=4.

9. DCs are primed by synaptic T-exosomes

We next assessed whether antigen-driven T-APC contacts trigger antiviral responses in recipient cells through the transfer of exosomal components. Gene expression analysis revealed that DCs upregulated ISGs upon immune cognate interactions with OT-II CD4+T cells **(Figure R24a)**. Control or SEE-pulsed Raji B cells were co-cultured with CD63GFP-expressing J77 T cells and then sorted according to the level of GFP-labeled exosome uptake **(Figure R24b)**. Raji B cells with higher acquisition of T cell exosomes showed more potent antiviral responses, as measured by their increased expression of Cxcl10 **(Figure R24c)**, supporting that exosome transfer during antigen-driven immune contacts primes antiviral responses in DCs.

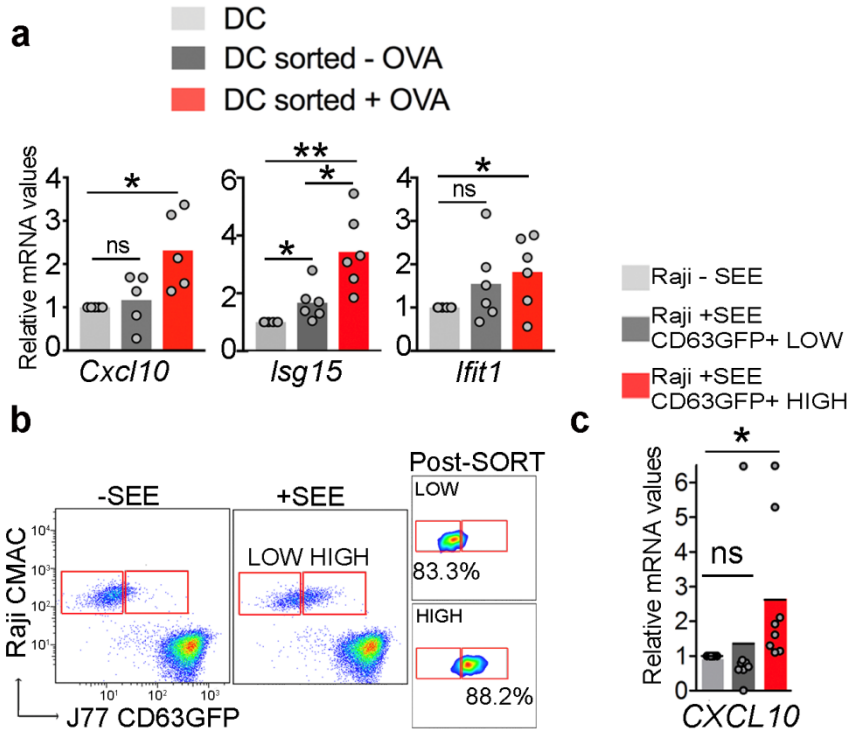

Figure R24. Cognate interations induce antiviral response in DC. (a) qRT-PCR analysis of the DC antiviral response upon antigen-dependent contacts. Gene expression was analyzed in sorted DCs after 16h conjugate formation. Data shows mean from five independent experiments. t-test *P-value<0.05. **(b)** Flow cytometry analysis of exosome uptake after co-culture of J77 T cells stably expressing CD63GFP with unprimed or SEE-primed Raji B cells. After immune interactions, Raji B cells (CMAC) were sorted according to the level of exosome uptake (CD63GFP content). Dot plots show the GFP signal in pre-sort and post-sort Raji populations. **(c)** Chart shows qRT-PCR analysis of Cxcl10 in low and high exosome uptake SEE-primed Raji B cell populations. Mean. n=3. t-test *P-value<0.05.

10. Primed DCs are more resistant to vaccinia infection

To assess the effect of exosome-boosted antiviral responses in recipient cells, we incubated DCs with T cell exosomes, infected them with GFP-expressing recombinant vaccinia virus, and monitored virus spreading and infection. Pre-incubation of DCs with T cell exosomes reduced viral infection, as measured by the number of vaccinia-GFP-positive DCs **(Figure R25)**.

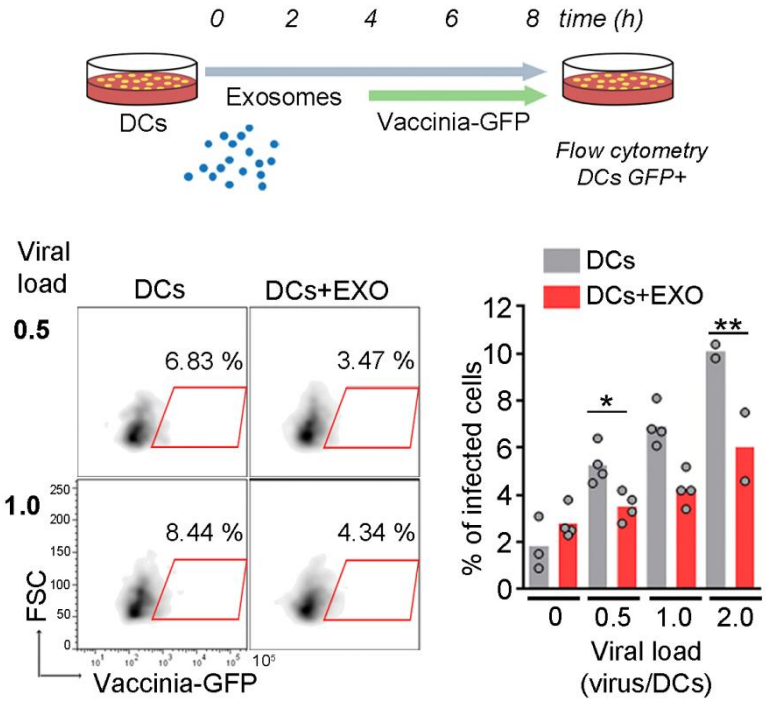

Figure R25. Exosomes protect primed DC against vaccinia. Upper panel, Time flow for the analysis of exosome-mediated antiviral protection. DCs were incubated for 4 h with T cell exosomes, infected with vaccinia-GFP, and analyzed for the level of infection by flow cytometry. Lower Left, Dot plots of DCs infected with vaccinia-GFP with or without exosome pre-treatment. Lower Right, Percentage of infected DCs at different viral loads with or without exosome pre-treatment. Mean; n=4; t-test *P-value<0.05, **P-value<0.01.

Antigen-dependent interactions between DCs and CD4+ T cells increased protection against further vaccinia virus infection of the DCs **(Figure R26a and R26c)**. This effect was dependent on T cell exosomes, since inhibition of their biogenesis by pretreatment of T cells with increasing concentrations of manumycin A, reduced DCs protection against subsequent viral infection **(Figure R26b)**, without interfering significantly with T cell viability and activation **(Figure R26c and R26d)**. Collectively, these results indicate that T cell exosomes delivered during antigen-dependent contacts boost inflammatory responses of DCs, protecting them against subsequent viral infection.

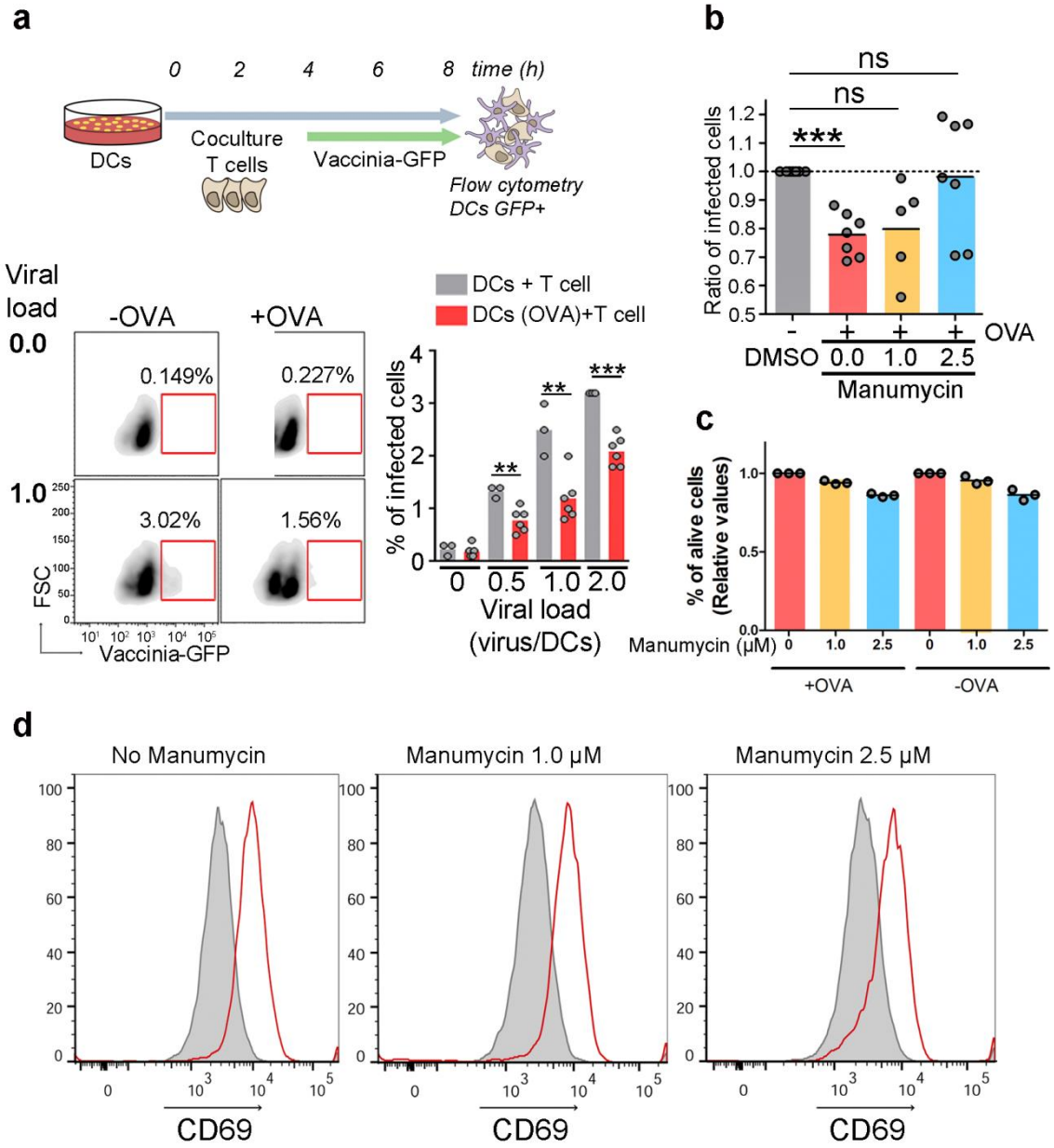

Figure R26. Antigen-driven immune interactions prime DCs to pathogen infection. Figure legend on the next page

Figure R26. Antigen-driven immune interactions prime DCs to pathogen infection. (a) Upper panel, Time flow for the analysis of exosome-mediated antiviral protection after immune cognate interactions. Unloaded or OVA peptide-loaded DCs were incubated for 4 h with $CD4^+$OT-II T cells, infected with vaccinia-GFP, and analyzed for the level of infection by flow cytometry. Lower Left, Dot plots of DCs (gated on CD11c) infected with vaccinia-GFP in the presence or absence of OVA peptide. Lower Right, Percentage of infected DCs at different viral loads in the presence or absence of antigen-dependent immune contacts. Mean; n=3-6; t-test *P-value<0.05, **P-value<0.01, ***P-value<0.0001 **(b)** Unloaded or OVA peptide-loaded DCs were incubated for 4 h with $CD4^+$OT-II T cells pretreated with increasing amounts of manumycin, infected with vaccinia-GFP, and analyzed for the level of infection by flow cytometry. Graph shows the ratio of infected DCs. Right graph, **(c)** Percentage of alive primary T lymphoblasts upon pre-treatment with increasing concentrations of manumycin for 2 h (vehicle = 0, 1 and 2.5 µM) and activation with OVA-pulsed dendritic cells for an additional 4 h period at a 5:1 ratio T cell: DCs. Manumycin was present during activation. Cell survival was measured by FACs, based on exclusion of DAPI staining. All values are relative to survival of non-treated cells. Mean percentage of T cell death was 13.8 % at maximal manumycin concentration. Data represent three independent experiments. **(d)** T lymphoblasts treated with manumycin for 16 h (vehicle = 0, 1 and 2.5 µM) and concomitant activation with anti-CD3 and anti-CD28 monoclonal Abs were stained with anti-CD69 as a measure of T cell activation. Histograms show a representative experiment out of four. No significant changes were observed in CD69 levels.

Discussion

Discussion

Here we present evidence highlighting a new pathway for intercellular communication during immune cognate interactions. Exosomes are crucial mediators for cellular communication; however, the mechanisms underlying the exchange of information are still unclear. In this study, we describe an immune cellular mechanism where mtDNA and mitochondrial components are loaded into exosomes that elicit a response in the antigen-presenting cell. The system for mitochondrial loading into multivesicular bodies is still undefined. We have shed light on how those two compartments influence functionally each other. In addition, our results show that upon non-related cognate encounters with T cells, primed dendritic cells are more resistant to viral infections. Knowledge of basic mechanisms that fine tune immune responses is relevant for future diagnostic and therapeutic applications.

1. Mitochondrial material is loaded into a specific population of extracellular vesicles

T cells secrete a great variety of EV. Depending on its origin they are classified in specific categories, i.e. microvesicles and exosomes. As previously mentioned, ILV are a mixed population of vesicles; when released by fusion of MVB with the plasma membrane the resulting exosomes are most likely a mixed population of vesicles with a common endosomal origin but different lipid and cargo composition [89,198].

Vesicle heterogeneity is evident when exosome synthesis and secretion is induced; for example upon activation of CD4 T cell some vesicle subpopulations increase significantly more than the other subpopulations, which indicates that T cells differentially regulate the release of distinct vesicle subpopulations depending on their activation status [199]. Inhibition of exosome release pathways does not affect all exosomal markers in the same way; for example Rab27 silencing decreases the secretion of classical markers such as CD63 or Tsg101, however it does barely affect CD9 release [198]. Genetic content of exosome subpopulations can vary as well; cancer cells secrete several types of exosomes and they differ on size and miRNA composition [200]. Moreover, vesicles secreted by the same polarized cell can vary depending on the subcellular localization where they are secreted [97–99,201]. For example, vesicles from polarized epithelial cells have different densities and co-fractionate with different exosomal markers depending on basolateral or apical secretion which are independent mechanisms [97]. Together, independent regulation of exosomal subpopulations and subcellular directed exosome secretion strongly suggests the existence of specialized mechanisms that control the selective

sorting of cargo into these vesicles and the transport of specific MVB repertoires to the membrane.

Taking into account that there are at least three mechanisms for ILV formation that act independently or coordinately, it is plausible that other mechanisms for vesicle formation exist and they are not yet described [80,202]. In Figure R4b and R6b we can observe a mild shift in the PCR product amplification and the proteins with mitochondrial origin respect from the classical exosomal markers. This may be due to slight differences in lipid composition between the **mitochondrial-containing extracellular vesicles** (mtExo) and vesicles containing classical markers which would change their density and thus their fractioning properties. In addition, there is only a partial colocalization of DNA and CD81 compared with complete co-localization for Tsg101 and CD81. These results suggest that although those populations share physical properties and their secretion is likely controlled by the MVB secretory pathway, they might differ in composition and probably in biogenesis. mtExo can be a subpopulation released by the fusion of MVB with the plasma membrane, but its origin could be different from the ILV which with they share space. They could even partially share lipid and protein composition and sucrose gradient could be insufficient to distinguish these two different populations.

At any rate, we frequently term exosomes those vesicles that precipitate upon ultracentrifugation at 100.000g. This pellet is enriched in exosomes, but it also may contain other EV and protein aggregates [203]. The greatest problem when studying EV is the difficulty in discriminating singular vesicles and in separating them in specific populations. Even when fractioning within a continuous band in the sucrose gradient, high density and low density subfractions from the "same" population differ in protein and RNA composition. Therefore, cells release distinct exosome subpopulations with unique compositions that elicit differential effects on recipient cells [204]. New technology is required to study in depth the different exosomal populations; only with single vesicle analysis we will be able to dissect the heterogeneous mechanisms of exosome biogenesis and secretion. A proof of concept for single vesicle microscopy is performed with TIRF microscopy techniques which allow us to challenge cells and observe individually fresh obtained vesicles, and then to classify them into subpopulations depending on their protein composition. Combined with single vesicle cytometry [205] and Omic analysis those techniques give us extra information about vesicles, using key markers to sort and analyze these enriched fractions [203].

We hypothesized that the selective secretion of mtExo is induced during T cell activation. This would imply that during cognate interactions an enriched population of exosomes containing mitochondrial components is secreted to the synaptic cleft achieving high concentration of vesicles in this confined space. This process makes possible a targeted delivery of exosomal components and the induction of a response in the antigen-presenting cell.

2. Pathway for mitochondrial content harboring into multivesicular bodies: Mitochondrial derived vesicles

Organelles are integrated into cellular networks regulating many cellular processes including metabolic interaction, intracellular signaling, cellular maintenance, regulation of programmed cell death/cell survival, and pathogen defense [206]. Apart from cytoskeleton, membrane contacts organize the position and motility of organelles. Examples of organelle interaction are mitochondria and endoplasmic reticulum contact sites (MERCs) [207], mitochondria and peroxisomes [208], mitochondria and lysosomes and autophagosomes [209,210]. In addition, the endosomal system directly interacts with mitochondria [211–214]. These contacts are dependent on Drp1, a mitochondrial fission protein present in both organelles [209]. However, there is still much to know about these complex networks.

We have found that mitochondria and multivesicular bodies are tightly linked, since disruption of the endosomal pathway also impairs mitochondrial homeostasis. Specifically, there is an increase in mitochondrial mass and in ROS, and a decrease in mitochondrial OXPHOS. In addition, when a constitutively active isoform of Rab7 was expressed in cells we detect a great accumulation of mitochondrial components inside the enlarged late endosomes. Moreover, we observe a preferential co-localization of mitochondrial proteins with components of the late stages of endosomal pathway. When cells are challenged with the uncoupler FCCP, that causes mitochondrial damage, we detect a higher localization of mitochondrial components within late endosome than within early endosomes. Our observation that mtDNA and mtDNA-binding proteins load into EVs in an autophagy-independent manner indicates the existence of an additional targeting mechanism to the MVB. The role of mitochondrial component release as a danger indicator to surrounding cells is well documented [195].

Our data suggest that the MVB endosomal route can target these components actively into exosomes. Although the signals that mediate the loading and incorporation of mitochondrial components into late endosomes/MVBs remain unidentified, an attractive possibility is that small organelle fragments containing mitochondrial nucleoids might bud toward the cytosol depending on their oxidative status, and would be subsequently loaded and incorporated into the endolysosomal compartment for their degradation or secretion. Cytosolic accumulation of mtDNA has been described following mitochondrial dysfunction and inflammatory stimulation [195,215], and a similar process may operate in the release of mtDNA to the cytoplasm and its subsequent incorporation into ILVs during MVB maturation.

Mitochondria is a highly compartmentalized organelle; release of mitochondrial components into the cytosol usually involves strong signaling in cells in an autologous manner [167]. Loss of mitochondrial permeability leads to Cytochrome c release and Caspase activation that ends in apoptosis; it is likely that mitochondrial loading into ILV is mediated by a highly regulated mechanism that protects the secreting cell from signaling of free mitochondrial content in cytosol [216].

Alternatively, we propose that mitochondrial cargo is delivered into MVB through a relatively new described mechanism. This system does not require mitochondrial depolarization, autophagy signaling or mitochondrial fission [217] and it would be a safe way to deliver dangerous material without damaging the secreting cell. It has been recently shown that small vesicles, called mitochondrial-derived vesicles (MDV), with a size ranging between 60-100nm bud out from mitochondria. MDV connect mitochondria with other organelles and transport mitochondrial components into lysosomes, peroxisomes and MVBs. MDV are essential for the correct homeostasis of mitochondria and help to get rid of unwanted material that can damage the organelle [218,219]. PINK1 and Parkin are some of the described proteins involved in the formation of MDV [220]. We postulate that they might participate in the loading of mitochondrial components into exosomes by fusion with MVB [217,221] and instead of being degraded by lysosomes, MVB could fuse with plasma membrane release a mix of bona fide exosomes together with MDV **(Figure D1)**.

However, we found that the loading of mitochondrial cargo into exosomes is independent of autophagy. In the same manner, MDV transport to lysosomes is ATG5 and LC-3 independent [217], which would support that even silencing autophagy MDV fuse with MVB and mtExo are still secreted.

This model would also explain why we detect separate vesicles containing DNA or exosomal markers such as CD81 by TIRF microscopy. Considering their similarity in size and their endosomal pathway dependence, we can be obtaining two different populations of vesicles in our samples and mixing them due to the lack of resolution of current available techniques.

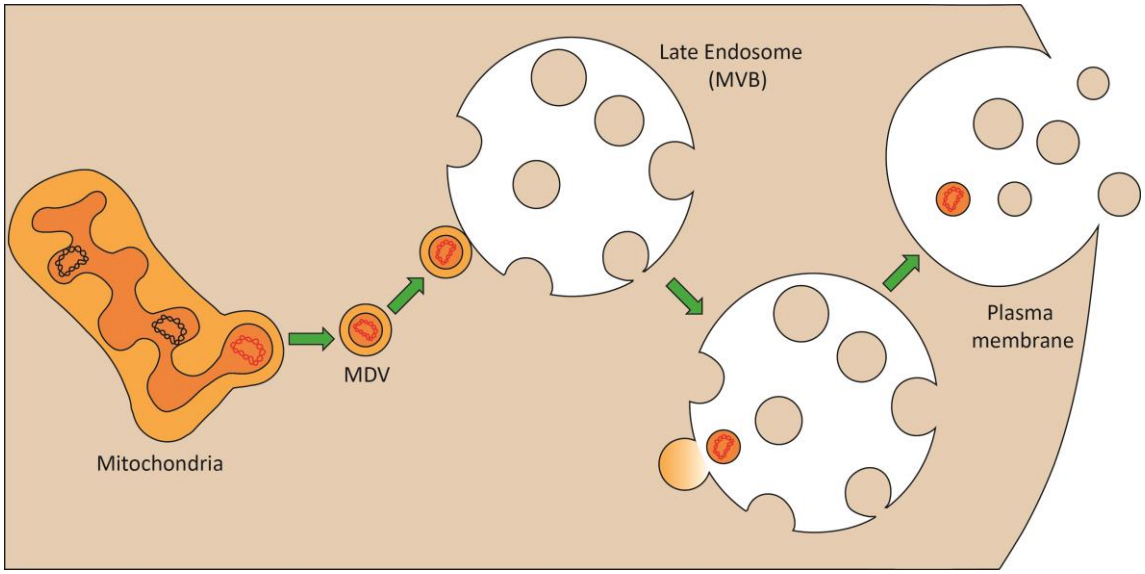

Figure D1. Proposed model for mitochondrial cargo loading into MVB. Mitochondrial-derived vesicles are extruded from mitochondria carrying oxidized cargo (in red) and unfolded proteins. After they fuse with late endosomes MDV release their single membrane cargo into MVB. After maturation MVB fuse with plasma membrane secreting single-membrane MDV and bona fide exosomes to the extracellular media.

3. Physiological cause for mtDNA release in exosomes

Exosomes were first described in reticulocytes[54,222]; initially they were proposed to represent cellular waste [223]. Nowadays, it is clear that apart from being and alternative way of releasing waste product they are essential for maintaining cellular homeostasis and for cell-cell communication [56,104]. We have addressed the role of mitochondrial-containing extracellular vesicles in the T cell-DC interaction; however, there are still several unknown issues in the secretion of mitochondrial content at the T cell side.

In some specific cases, mitochondrial transfer allows the exogenous replacement of damaged mitochondria, thereby rescuing mitochondrial defects [154]. However the effects of mitochondrial release in the secreting cell is not totally understood. The dynamics of mitochondrial networks and their selective degradation or biogenesis maintain a healthy mitochondria repertoire. Constant cycles of fusion and fission promote the intermixing and

homogenization of mitochondrial proteins, lipids and DNA between discrete organelles within the same cell [151]. The selective depletion of mitochondria through mitophagy eliminates deleterious mitochondrial mutations in heteroplasmic cells, restoring ATP levels and mitochondrial function [224–226]. Therefore cells need ways to get rid of damaged mitochondrial material. Mitophagy requires several cell resources and it is an energy consuming process once activated. Even though mtDNA can be degraded by the replication machinery [227] o by autophagy [228], there are other mitophagy/autophagy-independent pathways for degrading the damaged mtDNA that are still elusive. Moretton and colleagues described that there is a rapid loss of mtDNA upon a massive double strand break in mitochondrial genome which is neither dependent of exo/endonucleases nor autophagy [229]. The mode of mtDNA degradation may be determined by the cell type and oxidative stress [230]. Releasing damaged or aged mtDNA through the endosomal secreting pathway can be an appealing system to release stress or mtDNA double strand breaks without the need of starting a mitophagy program. Indeed, genomic DNA damage increases exosome secretion in a p53 and TSAP6-dependent manner [231]. Retention of damaged and oxidized mitochondrial components into the mitochondria is extremely harmful for cell homeostasis. Degradation of mitochondria by autophagy represents an extreme attempt to maintain cell homeostasis, although there are other mechanisms to maintain mitochondrial quality control in steady state or mild damage. Mitochondrial cargo release through MDV can be a way for releasing stress and protect cells from entering in mitophagy [219]. Therefore, exosome secretion could be a pathway for cell stress relieve [232]. As a matter of fact, there are more exosomes in the plasma of virus-infected individuals, where mitochondrial proteins are overrepresented and that contain markers of metabolic and mitochondrial stress [233]. Our results demonstrating the presence of oxidized DNA in exosomes suggest that these EVs may cooperate to manage cellular damage by releasing mitochondrial proteins and oxidized-DNA, acting as an “escape valve” to partially expel mitochondrial damage outside the cell. Recently, a role for exosomes in the secretion of harmful genomic DNA has been documented [104]. Damaged mtDNA is loaded in exosomes of epithelial cells and released to the extracellular media [234]. Supporting this role for exosomes in the preservation of cellular homeostasis[235], we found that inhibition of exosome biogenesis or secretion impair mitochondrial structure and function. A recent study identified that under stress conditions Caenorhabditis elegans secretes large vesicles containing protein aggregates and organelles for maintaining mitochondrial homeostasis and quality control [236]. Upon cell stress, MDV are preferentially loaded with oxidized cargo; the presence of oxidized mtDNA in exosomes also supports that this subpopulation of vesicles comes from a MDV origin and helps mitochondria homeostasis **(Figure D1)** [237].

Our working hypothesis is that mtExo are used as a signal to alert about the status of the donor cell to the surrounding cells by playing a dual role; on one hand, protecting the donor cell from mitochondrial dysfunction and, on the other hand, alerting receptor cells from a potential damage in the local environment. Whereas exosomes facilitate the secretion of harmful or damaged mitochondrial components and sustain mitochondrial function is a possibility that warrants further investigation.

4. Functional mtDNA delivery in antigen presenting cells

The immune synapse only covers the 20% of cell membrane and still it is a platform for cellular communication; clear examples are receptor signaling, cytokine secretion and induced cytolysis. There is no need for high amounts of messenger secretion to mount a response in the receptor cell. The encapsulation of signaling molecules inside the synaptic cleft allows reaching relative high concentrations of molecules that can trigger the signaling. Exosomal secretion inside the synaptic cleft grants high relative levels of EV per surface, which probably makes possible the induction of complete antiviral responses in the APC. However, the functional delivery of exosomal cargo into receptor cells is still not fully studied.

Exosomes allow functional delivery of genetic material to receptor cells. Specifically, miRNAs loaded in exosomes reach acceptor cells and repress target mRNAs [55,113]. In addition, cells can also secrete genomic DNA that is uptaken by recipient cells and translocated to the nucleus where it recruits nuclear factor κB (NF-κB), and is transcribed. In agreement with our data, DNA was shown to be within the exosomes rather than exposed outside [238]. Furthermore, genomic DNA delivery is functional since the exosomal delivery of the mutated gene H-Ras stimulates proliferation in recipient cells [239]. Finally, mitochondrial genes have been reported to be transferred through vesicles [234,240]. Although widely observed in prokaryotes, horizontal gene transfer (HGT) is in general a rare phenomenon in metazoans. However, HGT in eukaryotes might be less rare than previously anticipated [241]. HGT between species of Saccharomyces has been postulated during the evolution of modern yeast species [242]. Likewise, asexual bdelloid rotifers have experienced extensive HGT from non-metazoan genes [243], which might have compensated the lack of genetic heterogeneity due to the absence of sexual recombination [244]. One interesting example is the horizontal transfer of entire genomes via mitochondrial fusion in the angiosperm Amborella. Specifically, Amborella mtDNA includes a diverse collection of foreign sequences corresponding to about six genome equivalents of mtDNA acquired from mosses, angiosperms and green algae [245]. One of the first evidence of in vivo horizontal mitochondrial gene transfer was found in a transmissible canine venereal tumor (CTVT), which is a highly adapted form of cancer that is transmitted as an

allograft during mating of feral dogs. Phylogenetic evidence supports that CTVT cells periodically acquire mitochondria from their hosts to support long-term survival. Gene transfer events might rescue CTVT mitochondrial function, allowing the tumor to overcome the high mutation rate that would promote the accumulation of deleterious mutations in their own mitochondria [246].

Transfer of entire mitochondria between cells or acquisition of mitochondria from the environment in a functional and transmissible way has been demonstrated in culture cells [152,247,248], and in vivo in a cancer context [157,246,249]. Recent reports suggest that the intercellular transmission in vivo of mitochondria and/or mitochondrial components exerts a beneficial effect on the recipient damaged cells [153–155]. The benefits in all cases are attributed to the assumption that entire healthy functional mitochondria travel and colonize the recipient cells. However, the use of interspecies mix for donor cells in some cases and the lack of evidence of long lasting colonization of the recipient cells by the foreign mtDNA question this interpretation. The role of the intercellular transmission of defined mitochondrial components and specifically mtDNA as part of a complex intercellular signaling mechanism, raises the possibility that the observed beneficial effects of transmission of mitochondrial components would be consequences of activation of survival pathways rather than the transmission of fully functional organelles able to colonize the recipient cells. This could, for instance, explain the positive effects of interspecies (human/mice) experiments, since the interspecies incompatibility between nuclear and mtDNA is well described. In this study, we have shown that mtDNA is completely represented in the exosomal fraction, although we have not clarified the integrity of this genetic material. Our results indicate that there is a functional delivery of mtDNA to recipient cells upon cognate interactions. Interestingly, this transfer occurs in an unidirectional manner, from the T cell side to the APC side, as it was previously reported with other exosomal markers [55]. Nonetheless, we do not address whether whole mitochondria are transferred and whether this exchange could restore impaired mitochondrial respiration. Due to the size of exosomes and the minimal dimension of a functional mitochondrion it is not probable that entire functional units are transferred. However, if complete copies of mtDNA integrate in the mitochondria of receptor cells, it could be sufficient to replicate and restore respiration and mitochondrial functions. In fact, horizontal transfer of mtDNA occurrs in cancer cells, associated with increased self-renewal potential of these cells and tumor-initiating efficacy [157]. Cancer-stem like cells secrete extracellular vesicles carrying full mitochondrial genome, which induces exit from metabolic dormancy of other tumor cells [240]. Nevertheless, authors did not characterize properly the EV, which are probably are bigger vesicles than

exosomes, such as microvesicles. In other study, using an ImageStream imaging flow cytometer for single particle analysis, different sized extracellular vesicles from bronchoalveolar lavage contained mitochondrial components that were delivered and internalized into the mitochondrial network from the receptor cells and changed their pro-inflammatory function [234,250]. Islam and colleagues have described that mitochondria are transferred from bone-marrow-derived stromal cells to pulmonary alveoli in a connexin 43-dependent manner [155]. In addition, connexin 43 located in exosomes forming hexameric channels, facilitate the delivery of heterologous DNA and the exosomal uptake by target cells [115]. Together, these results reveal a possible mechanism for functional DNA delivery to the target cell where DNA could change its metabolic pattern or trigger inflammatory signalling. The mechanisms determining whether DNA is degraded, exported to the cytosol or integrated in the corresponding organelle are still elusive.

Finally, we describe a mouse system comprising two different haplotypes that can be differentiated by RFLP which is a suitable model for tracking mitochondrial effective transfer trace back. This model can be used for many exosomal transfer applications; it would be interesting to ascertain whether in a heteroplasmic cell an haplotype is predominantly selected and if the other is secreted via exosomes as a way to releas stress [194,251,252]. Finally, it would be interesting to deep in the transfer of healthy mtDNA to dendritic cells containing damaged DNA and study whether a healthy phenotype is recover or not. Thus, a clear understanding on the mechanisms mediating mitochondrial transmission will shed light on how mitochondrial transfer is regulated and can be exploited for therapeutic purposes.

5. Antiviral response induction upon exosome uptake in dendritic cells

Our results show the specificity of the type of cellular response evoked by the DNA packaged into EVs: type I IFN response and expression of ISGs. Although nuclear DNA is the main endogenous ligand for cGAS, growing evidence indicates a role for mtDNA as a ligand for cGAS in certain conditions. Mitochondrial DNA as well as other mitochondrial constituents such as N-formyl peptides (NFPs), mitochondrial lipids such as cardiolipin, or nuclear-encoded mitochondrial proteins, can elicit a local or systemic innate immune response in conditions of massive episodes of cell damage [195]. Intriguingly, mtDNA can also be released in a rapid, 'catapult-like' manner by neutrophils to create ‘extracellular traps’ that exert antibacterial activity and activate the release of pro-inflammatory cytokines [176,253]. In this regard, secretion of interferogenic mtDNA by neutrophils in systemic lupus erythematosus (SLE) patients contributes to disease by activating the production of potent IFN type I responses [173,254].

Likewise, lymphocytes eject interferogenic mtDNA webs in response to CpG and triggers antiviral signaling in monocytes [255]

The Intracellular accumulation of mtDNA molecules in the cytosol upon mtDNA stress has been also shown to activate type I IFNs response through the cGAS/STING pathway [167], contributing to the acquisition of an antiviral state. Our results demonstrate that in DCs, the DNA present in EVs activate type I IFN responses and expression of ISGs. The contribution of cytoplasmic sensors, e.g. STING, appears to be only partial, and other DNA receptors localized at the endosome or the plasma membrane could also detect the DNA present on the surface or the lumen of EVs and activate interferon-response factors, thus contributing to the induction of a potent antiviral response. Then, understanding which sensors or receptors detect the DNA transported in EVs; and whether the mechanisms (endocytosis, phagocytosis, back-fusion of endosomes) by which vesicular content is acquired by recipient cells affect DNA responses are questions that deserve further investigation. In this study, we have found that the DNA-sensing responses were abrogated in an IRF3-dependent manner. Also, elimination of exosomal DNA, either by DNase treatment or overexpression of DNase II fused to the intraluminal domain of the exosome-enriched protein CD63, significantly reduced the expression of antiviral related genes. However, we cannot rule out the contribution of other EVs constituents in triggering innate immune signaling in DCs. For example, Tfam serves as a danger signal that augments DNA signaling in plasmacitoid dendritic cells [256]. Another possibility is that mtDNA present in vesicles signals through different pathways; specifically, mtDNA associates with Z-binding protein (ZBP1), which recruits the TANK-binding kinase 1 (TBK1) and interferon regulatory factor 3 (IRF3). Those factors migrate to the nucleus and activate an inflammatory response in a STING independent manner [234]. Finally, vesicles containing mtDNA can also activate other pathways such as the inflammasome [257]. Therefore, signaling coming from mtExo are most likely conformed by mixed pathways that overall display a combined inflammatory response

6. Physiological purpose of DC priming

Besides the well-characterized role of IS in instructing T cell activation, it also transmits intracellular signals to the DC side [258]. Upon IS formation, the DC rapidly increases the concentration of MHC class II molecules on the membrane of the synaptic contact to strengthen antigen presentation to cognate T cells [259,260]. DC cytoskeleton undergoes substantial rearrangements during IS formation, allowing the polarization of different compartments such as endosomes and mitochondria [141]. MTOC relocation also grants polarized cytokine secretion [261].

The establishment of immune cognate interactions between T cells and APC is a key element of T cell activation, i.e. the conversion of naive T cells into effector cells, leading to the efficient clearance of pathogens through the adaptive arm of the immune response. This study demonstrates that this signal displays retrograde feedback, in which the T cell imposes additional changes to the activity of the APC, priming those post-synaptic DC (psDC) to respond better in the case of subsequent infections by the same pathogen, or a similar one. We have also identified EVs as the vessels of the information that triggers these changes in DCs, promoting an antiviral response with induction of IFN-related stimulated genes. A key observation is that these effects require antigenic stimulation. This is crucial because it ensures that the acquisition of inflammatory (or antiviral) traits is limited to situations in which a specific stimulus, i.e. the pathogen, is triggering these responses. It also has the potential to drastically alter the fate of the DC. DC supposedly die in lymph nodes after cognate interactions. This is based on evidence of the onset of autoimmune disease when DC apoptosis is inhibited [262]. We postulate that, even if DC are eliminated after activating naive T cells in an antigen specific-dependent manner, T cell exosomes could salvage the psDC by reverting the onset of the apoptotic program. This is consistent with the observation that DCs receive pro-survival signals after IS formation, reducing the percentages of apoptosis in vitro and in vivo [263]. Hence, the reported disappearance of DC from the lymph nodes after the IS [264] could be explained due to their programmed cell death but also due to their migration to other tissues, particularly if they have been fine-tuned by T cell exosomes. In fact, DC can live for 15 days in the lymph node after an immune challenge, and are able to present antigens ex vivo to CD4+ T cells [265]. There is scant evidence of this type of priming, but some indirect evidence points to the potential importance of this mechanism. For example, tissue-resident memory T cells (TRM) have been shown to allow superior protection to homologous infection compared to circulating memory T cells. These TRM can become instructors of innate immune system by initiating a local anti-viral state after reinfection that depends on the secretion of pro-

inflammatory cytokines such as TNF, IL-2 or IFN-γ that rapidly initiate an innate immune response in the infected tissues [266–268]. These experimental observations suggest the existence of cross-priming elements that are transferred by the exposure to one pathogen to improve the response against other pathogens. Hence, it is tempting to speculate a role for exosomes and DNA transfer in this enhanced anti-viral protection exerted by tissue-resident memory T cells.

The mechanism proposed here would function as a mechanism of innate memory, adapting the DC response during antigenic challenge. Obviously, DCs do not bear genetic mechanisms to modulate their ability to recognize antigens similar to the recombination observed in B cells and T cells. However, increasing evidence has demonstrated that DCs and macrophages bear long-lasting modifications to their epigenetic status after infection or vaccination, leading to enhanced responsiveness upon secondary stimulation by microbial pathogens, increased production of inflammatory mediators and enhanced capacity to eliminate infection [269]. We propose that T cell exosomes are powerful DC reprogramming tools that enhance the adaptation of the innate cell against the pathogen. Although this is obviously a short-ranged mechanism, the delivery of T cell exosomes to circulating fluids and their subsequent capture by distant APC could play a significant role in boosting vaccination and the induction of long-distance preparation against infection.

7. Concluding remarks

In summary, this study provides a physiological mechanism for the transfer of mitochondrial components and genome transfer in the context of immune cognate interactions, laying the foundation of a model in which the transfer of DNA between immune cells constitutes a signal-dependent mechanism for alerting responses in innate immune cells. We postulate that mitochondrial components are loaded into MVB of T cells during activation or a stress situation. Those components are released in exosomes-like vesicles to the synaptic cleft when MVB fuse with plasma membrane and they are uptaken by the DC. mtDNA contained in those vesicles triggers a transcriptomic remodeling through the cGas/STING pathway. The main affected genes in primed DC are those from pathogen defense pathways, specifically the antiviral response. Consistently, primed DC are more protected against vaccinia infection *in vitro* **(Figure D2)**.

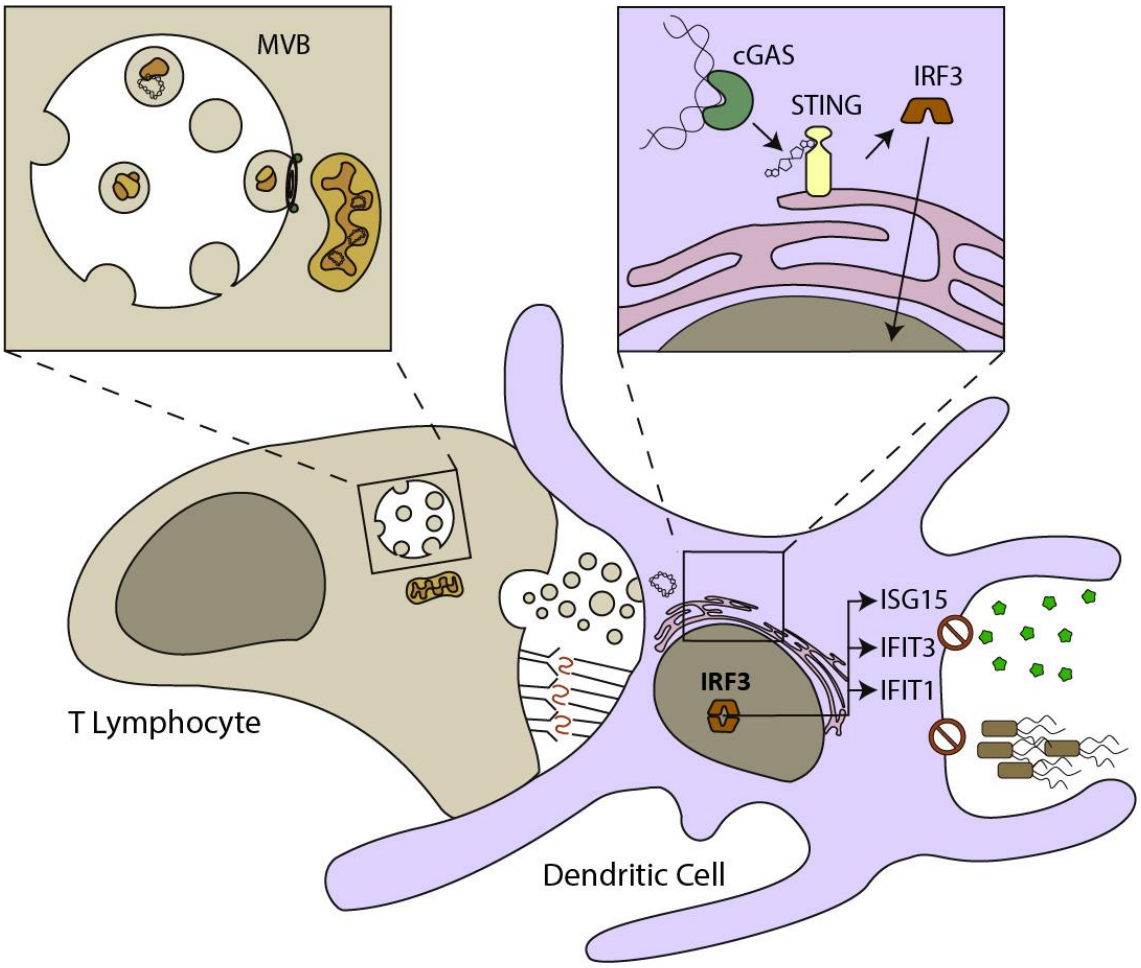

Figure D2. Proposed model for the experimental conclusions. T Lymphocytes load mitochondrial components into ILV of the MVB. Vesicles are released during cognate interactions and mtDNA is incorporated in DC where it triggers antiviral signaling through the cGAS/STING pathway. Due to this interaction primed DC are more protected against further pathogen infections.

Although there are many aspects of our research where more investigation is needed, this study opens a very interesting field. During many years DC were supposed to present antigens and once their mission was accomplished they died [262]. However data show that upon antigen-driven contacts DC induce pro-survival signals, have lower percentages of apoptosis [263] and they can live for more than 15 days after the interaction in the lymph node [264]. In addition, their mitochondria cluster and local autophagy is induced with homeostatic purposes [141]. Finally, our data show that upon cognate interaction psDC acquire an antiviral program and they are more protected. Those data are supported by a study where it is shown that this also happens in DC in vivo [270]. Even if after immune synapse many DC die, some of these post-synaptic Dendritic Cells activate a program that improves their performance [271].

This specific repertoire of cells could have a role in subsequent infections and there is an exciting new field of study that probably can unveil new modes to improve vaccination and fight against infective diseases.

Conclusions

Conclusions

The findings presented herein support the following conclusions:

1. Exosomes isolated from T Lymphocytes are loaded with a repertoire of mitochondrial proteins where mitochondrial DNA binding proteins are enriched.

2. T Lymphocytes shuttle genomic and mitochondrial DNA in exosomes. DNA in exosomes is partially oxidized and it is only present in a specific exosomal subpopulations.

3. Mitochondrial proteins and DNA segregate into multivesicular bodies and the exosomal secretory pathway to reach exosomes.

4. Biogenesis and Release of exosomes regulate mitochondrial function and homeostasis.

5. Mitochondrial proteins and DNA are transferred from T cells to dendritic cells in a unidirectional manner during immune synapsis.

6. DNA contained in exosomes activates the expression of antiviral genes through cGAS/STING-IRF3 pathway in dendritic cells due to exosome uptake.

7. Synaptic exosomes secreted by T cells during cognate interactions prime dendritic cells and protect them against subsequent viral infections.

Conclusiones

Conclusiones

Los resultados presentados en esta tesis apoyan las siguientes conclusiones:

1. Los exosomas provenientes de linfocitos T contienen proteínas mitocondriales entre las que se encuentran especialmente enriquecidas las proteínas de unión a ADN mitocondrial.

2. Los exosomas secretados por los linfocitos T están cargados de ADN genómico y mitocondrial. El ADN de los exosomas está parcialmente oxidado y sólo está presente en una subpoblación específica de exosomas.

3. Las proteínas mitocondriales y el ADN se acumulan en cuerpos multivesiculares y de esta manera llegan a los exosomas.

4. La biogénesis y liberación de exosomas regulan la homeostasis y la función mitocondrial.

5. Las proteínas y El ADN mitocondriales se transfieren de los linfocitos T a las células dendríticas de una manera unidireccional durante la sinapsis inmune.

6. El ADN contenido en los exosomas activa la expresión de los genes antivirales a través de la vía cGAS/STING-IRF3 en las células dendríticas cuando estas captan e incorporan los exosomas de los linfocitos.

7. Los exosomas secretados por las células T durante la sinapsis inmune pre-activan a las células dendríticas y las protegen contra infecciones virales posteriores.

References

References

1. Abbas, A. K., Lichtman, A. H., Pillai, S. & Preceded by: Abbas, A. K. *Cellular and molecular immunology*. (2017).

2. Dustin, M. L. & Choudhuri, K. Signaling and Polarized Communication Across the T Cell Immunological Synapse. *Annu. Rev. Cell Dev. Biol.* **32**, 303–325 (2016).

3. Monks, C. R., Freiberg, B. A., Kupfer, H., Sciaky, N. & Kupfer, A. Three-dimensional segregation of supramolecular activation clusters in T cells. *Nature* **395**, 82–86 (1998).

4. Cai, E. *et al.* Visualizing dynamic microvillar search and stabilization during ligand detection by T cells. *Science (80-.).* (2017).

5. Kim, H. R. *et al.* T cell microvilli constitute immunological synaptosomes that carry messages to antigen-presenting cells. *Nat. Commun.* (2018).

6. Wülfing, C., Sjaastad, M. D. & Davis, M. M. Visualizing the dynamics of T cell activation: intracellular adhesion molecule 1 migrates rapidly to the T cell/B cell interface and acts to sustain calcium levels. *Proc. Natl. Acad. Sci. U. S. A.* **95**, 6302–7 (1998).

7. Robles-Valero, J. *et al.* Integrin and CD3/TCR activation are regulated by the scaffold protein AKAP450. *Blood* **115**, 4174–4184 (2010).

8. Comrie, W. A., Babich, A. & Burkhardt, J. K. F-actin flow drives affinity maturation and spatial organization of LFA-1 at the immunological synapse. *J. Cell Biol.* (2015).

9. Van Der Merwe, P. A. & Dushek, O. Mechanisms for T cell receptor triggering. *Nature Reviews Immunology* (2011).

10. Valitutti, S., Dessing, M., Aktories, K., Gallati, H. & Lanzavecchia, A. Sustained signaling leading to T cell activation results from prolonged T cell receptor occupancy. Role of T cell actin cytoskeleton. *J. Exp. Med.* **181**, 577–84 (1995).

11. Lee, K.-H. *et al.* T Cell Receptor Signaling Precedes Immunological Synapse Formation. *Science (80-.).* **295**, 1539–1542 (2002).

12. He, H.-T. & Marguet, D. T-cell antigen receptor triggering and lipid rafts: a matter of space and time scales. Talking Point on the involvement of lipid rafts in T-cell activation. *EMBO Rep.* **9**, 525–530 (2008).

13. Grakoui, A. *et al.* The immunological synapse: a molecular machine controlling T cell activation. *Science* **285**, 221–7 (1999).

14. Varma, R., Campi, G., Yokosuka, T., Saito, T. & Dustin, M. L. T cell receptor-proximal signals are sustained in peripheral microclusters and terminated in the central supramolecular activation cluster. *Immunity* **25**, 117–127 (2006).

15. DeMond, A. L., Mossman, K. D., Starr, T., Dustin, M. L. & Groves, J. T. T cell receptor microcluster transport through molecular mazes reveals mechanism of translocation. *Biophys J* **94**, 3286–3292 (2008).

16. Yi, J., Wu, X. S., Crites, T. & Hammer 3rd, J. A. Actin retrograde flow and actomyosin II arc contraction drive receptor cluster dynamics at the immunological synapse in Jurkat T cells. *Mol Biol Cell* **23**, 834–852 (2012).

17. Ilani, T., Vasiliver-Shamis, G., Vardhana, S., Bretscher, A. & Dustin, M. L. T cell antigen receptor signaling and immunological synapse stability require myosin IIA. *Nat Immunol* **10**, 531–539 (2009).

18. Freiberg, B. A. *et al.* Staging and resetting T cell activation in SMACs. *Nat Immunol* **3**, 911–917 (2002).

19. Sykulev, Y., Joo, M., Vturina, I., Tsomides, T. J. & Eisen, H. N. Evidence that a single peptide-MHC complex on a target cell can elicit a cytolytic T cell response. *Immunity* **4**, 565–571 (1996).

20. Benvenuti, F. *et al.* Requirement of Rac1 and Rac2 expression by mature dendritic cells for T cell priming. *Science (80-.).* **305**, 1150–1153 (2004).

21. Al-Alwan, M. M. *et al.* Cutting edge: dendritic cell actin cytoskeletal polarization during immunological synapse formation is highly antigen-dependent. *J Immunol* **171**, 4479–4483 (2003).

22. Al-Alwan, M. M., Rowden, G., Lee, T. D. & West, K. A. The dendritic cell cytoskeleton is critical for the formation of the immunological synapse. *J Immunol* **166**, 1452–1456 (2001).

23. Mayya, V. *et al.* Durable Interactions of T Cells with T Cell Receptor Stimuli in the Absence of a Stable Immunological Synapse. *Cell Rep* **22**, 340–349 (2018).

24. Martín-cófreces, N. B., Vicente-manzanares, M. & Sanchez-Madrid, F. Adhesive Interactions Delineate the Topography of the Immune Synapse. **6**, 1–10 (2018).

25. Martin-Cofreces, N. B. & Sanchez-Madrid, F. Sailing to and Docking at the Immune Synapse: Role of Tubulin Dynamics and Molecular Motors. *Front Immunol* **9**, 1174 (2018).

26. Fritzsche, M. *et al.* Cytoskeletal actin dynamics shape a ramifying actin network underpinning immunological synapse formation. *Sci Adv* **3**, e1603032 (2017).

27. Huse, M., Lillemeier, B. F., Kuhns, M. S., Chen, D. S. & Davis, M. M. T cells use two directionally distinct pathways for cytokine secretion. *Nat Immunol* **7**, 247–255 (2006).

28. Martin-Cofreces, N. B. *et al.* MTOC translocation modulates IS formation and controls sustained T cell signaling. *J Cell Biol* **182**, 951–962 (2008).

29. Kupfer, A. & Dennert, G. Reorientation of the microtubule-organizing center and the Golgi apparatus in cloned cytotoxic lymphocytes triggered by binding to lysable target cells. *J Immunol* **133**, 2762–2766 (1984).

30. Kupfer, A., Dennert, G. & Singer, S. J. The reorientation of the Golgi apparatus and the microtubule-organizing center in the cytotoxic effector cell is a prerequisite in the lysis of bound target cells. *J Mol Cell Immunol* **2**, 37–49 (1985).

31. Kupfer, A., Mosmann, T. R. & Kupfer, H. Polarized expression of cytokines in cell conjugates of helper T cells and splenic B cells. *Proc Natl Acad Sci U S A* **88**, 775–779 (1991).

32. Huse, M., Le Floc'h, A. & Liu, X. From lipid second messengers to molecular motors: microtubule-organizing center reorientation in T cells. *Immunol Rev* **256**, 95–106 (2013).

33. Kuhne, M. R. *et al.* Linker for activation of T cells, zeta-associated protein-70, and Src homology 2 domain-containing leukocyte protein-76 are required for TCR-induced microtubule-organizing center polarization. *J Immunol* **171**, 860–866 (2003).

34. Lo, W. L. *et al.* Lck promotes Zap70-dependent LAT phosphorylation by bridging Zap70 to LAT. *Nat Immunol* **19**, 733–741 (2018).

35. Babich, A. *et al.* F-actin polymerization and retrograde flow drive sustained PLCgamma1 signaling during T cell activation. *J Cell Biol* **197**, 775–787 (2012).

36. Spitaler, M., Emslie, E., Wood, C. D. & Cantrell, D. Diacylglycerol and protein kinase D localization during T lymphocyte activation. *Immunity* **24**, 535–546 (2006).

37. Quann, E. J., Merino, E., Furuta, T. & Huse, M. Localized diacylglycerol drives the polarization of the microtubule-organizing center in T cells. *Nat Immunol* **10**, 627–635 (2009).

38. Quann, E. J., Liu, X., Altan-Bonnet, G. & Huse, M. A cascade of protein kinase C isozymes promotes cytoskeletal polarization in T cells. *Nat Immunol* **12**, 647–654 (2011).

39. Combs, J. *et al.* Recruitment of dynein to the Jurkat immunological synapse. *Proc Natl Acad Sci U S A* **103**, 14883–14888 (2006).

40. Liu, X., Kapoor, T. M., Chen, J. K. & Huse, M. Diacylglycerol promotes centrosome polarization in T cells via reciprocal localization of dynein and myosin II. *Proc Natl Acad Sci U S A* **110**, 11976–11981 (2013).

41. Baixauli, F. *et al.* The mitochondrial fission factor dynamin-related protein 1 modulates T-cell receptor signalling at the immune synapse. *EMBO J.* **30**, 1238–50 (2011).

42. Calabia-Linares, C. *et al.* Endosomal clathrin drives actin accumulation at the immunological synapse. *J Cell Sci* **124**, 820–830 (2011).

43. Huse, M., Quann, E. J. & Davis, M. M. Shouts, whispers and the kiss of death: directional secretion in T cells. *Nat. Immunol.* **9**, 1105–1111 (2008).

44. Ueda, H., Morphew, M. K., McIntosh, J. R. & Davis, M. M. CD4+ T-cell synapses involve multiple distinct stages. *Proc Natl Acad Sci U S A* **108**, 17099–17104 (2011).

45. Poo, W. J., Conrad, L. & Janeway Jr., C. A. Receptor-directed focusing of lymphokine release by helper T cells. *Nature* **332**, 378–380 (1988).

46. Alcover, A., Alarcon, B. & Di Bartolo, V. Cell Biology of T Cell Receptor Expression and Regulation. *Annu Rev Immunol* **36**, 103–125 (2018).

47. Finetti, F. *et al.* The small GTPase Rab8 interacts with VAMP-3 to regulate the delivery of recycling T-cell receptors to the immune synapse. *J Cell Sci* **128**, 2541–2552 (2015).

48. Finetti, F. *et al.* Intraflagellar transport is required for polarized recycling of the TCR/CD3 complex to the immune synapse. *Nat Cell Biol* **11**, 1332–1339 (2009).

49. Martin-Cofreces, N. B. *et al.* End-binding protein 1 controls signal propagation from the T cell receptor. *EMBO J* **31**, 4140–4152 (2012).

50. Blas-Rus, N. *et al.* Aurora A drives early signalling and vesicle dynamics during T-cell activation. *Nat Commun* **7**, 11389 (2016).

51. Das, V. *et al.* Activation-induced polarized recycling targets T cell antigen receptors to the immunological synapse; involvement of SNARE complexes. *Immunity* **20**, 577–588 (2004).

52. Compeer, E. B. *et al.* A mobile endocytic network connects clathrin-independent receptor endocytosis to recycling and promotes T cell activation. *Nat Commun* **9**, 1597 (2018).

53. Pan, B. T. & Johnstone, R. M. Fate of the transferrin receptor during maturation of sheep reticulocytes in vitro: selective externalization of the receptor. *Cell* **33**, 967–78 (1983).

54. Harding, C., Heuser, J. & Stahl, P. Receptor-mediated endocytosis of transferrin and recycling of the transferrin receptor in rat reticulocytes. *J. Cell Biol.* **97**, 329–339 (1983).

55. Mittelbrunn, M. *et al.* Unidirectional transfer of microRNA-loaded exosomes from T cells to antigen-presenting cells. *Nat. Commun.* **2**, 282 (2011).

56. Mittelbrunn, M. & Sánchez-Madrid, F. Intercellular communication: diverse structures for exchange of genetic information. *Nat. Rev. Mol. Cell Biol.* **13**, 328–35 (2012).

57. Huotari, J. & Helenius, A. Endosome maturation. *EMBO J.* **30**, 3481–3500 (2011).

58. Nielsen, E., Severin, F., Backer, J. M., Hyman, A. A. & Zerial, M. Rab5 regulates motility of early endosomes on microtubules. *Nat. Cell Biol.* **1**, 376–382 (1999).

59. Rink, J., Ghigo, E., Kalaidzidis, Y. & Zerial, M. Rab Conversion as a Mechanism of Progression from Early to Late Endosomes. *Cell* **122**, 735–749 (2005).

60. Bucci, C., Thomsen, P., Nicoziani, P., McCarthy, J. & van Deurs, B. Rab7: A Key to Lysosome Biogenesis. *Mol. Biol. Cell* **11**, 467–480 (2000).

61. Vitelli, R. *et al.* Role of the Small GTPase RAB7 in the Late Endocytic Pathway. *J. Biol. Chem.* **272**, 4391–4397 (1997).

62. Collinet, C. *et al.* Systems survey of endocytosis by multiparametric image analysis. *Nature* **464**, 243–249 (2010).

63. Driskell, O. J., Mironov, A., Allan, V. J. & Woodman, P. G. Dynein is required for receptor sorting and the morphogenesis of early endosomes. *Nat. Cell Biol.* **9**, 113–120 (2007).

64. Hoepfner, S. *et al.* Modulation of Receptor Recycling and Degradation by the Endosomal Kinesin KIF16B. *Cell* **121**, 437–450 (2005).

65. Bananis, E., Murray, J. W., Stockert, R. J., Satir, P. & Wolkoff, A. W. Microtubule and Motor-Dependent Endocytic Vesicle Sorting in Vitro. *J. Cell Biol.* **151**, 179–186 (2000).

66. Aniento, F., Emans, N., Griffiths, G. & Gruenberg, J. Cytoplasmic dynein-dependent vesicular transport from early to late endosomes [published erratum appears in J Cell Biol 1994 Feb;124(3):397]. *J. Cell Biol.* **123**, 1373–1387 (1993).

67. Brown, C. L. *et al.* Kinesin-2 is a Motor for Late Endosomes and Lysosomes. *Traffic* **6**, 1114–1124 (2005).

68. Jordens, I. *et al.* The Rab7 effector protein RILP controls lysosomal transport by inducing the recruitment of dynein-dynactin motors. *Curr. Biol.* **11**, 1680–5 (2001).

69. Johansson, M. *et al.* Activation of endosomal dynein motors by stepwise assembly of Rab7–RILP–p150Glued, ORP1L, and the receptor βIII spectrin. *J. Cell Biol.* **176**, 459 (2007).

70. Progida, C. & Bakke, O. Bidirectional traffic between the Golgi and the endosomes – machineries and regulation. *J. Cell Sci.* **129**, jcs.185702 (2016).

71. Hessvik, N. P. & Llorente, A. Current knowledge on exosome biogenesis and release. *Cell. Mol. Life Sci.* **75**, 193–208 (2018).

72. Villarroya-Beltri, C., Baixauli, F., Gutierrez-Vazquez, C., Sanchez-Madrid, F. & Mittelbrunn, M. Sorting it out: regulation of exosome loading. *Semin Cancer Biol* **28**, 3–13 (2014).

73. Baietti, M. F. *et al.* Syndecan–syntenin–ALIX regulates the biogenesis of exosomes. *Nat. Cell Biol.* **14**, 677–685 (2012).

74. Colombo, M., Raposo, G. & Théry, C. Biogenesis, Secretion, and Intercellular Interactions of Exosomes and Other Extracellular Vesicles. *Annu. Rev. Cell Dev. Biol.* **30**, 255–289 (2014).

75. Alonso Y Adell, M., Migliano, S. M. & Teis, D. ESCRT-III and Vps4: a dynamic multipurpose tool for membrane budding and scission. *FEBS J.* **283**, 3288–3302 (2016).

76. Bache, K. G., Brech, A., Mehlum, A. & Stenmark, H. Hrs regulates multivesicular body formation via ESCRT recruitment to endosomes. *J. Cell Biol.* **162**, 435–42 (2003).

77. Raiborg, C. *et al.* Hrs sorts ubiquitinated proteins into clathrin-coated microdomains of early endosomes. *Nat. Cell Biol.* **4**, 394–398 (2002).

78. Razi, M. & Futter, C. E. Distinct Roles for Tsg101 and Hrs in Multivesicular Body Formation and Inward Vesiculation. *Mol. Biol. Cell* **17**, 3469–3483 (2006).

79. Bache, K. G. *et al.* The ESCRT-III Subunit hVps24 Is Required for Degradation but Not Silencing of the Epidermal Growth Factor Receptor. *Mol. Biol. Cell* **17**, 2513–2523 (2006).

80. Trajkovic, K. *et al.* Ceramide Triggers Budding of Exosome Vesicles into Multivesicular Endosomes. *Science (80-.).* **319**, 1244–1247 (2008).

81. Yuyama, K., Sun, H., Mitsutake, S. & Igarashi, Y. Sphingolipid-modulated Exosome Secretion Promotes Clearance of Amyloid-β by Microglia. *J. Biol. Chem.* **287**, 10977–10989 (2012).

82. Xu, Y. *et al.* Macrophages transfer antigens to dendritic cells by releasing exosomes containing dead-cell-associated antigens partially through a ceramide-dependent pathway to enhance CD4 $^{+}$ T-cell responses. *Immunology* **149**, 157–171 (2016).

83. Kajimoto, T., Okada, T., Miya, S., Zhang, L. & Nakamura, S. Ongoing activation of sphingosine 1-phosphate receptors mediates maturation of exosomal multivesicular endosomes. *Nat. Commun.* **4**, 2712 (2013).

84. Kajimoto, T. *et al.* Involvement of Gβγ subunits of G $_{i}$ protein coupled with S1P receptor on multivesicular endosomes in F-actin formation and cargo sorting into exosomes. *J. Biol. Chem.* **293**, 245–253 (2018).

85. Mohamed, N. N. I., Okada, T., Kajimoto, T. & Nakamura, S.-I. Essential Role of Sphingosine Kinase 2 in the Regulation of Cargo Contents in the Exosomes from K562 Cells. *Kobe J. Med. Sci.* **63**, E123–E129 (2018).

86. Escola, J.-M. *et al.* Selective Enrichment of Tetraspan Proteins on the Internal Vesicles of Multivesicular Endosomes and on Exosomes Secreted by Human B-lymphocytes. *J. Biol. Chem.* **273**, 20121–20127 (1998).

87. Rocha-Perugini, V., Sánchez-Madrid, F. & Martínez del Hoyo, G. Function and Dynamics of Tetraspanins during Antigen Recognition and Immunological Synapse Formation. *Front. Immunol.* **6**, 653 (2016).

88. van Niel, G. *et al.* The Tetraspanin CD63 Regulates ESCRT-Independent and -Dependent Endosomal Sorting during Melanogenesis. *Dev. Cell* **21**, 708–721 (2011).

89. Edgar, J. R., Eden, E. R. & Futter, C. E. Hrs- and CD63-Dependent Competing Mechanisms Make Different Sized Endosomal Intraluminal Vesicles. *Traffic* **15**, 197–211 (2014).

90. Tamai, K. *et al.* Exosome secretion of dendritic cells is regulated by Hrs, an ESCRT-0 protein. *Biochem. Biophys. Res. Commun.* **399**, 384–390 (2010).

91. Stuffers, S., Sem Wegner, C., Stenmark, H. & Brech, A. Multivesicular Endosome Biogenesis in the Absence of ESCRTs. *Traffic* **10**, 925–937 (2009).

92. Ostrowski, M. *et al.* Rab27a and Rab27b control different steps of the exosome secretion pathway. *Nat. Cell Biol.* **12**, 19–30 (2010).

93. Villarroya-Beltri, C. *et al.* ISGylation controls exosome secretion by promoting lysosomal degradation of MVB proteins. *Nat. Commun.* **7**, (2016).

94. Villarroya-Beltri, C., Guerra, S. & Sanchez-Madrid, F. ISGylation - a key to lock the cell gates for preventing the spread of threats. *J Cell Sci* **130**, 2961–2969 (2017).

95. Li, Z. *et al.* Acetylation modification regulates GRP78 secretion in colon cancer cells. *Sci Rep* **6**, 30406 (2016).

96. Möbius, W. *et al.* Immunoelectron Microscopic Localization of Cholesterol Using Biotinylated and Non-cytolytic Perfringolysin O. *J. Histochem. Cytochem.* **50**, 43–55 (2002).

97. Chen, Q., Takada, R., Noda, C., Kobayashi, S. & Takada, S. Different populations of Wnt-containing vesicles are individually released from polarized epithelial cells. *Sci. Rep.* **6**, 35562 (2016).

98. Tauro, B. J. *et al.* Two Distinct Populations of Exosomes Are Released from LIM1863 Colon Carcinoma Cell-derived Organoids. *Mol. Cell. Proteomics* **12**, 587–598 (2013).

99. van Niel, G. *et al.* Intestinal epithelial cells secrete exosome-like vesicles. *Gastroenterology* **121**, 337–49 (2001).

100. Sinha, S. *et al.* Cortactin promotes exosome secretion by controlling branched actin dynamics. *J. Cell Biol.* **214**, 197–213 (2016).

101. Möbius, W. *et al.* Recycling compartments and the internal vesicles of multivesicular bodies harbor most of the cholesterol found in the endocytic pathway. *Traffic* **4**, 222–31 (2003).

102. Valadi, H. *et al.* Exosome-mediated transfer of mRNAs and microRNAs is a novel mechanism of genetic exchange between cells. *Nat. Cell Biol.* **9**, 654–9 (2007).

103. Thakur, B. K. *et al.* Double-stranded DNA in exosomes: a novel biomarker in cancer detection. *Cell Res* **24**, 766–769 (2014).

104. Takahashi, A., Okada, R., Nagao, K., Kawamata, Y. & Hanyu, A. Exosomes maintain cellular homeostasis by excreting harmful DNA from cells. *Nat. Commun.* **8**, 15287 (2017).

105. Kahlert, C. *et al.* Identification of double-stranded genomic DNA spanning all chromosomes with mutated KRAS and p53 DNA in the serum exosomes of patients with pancreatic cancer. *J Biol Chem* **289**, 3869–3875 (2014).

106. Guescini, M., Genedani, S., Stocchi, V. & Agnati, L. F. Astrocytes and Glioblastoma cells release exosomes carrying mtDNA. *J. Neural Transm.* **117**, 1–4 (2010).

107. Moreno-Gonzalo, O., Fernandez-Delgado, I. & Sanchez-Madrid, F. Post-translational add-ons mark the path in exosomal protein sorting. *Cell Mol Life Sci* **75**, 1–19 (2018).

108. Raiborg, C. & Stenmark, H. The ESCRT machinery in endosomal sorting of ubiquitylated membrane proteins. *Nature* **458**, 445–452 (2009).

109. Nikko, E. & Andre, B. Evidence for a direct role of the Doa4 deubiquitinating enzyme in protein sorting into the MVB pathway. *Traffic* **8**, 566–581 (2007).

110. Kunadt, M. *et al.* Extracellular vesicle sorting of α-Synuclein is regulated by sumoylation. *Acta Neuropathol.* **129**, 695–713 (2015).

111. Villarroya-Beltri, C. *et al.* Sumoylated hnRNPA2B1 controls the sorting of miRNAs into exosomes through binding to specific motifs. *Nat. Commun.* **4**, 2980 (2013).

112. Santangelo, L. *et al.* The RNA-Binding Protein SYNCRIP Is a Component of the Hepatocyte Exosomal Machinery Controlling MicroRNA Sorting. *Cell Rep* **17**, 799–808 (2016).

113. Montecalvo, A. *et al.* Mechanism of transfer of functional microRNAs between mouse dendritic cells via exosomes. *Blood* **119**, 756–766 (2012).

114. Gibbings, D. J., Ciaudo, C., Erhardt, M. & Voinnet, O. Multivesicular bodies associate with components of miRNA effector complexes and modulate miRNA activity. *Nat. Cell Biol.* **11**, 1143–9 (2009).

115. Soares, A. R. *et al.* Gap junctional protein Cx43 is involved in the communication between extracellular vesicles and mammalian cells. *Sci. Rep.* **5**, 13243 (2015).

116. Varela-Eirin, M. *et al.* Recruitment of RNA molecules by connexin RNA-binding motifs: Implication in RNA and DNA transport through microvesicles and exosomes. *Biochim. Biophys. Acta - Mol. Cell Res.* **1864**, 728–736 (2017).

117. Welton, J. L. *et al.* Cerebrospinal fluid extracellular vesicle enrichment for protein biomarker discovery in neurological disease; multiple sclerosis. *J. Extracell. Vesicles* **6**, 1369805 (2017).

118. Cheng, L., Sharples, R. A., Scicluna, B. J. & Hill, A. F. Exosomes provide a protective and enriched source of miRNA for biomarker profiling compared to intracellular and cell-free blood. *J. Extracell. vesicles* **3**, (2014).

119. Thind, A. & Wilson, C. Exosomal miRNAs as cancer biomarkers and therapeutic targets. *J. Extracell. Vesicles* **5**, 31292 (2016).

120. Quinn, J. F. *et al.* Extracellular RNAs: development as biomarkers of human disease. *J. Extracell. Vesicles* **4**, 27495 (2015).

121. Boukouris, S. & Mathivanan, S. Exosomes in bodily fluids are a highly stable resource of disease biomarkers. *Proteomics. Clin. Appl.* **9**, 358–67 (2015).

122. Pitt, J. M., Kroemer, G. & Zitvogel, L. Extracellular vesicles: masters of intercellular communication and potential clinical interventions. *J. Clin. Invest.* **126**, 1139–1143 (2016).

123. van Niel, G., D'Angelo, G. & Raposo, G. Shedding light on the cell biology of extracellular vesicles. *Nat. Rev. Mol. Cell Biol.* **19**, 213–228 (2018).

124. Raposo, G. & Stoorvogel, W. Extracellular vesicles: exosomes, microvesicles, and friends. *J Cell Biol* **200**, 373–383 (2013).

125. Tkach, M. & Thery, C. Communication by Extracellular Vesicles: Where We Are and Where We Need to Go. *Cell* **164**, 1226–1232 (2016).

126. Robbins, P. D. & Morelli, A. E. Regulation of immune responses by extracellular vesicles. *Nat. Rev. Immunol.* **14**, 195–208 (2014).

127. Blanchard, N. *et al.* TCR activation of human T cells induces the production of exosomes bearing the TCR/CD3/zeta complex. *J Immunol* **168**, 3235–3241 (2002).

128. Wahlgren, J., Karlson Tde, L., Glader, P., Telemo, E. & Valadi, H. Activated human T cells secrete exosomes that participate in IL-2 mediated immune response signaling. *PLoS One* **7**, e49723 (2012).

129. Jolly, C., Welsch, S., Michor, S. & Sattentau, Q. J. The regulated secretory pathway in CD4(+) T cells contributes to human immunodeficiency virus type-1 cell-to-cell spread at the virological synapse. *PLoS Pathog* **7**, e1002226 (2011).

130. Soares, H. HIV-1 Intersection with CD4 T Cell Vesicle Exocytosis: Intercellular Communication Goes Viral. *Front Immunol* **5**, 454 (2014).

131. Bukong, T. N., Momen-Heravi, F., Kodys, K., Bala, S. & Szabo, G. Exosomes from hepatitis C infected patients transmit HCV infection and contain replication competent viral RNA in complex with Ago2-miR122-HSP90. *PLoS Pathog* **10**, e1004424 (2014).

132. Choudhuri, K. *et al.* Polarized release of T-cell-receptor-enriched microvesicles at the immunological synapse. *Nature* **507**, 118–23 (2014).

133. Vardhana, S., Choudhuri, K., Varma, R. & Dustin, M. L. Essential role of ubiquitin and TSG101 protein in formation and function of the central supramolecular activation cluster. *Immunity* **32**, 531–540 (2010).

134. Esposito, L. *et al.* Investigation of soluble and transmembrane CTLA-4 isoforms in serum and microvesicles. *J Immunol* **193**, 889–900 (2014).

135. Friedman, J. R. & Nunnari, J. Mitochondrial form and function. *Nature* **505**, 335–343 (2014).

136. Angajala, A. *et al.* Diverse Roles of Mitochondria in Immune Responses: Novel Insights Into Immuno-Metabolism. *Front. Immunol.* **9**, 1605 (2018).

137. Sena, L. a *et al.* Mitochondria are required for antigen-specific T cell activation through reactive oxygen species signaling. *Immunity* **38**, 225–36 (2013).

138. Arsenio, J., Metz, P. J. & Chang, J. T. Asymmetric Cell Division in T Lymphocyte Fate Diversification. *Trends Immunol.* **36**, 670–683 (2015).

139. Baixauli, F. *et al.* Mitochondrial Respiration Controls Lysosomal Function during Inflammatory T Cell Responses. *Cell Metab* **22**, 485–498 (2015).

140. Quintana, A. *et al.* T cell activation requires mitochondrial translocation to the immunological synapse. *Proc. Natl. Acad. Sci.* **104**, 14418–14423 (2007).

141. Gómez-Cabañas, L. *et al.* Immunological Synapse Formation Induces Mitochondrial Clustering and Mitophagy in Dendritic Cells. *J. Immunol.* **202**, 1715–1723 (2019).

142. Lewis, R. S. Calcium signaling mechanisms in T lymphocytes. *Annu. Rev. Immunol.* **19**, 497–521 (2001).

143. Schwindling, C., Quintana, A., Krause, E. & Hoth, M. Mitochondria positioning controls local calcium influx in T cells. *J. Immunol.* **184**, 184–90 (2010).

144. Morlino, G. *et al.* Miro-1 Links Mitochondria and Microtubule Dynein Motors To Control Lymphocyte Migration and Polarity. *Mol. Cell. Biol.* **34**, 1412–1426 (2014).

145. MacAskill, A. F. *et al.* Miro1 Is a Calcium Sensor for Glutamate Receptor-Dependent Localization of Mitochondria at Synapses. *Neuron* **61**, 541–555 (2009).

146. Contento, R. L. *et al.* Adhesion shapes T cells for prompt and sustained T-cell receptor signalling. *EMBO J.* **29**, 4035–4047 (2010).

147. López-Doménech, G. *et al.* Miro proteins coordinate microtubule- and actin-dependent mitochondrial transport and distribution. *EMBO J.* **37**, 321–336 (2018).

148. Quintero, O. A. *et al.* Human Myo19 Is a Novel Myosin that Associates with Mitochondria. *Curr. Biol.* **19**, 2008–2013 (2009).

149. Gustafsson, C. M., Falkenberg, M. & Larsson, N.-G. Maintenance and Expression of Mammalian Mitochondrial DNA. *Annu. Rev. Biochem.* **85**, 133–160 (2016).

150. Kukat, C. *et al.* Cross-strand binding of TFAM to a single mtDNA molecule forms the mitochondrial nucleoid. *Proc. Natl. Acad. Sci.* **112**, 11288–11293 (2015).

151. Mishra, P. & Chan, D. C. Mitochondrial dynamics and inheritance during cell division, development and disease. *Nat. Rev. Mol. Cell Biol.* **15**, 634–46 (2014).

152. Spees, J. L., Olson, S. D., Whitney, M. J. & Prockop, D. J. Mitochondrial transfer between cells can rescue aerobic respiration. *Proc. Natl. Acad. Sci. U. S. A.* **103**, (2006).

153. Ahmad, T. *et al.* Miro 1 regulates intercellular mitochondrial transport & enhances mesenchymal stem cell rescue efficacy. EMBO J. **33**, (2014).

154. Hayakawa, K. *et al.* Transfer of mitochondria from astrocytes to neurons after stroke. *Nature* **535**, 551–555 (2016).

155. Islam, M. N. *et al.* Mitochondrial transfer from bone-marrow-derived stromal cells to pulmonary alveoli protects against acute lung injury. *Nat Med* **18**, 759–765 (2012).

156. Moschoi, R. *et al.* Protective mitochondrial transfer from bone marrow stromal cells to acute myeloid leukemic cells during chemotherapy. *Blood* (2016).

157. Tan, A. S. *et al.* Mitochondrial Genome Acquisition Restores Respiratory Function and Tumorigenic Potential of Cancer Cells without Mitochondrial DNA. *Cell Metab.* **21**, 81–94 (2015).

158. Cho, Y. M. *et al.* Mesenchymal stem cells transfer mitochondria to the cells with virtually no mitochondrial function but not with pathogenic mtDNA mutations. *PLoS One* **7**, 0–7 (2012).

159. Wang, X. & Gerdes, H.-H. Transfer of mitochondria via tunneling nanotubes rescues apoptotic PC12 cells. *Cell Death Differ.* **22**, 1181–91 (2015).

160. Guescini, M. *et al.* C2C12 myoblasts release micro-vesicles containing mtDNA and proteins involved in signal transduction. *Exp. Cell Res.* **316**, 1977–84 (2010).

161. Kahlert, C. *et al.* Identification of double-stranded genomic DNA spanning all chromosomes with mutated KRAS and p53 DNA in the serum exosomes of patients with pancreatic cancer. *J. Biol. Chem.* **289**, 3869–75 (2014).

162. Phinney, D. G. *et al.* Mesenchymal stem cells use extracellular vesicles to outsource mitophagy and shuttle microRNAs. *Nat. Commun.* **6**, 8472 (2015).

163. Ong, S.-G. & Wu, J. C. Exosomes as potential alternatives to stem cell therapy in mediating cardiac regeneration. *Circ. Res.* **117**, 7–9 (2015).

164. Nakamura, Y. *et al.* Mesenchymal-stem-cell-derived exosomes accelerate skeletal muscle regeneration. *FEBS Lett.* **589**, 1257–1265 (2015).

165. Khan, M. *et al.* Embryonic Stem Cell-Derived Exosomes Promote Endogenous Repair Mechanisms and Enhance Cardiac Function Following Myocardial Infarction. *Circ. Res.* **117**, 52–64 (2015).

166. Galluzzi, L., Kepp, O. & Kroemer, G. Mitochondria: master regulators of danger signalling. *Nat. Rev. Mol. Cell Biol.* **13**, 780–788 (2012).

167. West, A. P. *et al.* Mitochondrial DNA stress primes the antiviral innate immune response. *Nature* **520**, 553–557 (2015).

168. Zhang, Q. *et al.* Circulating mitochondrial DAMPs cause inflammatory responses to injury. *Nature* **464**, 104–7 (2010).

169. Weinberg, S. E., Sena, L. A. & Chandel, N. S. Mitochondria in the Regulation of Innate and Adaptive Immunity. *Immunity* **42**, 406–417 (2015).

170. Collins, L. V., Hajizadeh, S., Holme, E., Jonsson, I. & Tarkowski, A. Endogenously oxidized mitochondrial DNA induces in vivo and in vitro inflammatory responses. *J. Leukoc. Biol.* **75**, 995–1000 (2004).

171. Oka, T. *et al.* Mitochondrial DNA that escapes from autophagy causes inflammation and heart failure. *Nature* **485 VN**-, 251–255 (2012).

172. Shimada, K. *et al.* Oxidized Mitochondrial DNA Activates the NLRP3 Inflammasome during Apoptosis. *Immunity* **36**, 401–414 (2012).

173. Caielli, S. *et al.* Oxidized mitochondrial nucleoids released by neutrophils drive type I interferon production in human lupus. *J. Exp. Med.* **213**, 697–713 (2016).

174. Boudreau, L. H. *et al.* Platelets release mitochondria serving as substrate for bactericidal group IIA-secreted phospholipase a to promote inflammation. *Blood* **124**, 2173–2183 (2014).

175. Morshed, M. *et al.* NADPH oxidase-independent formation of extracellular DNA traps by basophils. *J. Immunol.* **192**, 5314–23 (2014).

176. Yousefi, S. *et al.* Catapult-like release of mitochondrial DNA by eosinophils contributes to antibacterial defense. *Nat Med* **14**, 949–953 (2008).

177. Ishikawa, K. *et al.* The innate immune system in host mice targets cells with allogenic mitochondrial DNA. *J. Exp. Med.* **207**, 2297–305 (2010).

178. Sauer, J. D. *et al.* The N-ethyl-N-nitrosourea-induced Goldenticket mouse mutant reveals an essential function of Sting in the in vivo interferon response to Listeria monocytogenes and cyclic dinucleotides. *Infect Immun* **79**, 688–694 (2011).

179. Thery, C., Amigorena, S., Raposo, G. & Clayton, A. Isolation and characterization of exosomes from cell culture supernatants and biological fluids. *Curr Protoc Cell Biol* **Chapter 3**, Unit 3 22 (2006).

180. Wisniewski, J. R., Zougman, A., Nagaraj, N. & Mann, M. Universal sample preparation method for proteome analysis. *Nat Methods* **6**, 359–362 (2009).

181. Bonzon-Kulichenko, E., Garcia-Marques, F., Trevisan-Herraz, M. & Vazquez, J. Revisiting peptide identification by high-accuracy mass spectrometry: problems associated with the use of narrow mass precursor windows. *J Proteome Res* **14**, 700–710 (2015).

182. Manders, E. M., Stap, J., Brakenhoff, G. J., van Driel, R. & Aten, J. A. Dynamics of three-dimensional replication patterns during the S-phase, analysed by double labelling of DNA and confocal microscopy. *J Cell Sci* **103 (Pt 3**, 857–862 (1992).

183. Théry, C. *et al.* Minimal information for studies of extracellular vesicles 2018 (MISEV2018): a position statement of the International Society for Extracellular Vesicles and update of the MISEV2014 guidelines. *J. Extracell. Vesicles* **7**, 1535750 (2018).

184. Zhang, Y. *et al.* Inflammasome-Derived Exosomes Activate NF-kappaB Signaling in Macrophages. *J Proteome Res* (2016).

185. Perez-Hernandez, D. *et al.* The intracellular interactome of tetraspanin-enriched microdomains reveals their function as sorting machineries toward exosomes. *J Biol Chem* **288**, 11649–11661 (2013).

186. Gilkerson, R. *et al.* The mitochondrial nucleoid: integrating mitochondrial DNA into cellular homeostasis. *Cold Spring Harb Perspect Biol* **5**, a011080 (2013).

187. Nolte-'t Hoen, E. N. *et al.* Deep sequencing of RNA from immune cell-derived vesicles uncovers the selective incorporation of small non-coding RNA biotypes with potential regulatory functions. *Nucleic Acids Res* **40**, 9272–9285 (2012).

188. Hammerling, B. C. *et al.* A Rab5 endosomal pathway mediates Parkin-dependent mitochondrial clearance. *Nat Commun* **8**, 14050 (2017).

189. Vanlandingham, P. A. & Ceresa, B. P. Rab7 regulates late endocytic trafficking downstream of multivesicular body biogenesis and cargo sequestration. *J Biol Chem* **284**, 12110–12124 (2009).

190. Cogliati, S. *et al.* Mitochondrial cristae shape determines respiratory chain supercomplexes assembly and respiratory efficiency. *Cell* **155**, 160–171 (2013).

191. Buck, M. D. *et al.* Mitochondrial Dynamics Controls T Cell Fate through Metabolic Programming. *Cell* **166**, 63–76 (2016).

192. Mizushima, N. & Levine, B. Autophagy in mammalian development and differentiation. *Nat Cell Biol* **12**, 823–830 (2010).

193. Fader, C. M., Sanchez, D., Furlan, M. & Colombo, M. I. Induction of autophagy promotes fusion of multivesicular bodies with autophagic vacuoles in k562 cells. *Traffic* **9**, 230–250 (2008).

194. Latorre-Pellicer, A. *et al.* Mitochondrial and nuclear DNA matching shapes metabolism and healthy ageing. *Nature* **535**, 561–565 (2016).

195. West, A. P. & Shadel, G. S. Mitochondrial DNA in innate immune responses and inflammatory pathology. *Nat Rev Immunol* (2017).

196. Chen, Q., Sun, L. & Chen, Z. J. Regulation and function of the cGAS-STING pathway of cytosolic DNA sensing. *Nat Immunol* **17**, 1142–1149 (2016).

197. Ishikawa, H., Ma, Z. & Barber, G. N. STING regulates intracellular DNA-mediated, type I interferon-dependent innate immunity. *Nature* **461**, 788–792 (2009).

198. Bobrie, A., Colombo, M., Krumeich, S., Raposo, G. & Théry, C. Diverse subpopulations of vesicles secreted by different intracellular mechanisms are present in exosome preparations obtained by differential ultracentrifugation. *J. Extracell. Vesicles* **1**, 18397 (2012).

199. van der Vlist, E. J. *et al.* CD4 $^{+}$ T cell activation promotes the differential release of distinct populations of nanosized vesicles. *J. Extracell. Vesicles* **1**, 18364 (2012).

200. Palma, J. *et al.* MicroRNAs are exported from malignant cells in customized particles. *Nucleic Acids Res.* **40**, 9125–9138 (2012).

201. Sreekumar, P. G. *et al.* αB Crystallin Is Apically Secreted within Exosomes by Polarized Human Retinal Pigment Epithelium and Provides Neuroprotection to Adjacent Cells. *PLoS One* **5**, e12578 (2010).

202. White, I. J., Bailey, L. M., Aghakhani, M. R., Moss, S. E. & Futter, C. E. EGF stimulates annexin 1-dependent inward vesiculation in a multivesicular endosome subpopulation. *EMBO J.* **25**, 1–12 (2006).

203. Kowal, J. *et al.* Proteomic comparison defines novel markers to characterize heterogeneous populations of extracellular vesicle subtypes. *Proc. Natl. Acad. Sci. U. S. A.* (2016).

204. Willms, E. *et al.* Cells release subpopulations of exosomes with distinct molecular and biological properties. *Sci. Rep.* **6**, 22519 (2016).

205. Mastoridis, S. *et al.* Multiparametric Analysis of Circulating Exosomes and Other Small Extracellular Vesicles by Advanced Imaging Flow Cytometry. *Front. Immunol.* **9**, 1583 (2018).

206. Schrader, M., Godinho, L. F., Costello, J. L. & Islinger, M. The different facets of organelle interplay-an overview of organelle interactions. *Front. cell Dev. Biol.* **3**, 56 (2015).

207. Martinvalet, D. The role of the mitochondria and the endoplasmic reticulum contact sites in the development of the immune responses. *Cell Death Dis.* **9**, 336 (2018).

208. Sugiura, A., Mattie, S., Prudent, J. & McBride, H. M. Newly born peroxisomes are a hybrid of mitochondrial and ER-derived pre-peroxisomes. *Nature* **542**, 251–254 (2017).

209. Itoh, K. *et al.* A brain-enriched Drp1 isoform associates with lysosomes, late endosomes, and the plasma membrane. *J. Biol. Chem.* **293**, 11809–11822 (2018).

210. Green, D. R., Galluzzi, L. & Kroemer, G. Mitochondria and the Autophagy-Inflammation-Cell Death Axis in Organismal Aging. *Science (80-.).* **333**, 1109–1112 (2011).

211. Sheftel, A. D., Zhang, A.-S., Brown, C., Shirihai, O. S. & Ponka, P. Direct interorganellar transfer of iron from endosome to mitochondrion. *Blood* **110**, 125–132 (2007).

212. Hamdi, A. *et al.* Erythroid cell mitochondria receive endosomal iron by a “kiss-and-run” mechanism. *Biochim. Biophys. Acta - Mol. Cell Res.* **1863**, 2859–2867 (2016).

213. Soto-Heredero, G., Baixauli, F. & Mittelbrunn, M. Interorganelle Communication between Mitochondria and the Endolysosomal System. *Front. Cell Dev. Biol.* **5**, 95 (2017).

214. Cioni, J.-M. *et al.* Late Endosomes Act as mRNA Translation Platforms and Sustain Mitochondria in Axons. *Cell* **176**, 56-72.e15 (2019).

215. Nakahira, K. *et al.* Autophagy proteins regulate innate immune responses by inhibiting the release of mitochondrial DNA mediated by the NALP3 inflammasome. *Nat Immunol* **12**, 222–230 (2011).

216. Wang, C. & Youle, R. J. The role of mitochondria in apoptosis*. *Annu. Rev. Genet.* **43**, 95–118 (2009).

217. Soubannier, V. *et al.* A vesicular transport pathway shuttles cargo from mitochondria to lysosomes. *Curr. Biol.* **22**, 135–41 (2012).

218. Cadete, V. J. J. *et al.* Formation of mitochondrial-derived vesicles is an active and physiologically relevant mitochondrial quality control process in the cardiac system. *J. Physiol.* **594**, 5343–5362 (2016).

219. Sugiura, A., McLelland, G. L., Fon, E. A. & McBride, H. M. A new pathway for mitochondrial quality control: mitochondrial-derived vesicles. *EMBO J* **33**, 2142–2156 (2014).

220. Mclelland, G., Soubannier, V., Chen, C. X., Mcbride, H. M. & Fon, E. A. Parkin and PINK 1 function in a vesicular trafficking pathway regulating mitochondrial quality control. **33**, 282–296 (2014).

221. McLelland, G.-L., Lee, S. A., McBride, H. M. & Fon, E. A. Syntaxin-17 delivers PINK1/parkin-dependent mitochondrial vesicles to the endolysosomal system. *J. Cell Biol.* **214**, 275–291 (2016).

222. Pan, B. T., Teng, K., Wu, C., Adam, M. & Johnstone, R. M. Electron microscopic evidence for externalization of the transferrin receptor in vesicular form in sheep reticulocytes. *J. Cell Biol.* **101**, 942–948 (1985).

223. Johnstone, R. M., Adam, M., Hammond, J. R., Orr, L. & Turbide, C. Vesicle formation during reticulocyte maturation. Association of plasma membrane activities with released vesicles (exosomes). *J. Biol. Chem.* **262**, 9412–20 (1987).

224. Dai, Y. *et al.* Rapamycin drives selection against a pathogenic heteroplasmic mitochondrial DNA mutation. *Hum. Mol. Genet.* **23**, 637–47 (2014).

225. Suen, D.-F., Narendra, D. P., Tanaka, A., Manfredi, G. & Youle, R. J. Parkin overexpression selects against a deleterious mtDNA mutation in heteroplasmic cybrid cells. *Proc. Natl. Acad. Sci.* **107**, 11835–11840 (2010).

226. Valenci, I., Yonai, L., Bar-Yaacov, D., Mishmar, D. & Ben-Zvi, A. Parkin modulates heteroplasmy of truncated mtDNA in Caenorhabditis elegans. *Mitochondrion* **20**, 64–70 (2015).

227. Peeva, V. *et al.* Linear mitochondrial DNA is rapidly degraded by components of the replication machinery. *Nat. Commun.* **9**, 1727 (2018).

228. Medeiros, T. C., Thomas, R. L., Ghillebert, R. & Graef, M. Autophagy balances mtDNA synthesis and degradation by DNA polymerase POLG during starvation. *J. Cell Biol.* **217**, 1601–1611 (2018).

229. Moretton, A. *et al.* Selective mitochondrial DNA degradation following double-strand breaks. *PLoS One* **12**, e0176795 (2017).

230. Shokolenko, I. N., Wilson, G. L. & Alexeyev, M. F. The “fast” and the “slow” modes of mitochondrial DNA degradation. *Mitochondrial DNA* **27**, 490–498 (2016).

231. Lespagnol, A. *et al.* Exosome secretion, including the DNA damage-induced p53-dependent secretory pathway, is severely compromised in TSAP6/Steap3-null mice. *Cell Death Differ.* **15**, 1723–1733 (2008).

232. Hessvik, N. P. *et al.* PIKfyve inhibition increases exosome release and induces secretory autophagy. *Cell. Mol. Life Sci.* **73**, 4717–4737 (2016).

233. Jeannin, P. *et al.* Proteomic analysis of plasma extracellular vesicles reveals mitochondrial stress upon HTLV-1 infection. *Sci. Rep.* **8**, 5170 (2018).

234. Szczesny, B. *et al.* Mitochondrial DNA damage and subsequent activation of Z-DNA binding protein 1 links oxidative stress to inflammation in epithelial cells. *Sci. Rep.* **8**, 914 (2018).

235. Kalluri, R. & LeBleu, V. S. Discovery of Double-Stranded Genomic DNA in Circulating Exosomes. *Cold Spring Harb. Symp. Quant. Biol.* **81**, 275–280 (2016).

236. Melentijevic, I. *et al.* C. elegans neurons jettison protein aggregates and mitochondria under neurotoxic stress. *Nature* **542**, 367–371 (2017).

237. Soubannier, V., Rippstein, P., Kaufman, B. a, Shoubridge, E. a & McBride, H. M. Reconstitution of mitochondria derived vesicle formation demonstrates selective enrichment of oxidized cargo. *PLoS One* **7**, e52830 (2012).

238. Cai, J. *et al.* Extracellular vesicle-mediated transfer of donor genomic DNA to recipient cells is a novel mechanism for genetic influence between cells. *J. Mol. Cell Biol.* **5**, 227–238 (2013).

239. Lee, T. H. *et al.* Oncogenic ras-driven cancer cell vesiculation leads to emission of double-stranded DNA capable of interacting with target cells. *Biochem. Biophys. Res. Commun.* **451**, 295–301 (2014).

240. Sansone, P. *et al.* Packaging and transfer of mitochondrial DNA via exosomes regulate escape from dormancy in hormonal therapy-resistant breast cancer. *Proc. Natl. Acad. Sci.* **114**, E9066–E9075 (2017).

241. Crisp, A., Boschetti, C., Perry, M., Tunnacliffe, A. & Micklem, G. Expression of multiple horizontally acquired genes is a hallmark of both vertebrate and invertebrate genomes. *Genome Biol.* **16**, 50 (2015).

242. Marinoni, G. *et al.* Horizontal transfer of genetic material among Saccharomyces yeasts. *J. Bacteriol.* **181**, 6488–96 (1999).

243. Gladyshev, E. A., Meselson, M. & Arkhipova, I. R. Massive Horizontal Gene Transfer in Bdelloid Rotifers. *Science (80-.).* **320**, 1210–1213 (2008).

244. Eyres, I. *et al.* Horizontal gene transfer in bdelloid rotifers is ancient, ongoing and more frequent in species from desiccating habitats. *BMC Biol.* **13**, 90 (2015).

245. Rice, D. W. *et al.* Horizontal Transfer of Entire Genomes via Mitochondrial Fusion in the Angiosperm Amborella. *Science (80-.).* **342**, 1468–1473 (2013).

246. Rebbeck, C. A., Leroi, A. M. & Burt, A. Mitochondrial capture by a transmissible cancer. *Science (80-.).* **331**, 303 (2011).

247. Clark, M. A. & Shay, J. W. Mitochondrial transformation of mammalian cells. *Nature* **295**, 605–607 (1982).

248. Manfredi, G., Thyagarajan, D., Papadopoulou, L. C., Pallotti, F. & Schon, E. A. The fate of human sperm-derived mtDNA in somatic cells. *Am J Hum Genet* **61**, 953–960 (1997).

249. Dong, L. F. *et al.* Horizontal transfer of whole mitochondria restores tumorigenic potential in mitochondrial DNA-deficient cancer cells. *Elife* **6**, (2017).

250. Hough, K. P. *et al.* Exosomal transfer of mitochondria from airway myeloid-derived regulatory cells to T cells. *Redox Biol.* **18**, 54–64 (2018).

251. Li, M., Schröder, R., Ni, S., Madea, B. & Stoneking, M. Extensive tissue-related and allele-related mtDNA heteroplasmy suggests positive selection for somatic mutations. *Proc. Natl. Acad. Sci. U. S. A.* **112**, 2491–6 (2015).

252. Sharpley, M. S. *et al.* Heteroplasmy of Mouse mtDNA Is Genetically Unstable and Results in Altered Behavior and Cognition. *Cell* **151**, 333–343 (2012).

253. Branzk, N. *et al.* Neutrophils sense microbe size and selectively release neutrophil extracellular traps in response to large pathogens. *Nat Immunol* **15**, 1017–1025 (2014).

254. Lood, C. *et al.* Neutrophil extracellular traps enriched in oxidized mitochondrial DNA are interferogenic and contribute to lupus-like disease. *Nat Med* **22**, 146–153 (2016).

255. Ingelsson, B. *et al.* Lymphocytes eject interferogenic mitochondrial DNA webs in response to CpG and non-CpG oligodeoxynucleotides of class C. *Proc. Natl. Acad. Sci. U. S. A.* **115**, E478–E487 (2018).

256. Julian, M. W. *et al.* Mitochondrial transcription factor A serves as a danger signal by augmenting plasmacytoid dendritic cell responses to DNA. *J. Immunol. (Baltimore, Md. 1950)* **189**, 433–443 (2012).

257. Tsilioni, I. & Theoharides, T. C. Extracellular vesicles are increased in the serum of children with autism spectrum disorder, contain mitochondrial DNA, and stimulate human microglia to secrete IL-1β. *J. Neuroinflammation* **15**, 239 (2018).

258. Verboogen, D. R. J. *et al.* The dendritic cell side of the immunological synapse. *Biomol. Concepts* **7**, 17–28 (2016).

259. Boes, M. *et al.* T-cell engagement of dendritic cells rapidly rearranges MHC class II transport. *Nature* **418**, 983–988 (2002).

260. Boes, M. *et al.* T Cells Induce Extended Class II MHC Compartments in Dendritic Cells in a Toll-Like Receptor-Dependent Manner. *J. Immunol.* **171**, 4081–4088 (2003).

261. Pulecio, J. *et al.* Cdc42-mediated MTOC polarization in dendritic cells controls targeted delivery of cytokines at the immune synapse. *J. Exp. Med.* **207**, 2719–2732 (2010).

262. Chen, M. & Wang, J. Programmed cell death of dendritic cells in immune regulation. *Immunol Rev* **236**, 11–27 (2010).

263. Riol-Blanco, L. *et al.* Immunological synapse formation inhibits, via NF-kappaB and FOXO1, the apoptosis of dendritic cells. *Nat Immunol* **10**, 753–760 (2009).

264. Ingulli, E., Mondino, A., Khoruts, A. & Jenkins, M. K. In vivo detection of dendritic cell antigen presentation to CD4(+) T cells. *J Exp Med* **185**, 2133–2141 (1997).

265. Garg, S. *et al.* Genetic tagging shows increased frequency and longevity of antigen-presenting, skin-derived dendritic cells in vivo. *Nat Immunol* **4**, 907–912 (2003).

266. Ariotti, S. *et al.* T cell memory. Skin-resident memory CD8(+) T cells trigger a state of tissue-wide pathogen alert. *Science (80-.).* **346**, 101–105 (2014).

267. Iijima, N. & Iwasaki, A. T cell memory. A local macrophage chemokine network sustains protective tissue-resident memory CD4 T cells. *Science (80-.).* **346**, 93–98 (2014).

268. Schenkel, J. M. *et al.* T cell memory. Resident memory CD8 T cells trigger protective innate and adaptive immune responses. *Science (80-.).* **346**, 98–101 (2014).

269. Netea, M. G. *et al.* Trained immunity: A program of innate immune memory in health and disease. *Science (80-.).* **352**, aaf1098 (2016).

270. Curato, C. *et al.* DC Respond to Cognate T Cell Interaction in the Antigen-Challenged Lymph Node. *Front. Immunol.* **10**, 863 (2019).

271. Rodriguez-Fernandez, J. L., Riol-Blanco, L. & Delgado-Martin, C. What Is the Function of the Dendritic Cell Side of the Immunological Synapse? *Sci. Signal.* **3**, re2–re2 (2010).

Annexes

Annexes

1. Publications related with this work (included):

I. **Torralba D**, Baixauli F, Villarroya-Beltri C, Fernández-Delgado I, Latorre-Pellicer A, Acín-Pérez R, Martín-Cófreces NB, Jaso-Tamame ÁL, Iborra S, Jorge I, González-Aseguinolaza G, Garaude J, Vicente-Manzanares M, Enríquez JA, Mittelbrunn M, Sánchez-Madrid F. Priming of dendritic cells by DNA-containing extracellular vesicles from activated T cells through antigen-driven contacts. Nat Commun. 2018 Jul 9;9(1):2658. doi: 10.1038/s41467-018-05077-9.

II. Villarroya-Beltri C, Baixauli F, Mittelbrunn M, Fernández-Delgado I, **Torralba D**, Moreno-Gonzalo O, Baldanta S, Enrich C, Guerra S, Sánchez-Madrid F. ISGylation controls exosome secretion by promoting lysosomal degradation of MVB proteins. Nat Commun. 2016 Nov 24;7:13588. doi: 10.1038/ncomms13588.

2. Reviews related with this work (not included):

I. **Torralba D**, Baixauli F, Sánchez-Madrid F. Mitochondria Know No Boundaries: Mechanisms and Functions of Intercellular Mitochondrial Transfer. Front Cell Dev Biol. 2016 Sep 28;4:107. eCollection 2016. Review.

II. **Torralba D**, Martín-Cófreces NB, Sanchez-Madrid F. Mechanisms of polarized cell-cell communication of T lymphocytes. Immunol Lett. 2019 May;209:11-20. doi: 10.1016/j.imlet.2019.03.009. Epub 2019 Apr 5. Review.

3. Other articles not related with this work:

I. Saiz ML, Cibrian D, Ramírez-Huesca M, **Torralba D**, Moreno-Gonzalo O, Sánchez-Madrid F. Tetraspanin CD9 Limits Mucosal Healing in Experimental Colitis. Front Immunol. 2017 Dec 19;8:1854. doi: 10.3389/fimmu.2017.01854. eCollection 2017.